

**STUDY OF SHEAR DRIVEN ELECTRON
MAGNETOHYDRODYNAMIC (EMHD)
INSTABILITIES IN PLASMAS**

By

**GURUDATT GAUR
PHYS06200704008**

INSTITUTE FOR PLASMA RESEARCH, GANDHINAGAR.

*A thesis submitted to the
Board of Studies in Physical Sciences*

*In partial fulfillment of the requirements
For the Degree of*

DOCTOR OF PHILOSOPHY

of

HOMI BHABHA NATIONAL INSTITUTE



July, 2013

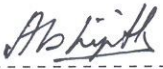
Homi Bhabha National Institute

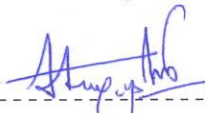
Recommendations of the Viva Voce Board

As members of the Viva Voce Board, we recommend that the dissertation prepared by **Gurudatt Gaur** entitled "Study of Shear Driven Electron Magnetohydrodynamic (EMHD) Instabilities in Plasmas" may be accepted as fulfilling the dissertation requirement for the Degree of Doctor of Philosophy.


----- Date : 29-10-2013
Chairman : Prof. Predhiman Kaw


----- Date : 29-10-2013
Convener : Prof. Amita Das


----- Date : 29-10-2013
Member : Prof. Abhijit Sen


----- Date : 29-10-2013
Member : Dr. Sudip Sengupta

Final approval and acceptance of this dissertation is contingent upon the candidate's submission of the final copies of the dissertation to HBNI.

I hereby certify that I have read this dissertation prepared under my direction and recommend that it may be accepted as fulfilling the dissertation requirement.


----- Date : 29-10-2013
Guide : Prof. Amita Das

STATEMENT BY AUTHOR

This dissertation has been submitted in partial fulfillment of requirements for an advanced degree at Homi Bhabha National Institute (HBNI) and is deposited in the Library to be made available to borrowers under rules of the HBNI.

Brief quotations from this dissertation are allowable without special permission, provided that accurate acknowledgement of source is made. Requests for permission for extended quotation from or reproduction of this manuscript in whole or in part may be granted by the Competent Authority of HBNI when in his or her judgment the proposed use of the material is in the interests of scholarship. In all other instances, however, permission must be obtained from the author.



Gurudatt Gaur

DECLARATION

I, hereby declare that the investigation presented in the thesis has been carried out by me. The work is original and the work has not been submitted earlier as a whole or in part for a degree/diploma at this or any other Institution or University.


Gurudatt Gaur

To my parents

ACKNOWLEDGEMENTS

It was hardly possible for me to complete this thesis without the precious support of a number of people. I take this opportunity to express my deepest gratitude to all of them.

I would like to start by thanking my thesis supervisor Prof. Amita Das for her valuable guidance, scholarly inputs and consistent support and encouragement I received throughout the tenure. She has been immensely patient in teaching me basic tools and concepts of plasma physics, as well as ignoring my naive acts at times. I largely owe it to her for whatever scientific understanding I have gained so far. I thank her for introducing me to the beautiful world of plasma physics.

I also intend to thank chairman of my doctoral committee Prof. Kaw for his kind association and invaluable time. I fall short of words to describe the great help I received from him over the years. I also thank the other doctoral committee members Prof. Abhijit Sen and Dr. Sudip Sengupta for monitoring the progress of my thesis work. Special thanks are due to Dr. Sudip Sengupta for critically reading my manuscripts and providing his valuable inputs.

I also owe many thanks to the faculty members Prof. Amita Das, Prof. Raghvendra Sigh, Prof. Jha, Dr. R. Ganesh, Dr. Prabal Chattopadhyay, Dr. Sudip Sengupta, Dr. S. Mukherjee, Dr. Joydeep Ghosh, Dr. Manoj Warriar for providing excellent training during course work. I am specially thankful to Dr. Prabal Chattopadhyay, who was the mentor of my project during the course work. I express my sincere thanks to Dean Academic, Dr. Mukherjee who has always offered the best to the students.

Stay at IPR was a wonderful experience in the company of many friends. I

am grateful to my batch-mates Tayyab, Sita, Kshitish, Ujjwal, Prabal, Deepak, Vikram, Ashwin, Sanjib, Arvind and Linthish for their affection. The first year days with them were the best fun. Unconditional support from Tayyab needs special mention. I would also like to thank my seniors Vikrant, Maya, Kishor, Anurag, Jugal, Sharad, Shekhar, Satya for their help and friendly attitude and my juniors Sanat, Sushil, Rameshwar, Pravesh, Sayak, Manjit, Aditya, Soumen, Vikram Dharodi, Rupendra, Neeraj, Vara for their love and support. I take this opportunity to thank Vikrant for being a great moral support, in tough times too.

I extend my thanks to Sharad K. Yadav, Sita Sundar and Sarveshwar Sharma for their association. With them, I could learn and do many things in this thesis. Special thanks to Bhavesh, Sanat and Vikram Dharodi for proof-reading of the thesis. Avadhesh also deserves a special mention for his timely help at several occasions. I thank Sharad, Bhavesh, Sanat, Vikram Dharodi and Avadhesh again for sharing their knowledge and experience during tea breaks. Thanks are also due to Aditya for providing suggestions on the Introduction.

I would also like to acknowledge people from computer center especially Ms. Sutapa Ranjan, Govind, Hemant, Shailendra and people from library especially Ms. Pragnya Pathak, Shravan, Shilpa and Smita for their continuous help. Thanks are also due to people from administration, accounts, stores, purchase and canteen for their co-operation throughout my Ph.D., without which it would have been a rather difficult task. Of course, the stay in the hostel would have been miserable without the delicious food prepared by our cooks Jeevlal and his wife. They deserve a big thanks for the good job. I also extend my thanks to Dept. of Atomic Energy, Govt. of India for providing me all the required facilities at my workplace and for the fellowship as well.

These were the blessings of my dear parents and best wishes of my family members, that I could see the completion of my Thesis. I wish to thank them all. I thank my father, for being the motivator, my mother, for being the inspiration and family members, for always standing by my side. I thank my wife Jyoti for taking care of our daughter Anwita and allowing me to focus. She also managed my other responsibilities very well that really took burden off me. But hereafter, *"Hum Saath Saath Hain"*.

Gurudatt Gaur

Contents

Synopsis	2
List of Figures	16
1 Introduction	23
1.1 Objective and Motivation	23
1.2 Electron Magnetohydrodynamic (EMHD) Model	26
1.2.1 Brief Description of Model and Its Applicability	26
1.2.2 Natural Scales in EMHD	29
1.2.3 Nonlinear Solutions of EMHD	30
1.3 A Review of Earlier Work on Shear Driven Instabilities in EMHD Domain	31
1.4 Scope of the Thesis	35
1.5 Summary of Chapters	38
2 Role of Natural Length and Time Scales on Electron Magnetohydrodynamic Kelvin Helmholtz Instability: 2D Studies	44
2.1 Introduction	45
2.2 Governing Equations	48
2.3 Role of Skin Depth	50

2.4	Role of Whistler Waves	54
2.4.1	Step Velocity Profile	55
2.4.2	Velocity Profile with Finite Shear Width	59
2.5	Nonlinear Simulations	61
2.6	Summary	68
3	Interplay of Kelvin Helmholtz and Kink Modes: 3D Studies	71
3.1	Introduction	72
3.2	Model and Governing Equations	75
3.3	Linear Instability	76
3.3.1	Local Analysis	77
3.3.2	Nonlocal Analysis: tanh-profile	78
3.4	Nonlinear Simulations	85
3.5	Summary	92
4	Stability of Isichenko Solutions of Electron Magnetohydrodynamic Model Against Shear Driven Modes	94
4.1	Introduction	95
4.2	Solutions of 2D EMHD	98
4.3	Nonlinear Simulations	101
4.4	Discussion	105
4.5	Summary	108
5	Summary and Future Scope	110
5.1	Summary and Conclusions	110
5.2	Future Scope	115
	Bibliography	117

SYNOPSIS

In this thesis, we study the collisionless instabilities driven due to the shear in the equilibrium electron current. These are the instabilities of sheared electron current configurations formed in a variety of physical situations e.g., fast z-pinches [1, 2], fast ignition phenomena of laser fusion [3, 4, 5, 6], collision less magnetic reconnections [7, 8, 9, 10, 11], plasma opening devices [12, 13, 14], inter planetary current-carrying plasmas [15, 16] etc. In these configurations, with equilibrium length scales smaller than the ion skin depth, the current flows faster than the Alfvén velocity. In these situations, ion response is ignored and a simplified Electron Magnetohydrodynamic (EMHD) model is evoked to study the stability of the current configurations.

EMHD model is a single fluid description of plasma in which only electron dynamics is of importance and ions provide merely a static, neutralizing background [17]. In our studies, the electrons have been treated as a cold, incompressible electron fluid of uniform density. In the cold fluid (plasma) description, effects due to thermal motion of particles are neglected. This is valid when the phase velocities are much larger than the thermal velocity of particles. In this situation, the corresponding velocity distribution function may be approximately a Dirac delta function centered at the macroscopic fluid velocity.

Since ions are stationary in EMHD, the electron flow velocity \vec{v} is directly related to the current density as, $\vec{J} = -ne\vec{v}$. In our case of uniform density electron fluid, the shear in the current is due to the shear in flow velocity. The shear in the current can also be generated due to the density gradient. However, the density gradient can not relax in a cold collisionless plasma so there is no free energy available for the excitation of instability [18]. Further, it has been shown that the

presence of current gradient due to density gradient alone, is unable to excite the instability. The free energy associated with the sheared flow configuration is necessary for the instability. Thus in our case the shear driven instability is essentially the velocity shear driven Kelvin Helmholtz (KH) instability. The KH instability is one of the prominent neutral fluid instabilities [19, 20] which destabilizes the interface separating the two fluids in relative motion. The development of instability leads to turbulence, transport of energy and momentum and dissipation and mixing of fluids. Extensive work has been devoted in literature to the investigation of 2D and 3D KH instability in the framework of EMHD [21, 22, 23, 24, 25].

The EMHD system closely resembles an incompressible hydrodynamic fluid system with additional features associated with the magnetized character of electron fluid. The electromagnetic character of EMHD fluid manifests itself in terms of natural length and time scales. Electron skin depth d_e is the natural length scale which arises on the account of electron inertia. Also, whistlers being the normal oscillatory modes of EMHD introduce the natural time scale (whistler periods). The neutral fluids, however, are devoid of any such specific length and/or time scales. We investigated the role of these natural scales of EMHD on KH instability in two dimensions. The perturbations are confined to the 2D plane consisting of shear and flow directions in which the major action of KH instability lies. The self consistent magnetic field, arising due to 2D sheared flow of electrons, is directed along the symmetry direction. Role of electron skin depth on the KH instability has been investigated and thereby a comparison between EMHD fluid and neutral hydrodynamic fluid has been provided. The EMHD model, for scales shorter than the electron skin depth, reduces to Navier Stokes (NS) equations in 2D for an incompressible neutral hydrodynamic limit. For NS fluid case, plot of the growth

rate of KH instability is a universal curve for different values of shear width when velocity is adjusted to accommodate for the length rescaling. However, it is observed that the growth rate for EMHD fluid case decreases as the shear width is increased in comparison to the electron skin depth. The instability is prominent only when the shear scale in the electron flow velocity is shorter than the electron skin depth. Moreover, the instability is of nonlocal type for finite shear width, as outlined in earlier studies also [22, 23]; a physical understanding of this has been provided in the Thesis.

We next study the role of whistlers on the 2D instability. The excitation of whistlers requires a finite component of wave vector along the direction of magnetic field. In earlier 2D EMHD studies of KH-like mode [22, 23], the equilibrium as well as the perturbed magnetic fields were directed along the symmetry direction along which no variations were permitted. Hence, whistlers were clearly not supported in these studies. Whistler modes were supported in later 3D studies [24, 25]. In those studies, however, the propagation direction of whistlers was orthogonal to the 2D plane in which KH action primarily occurs. To understand the role of whistlers on the instability, we introduce a uniform external magnetic field along the flow direction (in the plane of KH). In earlier studies, a single equation describing the evolution of magnetic field component along the symmetry direction was sufficient. However, we need to solve a set of coupled equations when whistlers are permitted in the system. This is essentially due to the fact that whistlers couple the in-plane magnetic field perturbations to the magnetic perturbations along the symmetry direction. The action of KH distorts the magnetic field to a sheared configuration. The tension caused due to the distortion tries to restore the magnetic field configuration and sets up oscillations at whistler frequency. The

process of excitation of whistlers costs the energy and makes the KH instability less favourable. The linear analysis shows that the growth rate reduces as the magnetic field strength is increased.

Nonlinear simulations have been carried out to understand the role of whistlers in the nonlinear regime of instability. For this purpose we use a nonlinear fluid code which uses flux corrected transport algorithm. The code solves 2D EMHD equations for tangent hyperbolic profile of equilibrium velocity. In the nonlinear regime of instability, in the absence of B_0 , a coherent vortex occupying the box size is formed [23]. This is because of two non-dissipative square invariants namely, energy and enstrophy, supported by two dimensional EMHD model. However, In the presence of B_0 , the nonlinear state is significantly changed from the ordered state of $B_0 = 0$ case. The long scale structures are formed only along the direction of B_0 and there is hardly any extension in structures along the transverse direction. This induces anisotropy in the system. The observed anisotropy is a characteristics of the nonlinear cascade mediated by whistlers [26, 27]. The nonlinear interaction of whistlers produces diminishing wave number parallel to B_0 . The perpendicular wave numbers, on the other hand, increase as the result of these interactions. We provide a quantitative estimate of anisotropy in the Fourier spectrum of two fields. Due to the anisotropic cascade, the KH instability induced mixing of the fluids, flowing in two directions, around the shear layer is less. Consequently, the flattening of shear layer is observed to be weaker. These studies on shear driven instabilities in EMHD along with whistlers would be of relevance in a number of physics situations. This kind of configuration is quite likely in laboratory experiments [28, 29] where the plasma is confined with the help of an axial magnetic field. Also the presence of electron beams in plasmas threaded by a magnetic field

is ubiquitous in nature. For instance, in ionosphere and magnetosphere [30], solar corona [31] and pulsars [32], etc., the equilibrium configuration considered in our work might exist.

We extend our studies to more realistic 3D instability. In the three dimensional regime of instability, when the variations along the direction of self-consistent equilibrium magnetic field are also allowed, a new mode exists in addition to KH mode. This is a local mode, termed as the kink mode, which lies in the plane of magnetic field and shear [24, 33]. The mode requires finite electron inertia and is driven by the gradient in the equilibrium velocity, unlike the KH mode which is driven by the curvature in equilibrium velocity. Since in EMHD, the shear in velocity is analogous to current-gradient, the KH mode has also been identified as current-gradient driven sausage mode. The interplay of two modes has been studied under various physical conditions.

The shear width ϵ is varied in comparison with the electron skin depth d_e . It has been observed that sausage mode is dominant for sharper shear width while, for broader shear width, kink is the dominant mode. This is consistent with the fact that the 2D instability is prominent only when the shear width is sharper than the electron skin depth. Stabilizing behaviour of uniform magnetic field along the flow direction (denoted as B_{00} here) has been investigated for 3D instability. Local analysis shows that it has no role on pure kink mode. However, it reduces the growth rate of mixed mode. The field reduces the pure sausage growth rate and hence dominant mode is kink in this case. Self consistent magnetic field was known to have no effect on 2D instability when the variations were suppressed along its direction. However, this magnetic field has stabilizing role on kink instability as shown by local dispersion relation obtained in earlier studies [24]. An external

uniform magnetic field C_0 along the direction of self consistent field would simply add to it. This would make the excitation of kink instability difficult with no role on pure sausage instability. This we indeed observe in our studies. The dominant mode for this case is pure sausage mode. We also carry out the simulations of the three dimensional instability with the help of a nonlinear fluid code. The linear growth rates of instabilities calculated in various simulations with different values of ϵ , B_{00} and C_0 are in agreement with linear theory.

The nonlinear state of instability is strongly turbulent in the 3D simulations, unlike the two dimensional case. The generation of turbulence is attributed to larger number of unstable modes in 3D and also non-existence of non-dissipative integral invariants of 2D. The generation of electromagnetic turbulence due to the action of shear driven instabilities has been shown to have important implications. This leads to the anomalous stopping of energetic electrons moving towards core in Fast Ignition, which are known to eventually create the ignition spot by dumping their energy to the core [25]. Also, in collisionless magnetic reconnections [21], the generation of turbulence may alter the mechanism by which the frozen in field condition breaks in the dissipative regime. The reconnections may also be facilitated by the anomalous viscosity and anomalous resistivity associated to the turbulence generation.

We have analyzed the spectral cascade features of the turbulence generated in the nonlinear state with and without B_{00} . In the absence of B_{00} , it is observed that the spectral cascade towards shorter scales is inhibited along the direction of flow as well as the direction of self-consistent magnetic field. The shortest scales are thus found to generate along the shear direction while, in other two directions the scales are typically longer. This induces significant anisotropy in the spectrum. In

simulations with the external magnetic field (B_{00}) present along the flow direction, we observe that the scales along the shear directions are more or less unchanged. However, along the other two directions, the scales are longer in comparison to the case when this magnetic field is not present. These results are in conformity with the whistler mediated spectral cascade features [26, 27]. We have also measured the nonlinear broadening of shear layer which provides the information on the effective viscous coefficient. The broadening of shear layer occurs much slowly for the case when magnetic field is present along the flow directions. In that case, the system evolution is governed by the kink mode which in the linear phase does not alter the 2D flow structure. The broadening occurs only at later nonlinear phase when the energy starts to trickle in other modes as well. We stress here that the studies on interplay of two modes under various physical conditions is important as it would largely affect the evolution of system, as discussed here.

The EMHD set of equations permits certain exact, nonlinear electron flow solutions obtained by Isichenko and Marnachev as the isolated, coherent structures [34]. The first variety of solutions are the rotating electron currents giving rise to monopolar magnetic fields. These monopolar solutions are radially symmetric and stationary solutions. The other variety includes the electron currents producing bipolar magnetic fields. These dipolar solutions are radially non-symmetric and propagate with constant speed in their axial direction. 2D evolution of monopoles and dipoles has been studied extensively by several authors which suggests that these structures are very robust and stable [35, 36]. The structures, specially dipoles, are known to have important applications. Recently, the dipole structures have been employed to simulate the behaviour of electron current pulses through an inhomogeneous plasma medium [37, 38]. In an another study, Sharad et al.

[38] showed a novel mechanism, the formation of current shock, through which the dipoles dissipate their energy and discussed the implications of their study to the fast ignition [3, 4, 5, 6]. The similar current pulses can be found to get formed in other phenomena such as fast magnetic reconnections [7, 8, 9, 10, 11], fast magnetic field transport [39, 40], laser plasma interactions [41], etc.

We have investigated the instability processes, sausage and kink, for the Isichenko solutions of EMHD equations. These solutions have regions where electron flow velocity/current is significantly sheared and hence can be susceptible to the said instabilities. As mentioned above, in their 2D evolution, the structures are very robust and stable [35, 36]. These studies do not support the kink mode, and the structures are stable to the sausage mode. The stability of structures against sausage mode has been argued on the following basis. For the EMHD structures, shear width as well as total extent of shear flow are typically of the order of electron skin depth. The total extent of shear flow limited in size does not permit the wave number to satisfy the instability criteria of sausage mode viz., $k_z \epsilon < 1$; here, ' k_z ' is the wavenumber along the flow direction and ' ϵ ' is the typical shear width [42]. Hence the structures are found to be stable in 2D studies. The kink mode, however, does not have to follow such restriction. It is thus of importance to know if the structures are stable to this mode. To address this question, we performed a three dimensional simulation study in which kink mode is also operative in addition to sausage mode. In simulations, the structures are seen to become unstable. The destabilization of structures has been attributed to the presence of local kink mode. The unstable behaviour of structures raises a question of their relevance in various phenomena as described in earlier studies [36, 38]. The magnitude of instability growth rate needs to be taken into consideration along with the time scales

involved in the various phenomena to investigate the relevance of these structures. A discussion on this issue has been provided in the thesis.

The thesis has been organized as follows. Chapter 1 presents the introduction of the Thesis. In Chapter 2, we discuss the role of natural length and time scales on shear driven 2D EMHD instability. Linear and nonlinear studies of shear driven 3D EMHD instability have been discussed in Chapter 3. In Chapter 4, stability of Isichenko solutions has been investigated against various shear driven modes. Finally, in Chapter 5, summary and conclusions of the Thesis have been outlined.

-
- [1] A. A. Chernov and V. V. Yankov, Soviet Journal of Plasma Physics **8**, 522 (1982).
 - [2] D. D. Ryutov, M. S. Derzon, and M. K. Matzen, Review of Modern Physics **72**, 000167 (2000).
 - [3] M. Tabak, J. Hammer, M. E. Glinsky, W. L. Kruer, S. C. Wilks, J. Woodworth, E. M. Campbell, M. D. Perry and R. J. Mason, Phys. Plasmas **1**, 1626 (1994).
 - [4] S. Hain and P. Mulsar, Physical Review Letters **86**, 1015 (2001).
 - [5] R. Kodama, P. A. Norraeys, K. Mima, A. E. Dangor, R. G. Evans, H. Fujita, Y. Kitagawa, K. Krushelnik, T. Miyakoshi, N. Miyanga, T. Norimatsu, S. J. Rose, T. Shozaki, K. Shigemori, A. Sumahara, M. Tampo, K. A. Tanaka, Y. Toyama, T. Yamanaka, and M. Zepf, Nature (London) **412**, 798 (2001); R. Kodama, H. Shiraga, K. Shigemori, Y. Toyama, S. Fujioka, H. Azechi, H. Fujita, H. Habarat, T. Hall, Y. Izawa, T. Jitsuno, Y. Kitagawa, K. M.

- Krushelnik, K. L. Lancaster, K. Mima, K. Nagai, M. Naki, M. Nishimura, T. Norimatsu, P. A. Norreys, S. Sakabe, K. A. Tanaka, A. Youssef, M. Zepf, and T. Yamanaka, *ibid.* **418**, 933 (2002); M. H. Key, *ibid.* **412**, 775 (2001).
- [6] K. A. Tanaka, R. Kodama, K. Mima, Y. Kitagawa, H. Fujita, N. Miyanaga, K. Nagai, T. Norimatsu, T. Sato, Y. Sentoku, K. Shigemori, A. Sunahara, T. Shozaki, M. tanpo, S. Tohyama, T. Yabuuchi, J. Sheng, T. Yamanaka, P. A. Norreys, R. Evanse, M. Zepf, K. Krushelnic, A. Dangor, R. Stephens, S. Hatchett, M. Tabak, and R. Turner, *Phys. Plasmas* **10**, 1925 (2003).
- [7] S. V. Bulanov, F. Pegoraro, and A.S. Sakharov, *Phys. Fluids B* **4**, 2499 (1992).
- [8] L. I. Rudakov, and J. D. Huba, *Phys. Rev. Lett.* **89**, 095002 (2002).
- [9] K. Avinash, S. Bulanov, T. Esirkepov, P. Kaw, F. Pegoraro, P. V. Sasorov, and A. Sen, *Phys. Plasmas* **5**, 2849 (1998).
- [10] F. Califano, N. Attico, F. Pegoraro, G. Bertin, and S. V. Bulanov, *Phys. Rev. Lett.* **86**, 5293 (2001).
- [11] L. Chacon, A. N. Simakov, and A. Zocco, *Phys. Rev. Lett.* **99**, 235001 (2007).
- [12] A. Fruchtman, A. A. Ivanov, and A. S. Kingsep, *Phys. of Plasmas* **5**, 1133 (1998).
- [13] R. Shpitalnik, A. Weingarten, K. Gomberoff, Ya. Krasik, and Y. Maron, *Phys. Plasmas* **5**, 792 (1998).

- [14] M. Sarfaty, R. Shpitalnik, R. Arad, A. Weingarten, Ya. E. Krasik, A. Fruchtman, and Y. Maron, *Phys. Plasmas* **2**, 2583 (1995).
- [15] A. Teste and G. K. Perks, *Phys. Rev. Lett.* **102**, 075003 (2009).
- [16] N. Jain and S. Sharma, *Phys. Plasmas* **16**, 050704 (2009).
- [17] A. S. Kingsep, K. V. Chukbar and V. V. Yankov, in *Reviews of Plasma Physics* (Consultants Bureau, New York, 1990), Vol. 16 and references therein.
- [18] S. Sundar and A. Das, *Phys. Plasmas* **17**, 042106 (2010).
- [19] S. Chandrasekhar, *Hydrodynamic and Hydromagnetic Stability* (Dover Publications, Inc., New York, 1981).
- [20] P. G. Drazin and W. H. Reid, *Hydrodynamic Stability* (Cambridge University Press, Cambridge, London, 1982).
- [21] J. F. Drake, R. G. Kleva and M. E. Mandt, *Phys. Rev. Lett.*, **73**, 1251 (1994). D. Biskamp, E. Schwarz, and J. F. Drake, *Phys. Rev. Lett.*, **76**, 1264 (1996); J. F. Drake, D. Biskamp and A. Zeiler, *Geophysical Research Letters* **24**, 2921 (1997).
- [22] A. Das and P. Kaw, *Phys. Plasmas* **8**, 4518 (2001).
- [23] N. Jain, A. Das, P. Kaw and S. Sengupta, *Phys. Plasmas* **10**, 29 (2003).
- [24] N. Jain, A. Das and P. Kaw, *Phys. Plasmas* **11**, 4390 (2004).
- [25] N. Jain, A. Das, P. Kaw and S. Sengupta, *Phys. Letts. A* **363**, 125 (2007); N. Jain, A. Das, P. Kaw and S. Sengupta, *Phys. Plasmas* **19**, 092305 (2012).

- [26] S. Dastgeer, A. Das, P. Kaw, and P. H. Diamond, *Phys. Plasmas* **7**, 571 (2000); S. Dastgeer, A. Das, and P. Kaw, *Phys. Plasmas* **7**, 1366 (2000).
- [27] C. S. Ng, A. Bhattacharjee, K. Germaschewski, and S. Galtier, *Phys. Plasmas* **10**, 1954 (2003).
- [28] R. L. Stenzel, J. M. Urrutia, and K. D. Strohmaier, *Phys. Rev. Lett.* **99**, 265005 (2007); R. L. Stenzel, J. M. Urrutia and K. D. Strohmaier, *Phys. Rev. Lett.* **101**, 135002 (2008).
- [29] G. Ravi, S. K. Mattoo, L. M. Awasthi, and V. P. Anitha, *Phys. Plasmas* **10**, 2194 (2003).
- [30] J.P.McFadden, C. .W .Carlson, R. E. Ergun, C. C. Chaston, F. S. Mozer, M. Temerin, D. M. Klumpar, E. G. Shelley, W. K. Peterson, E. Moebius, L. Kistler, R. Elphic, R. Strangeway, C. Cattell, R. Pfaff, *Geophys. Res. Lett.* **25**, 2045 (1998); G. Parks, L. J. Chen, M. Fillingim, M. McCarthy, *Space Sci. Rev.* **95**, 237 (2001).
- [31] R. Treumann and T. Terasawa, *Space Sci. Rev.* **99**, 135 (2001).
- [32] J. Arons, in *General Relativistic Polar Particle Acceleration and Pulsar Death* (Universal Academy Press, Tokyo, 1998), p. 339.
- [33] V. S. Lukin, *Phys. Plasmas*, **16**, 122105 (2009).
- [34] M. B. Isichenko, and A. N. Marnachev, *Sov. Phys. JETP* **66**, 702 (1987).
- [35] A. Das, *Plasma Phys. Control. Fusion* **41** A531 (1999).

- [36] S. Dastgeer (2000), *Coherent, Nonlinear and Turbulence Phenomena in Electron Magnetohydrodynamics Systems*: PhD Thesis, Institute for Plasma Research, Bhat, Gandhinagar - 382428, India
- [37] S. K. Yadav, A. Das and P. Kaw, Phys. Plasmas **15**, 062308 (2008).
- [38] S. K. Yadav, A. Das, P. Kaw and S. Sengupta Phys. Plasmas **16**, 040701 (2009).
- [39] S. I. Vainshtein, S. M. Chitre, and A. V. Olinto, Phys. Rev. E **61**, 4422 (2000).
- [40] M. Rheinhardt and U. Geppert, Phys. Rev. Lett. **88**, 1000103 (2002).
- [41] A. S. Sandhu, A. K. Dharmadhikari, P. P . Rajeev, G. R. Kumar, S. Sengupta, A. Das and P. K. Kaw,
- [42] S. K. Yadav and Amita Das, Phys. Plasmas **17**, 052306 (2010).

List of Figures

- 1.1 The schematic describes tearing and bending modes depending upon the orientation of perturbations relative to one dimensional equilibrium magnetic field $B_0(x)\hat{y}$. This magnetic field is created by an equilibrium electron flow $v_0(x)\hat{z}$ sheared along x direction. Perturbations lying in the vertical plane, containing magnetic field with a null-line, give rise to tearing instability. When the angle of perturbations is changed to lie in the horizontal plane of shear and flow, the instability changes from tearing type to bending type. Both the instabilities are driven by velocity shear or equivalently, current shear in system where electron dynamical response is only of relevance. 25
- 2.1 The plot of growth rate vs. $k_z\epsilon$ for the hydrodynamic case (thick curve). The growth rate has been obtained for a shear flow profile $v_0 = V_0 \tanh(x/\epsilon)$. The curve for the hydrodynamic case is universal for the choice of $\epsilon = 0.1f$ and $V_0 = 1.0f$. The curves with dots, circles and stars show the growth rate for an EMHD system for $f = 1, 3, 5$ respectively. 52

2.2	A schematic showing the flow configuration after KH destabilization in 2D. It can be seen that the destabilized flow configuration results in a sheared flow orthogonal to the original shear flow, with a shear width given by k_z^{-1} .	54
2.3	The growth rate (solid line) and the real frequency (dashed line) for the KH mode as a function of the in-plane magnetic field B_0 for a step electron velocity profile.	58
2.4	The KH growth rate as a function of $k_z\epsilon$ for a tangent hyperbolic shear flow profile. Here the solid, dotted and the curve with circles correspond to $B_0 = 0, 0.5$ and 1.0 respectively.	60
2.5	The evolution of perturbed energy for $B_0 = 0, 0.5, 1.0$ in subplots (a), (b) and (c) respectively.	62
2.6	Contour plots for the field b at various times for the nonlinear simulation of $B_0 = 0.0$ case.	63
2.7	Contour plots for the field b at various times for the nonlinear simulation of $B_0 = 1.0$ case.	64
2.8	Contour plots for the field $\tilde{\psi}$ at various times for the nonlinear simulation of $B_0 = 0.0$ case.	65
2.9	Contour plots for the field $\tilde{\psi}$ at various times for the nonlinear simulation of $B_0 = 1.0$ case.	66
2.10	The evolution of mean square wavenumbers for the b and ψ fields in the x and z directions.	67
2.11	The plot of z averaged electron flow velocity profile at various times for $B_0 = 0$ and $B_0 = 1$ in subplot (a) and subplot(b) respectively.	68

3.1	A schematic diagram showing the pure sausage (subplot (a)) and pure kink (subplot (b)) perturbations.	73
3.2	The subplot (a) shows the surface plot of the growth rate for the tangent hyperbolic velocity shear profile $\vec{v}_0(x) = \hat{z}V_0 \tanh(x/\epsilon)$ as a function of $k_z\epsilon$ and $k_y\epsilon$ for $B_{00} = 0$ and $C_0 = 0$. For this case $V_0 = 1.0$ and $\epsilon = 0.3$. In subplot (b) of the figure the same data for growth rate has been shown as a function of $k_z\epsilon$. The various curves show different values of k_y . For this case the kink growth rate for $k_y = 2, k_z = 0$ (equal to 0.52) is almost identical to the maximum growth rate of the sausage mode at $k_z\epsilon = 0.5, k_y = 0$ (equal to 0.54).	80
3.3	The subplot (a) shows the surface plot of the growth rate for the tangent hyperbolic velocity shear profile $\vec{v}_0(x) = \hat{z}V_0 \tanh(x/\epsilon)$ as a function of $k_z\epsilon$ and $k_y\epsilon$ for $B_{00} = 0$ and $C_0 = 0$. For this case $V_0 = 1.0$ and $\epsilon = 0.5$. In subplot (b) of the figure the same data for growth rate has been shown as a function of $k_z\epsilon$. The various curves show different values of k_y . For this case the kink growth rate for $k_y = 2, k_z = 0$ (equal to 0.43) is higher than the maximum growth rate of the sausage mode at $k_z\epsilon = 0.5, k_y = 0$ (equal to 0.27). The pure kink mode clearly dominates for this case.	81
3.4	Plot of the eigen functions of pure sausage mode ($k_y = 0$). The other parameter values are $V_0 = 1.0, \epsilon = 0.3, k_z = 1.7, B_{00} = 0.0$ and $C_0 = 0.0$	82
3.5	Plot of the eigen functions of pure kink mode ($k_z = 0$). The other parameter values are $V_0 = 1.0, \epsilon = 0.3, k_y = 2.0, B_{00} = 0.0$ and $C_0 = 0.0$	82

3.6	Variation of growth rate with $k_z\epsilon$ for different values of uniform magnetic field B_{00} along flow direction. The various parameters for this case are $V_0 = 1.0$, $C_0 = 0$, $\epsilon = 0.3$ and $k_y = 0.4$. The growth rate decreases as the value of B_{00} increases.	83
3.7	Variation of growth rate as a function of $k_z\epsilon$ for the case $B_{00} = 1.0$ with $V_0 = 1.0$, $C_0 = 0$ and $\epsilon = 0.3$. The various curves correspond to different values of k_y . For this case the kink growth rate for $k_y = 2, k_z = 0$ (equal to 0.52) is higher than the maximum growth rate of the sausage mode at $k_z\epsilon = 0.5, k_y = 0$ (equal to 0.39). The pure kink mode clearly dominates in this case.	84
3.8	The variation of growth rate as a function of $k_y\epsilon$ has been shown in subplot (a) for $k_z = 0$ <i>i.e.</i> pure kink modes and in subplot (b) for the value of $k_z = 1.7$. The different curves correspond to the different values of C_0 in two subplots. The other parameters are $V_0 = 1.0$, $B_{00} = 0$ and $\epsilon = 0.3$. It is clear from the two subplots that as the value of C_0 is increased the growth rate of kink consistently drops down whereas the pure sausage growth rate is not influenced by this field.	85

- 3.9 The evolution of perturbed energy with $V_0 = 1.0$, $C_0 = 0$ and $\epsilon = 0.3$ for $B_{00} = 0.0$ and $B_{00} = 1.0$ has been shown in subplots (a) and (b) respectively. The dashed lines shown alongside are having the slope equal to $2\gamma_i$, where γ_i is the growth rate of the maximally growing mode in the system. In subplot (a) the slope corresponds to growth rate of pure sausage mode (with $\gamma_i = 0.54$) whereas, in subplot (b) the slope corresponds to the growth rate of pure kink mode (with $\gamma_i = 0.52$) which is the maximally growing mode in the system for this case. 86
- 3.10 The evolution of perturbed energy with $V_0 = 1.0$, $C_0 = 0$ and $\epsilon = 0.1$ for $B_{00} = 0.0$ and $B_{00} = 1.0$ has been shown in subplots (a) and (b) respectively. The dashed lines shown alongside are having the slope equal to $2\gamma_i$, where γ_i is the growth rate of the maximally growing mode in the system. For two cases the values of γ_i are equal to 1.85 and 1.78 for subplots (a) and (b) respectively. The maximally growing mode for two cases is pure sausage mode. 87
- 3.11 The evolution of perturbed energy with $V_0 = 1.0$, $C_0 = 1.0$ and $\epsilon = 0.3$ for $B_{00} = 0.0$ and $B_{00} = 1.0$ has been shown in subplots (a) and (b) respectively. The dashed lines shown alongside are having the slope equal to $2\gamma_i$, where γ_i is the growth rate of the maximally growing mode in the system. For two cases the values of γ_i are equal to 0.54 and 0.39 for subplots (a) and (b) respectively. Here again the maximally growing mode for two cases is pure sausage mode. . . 88

3.12	The plot of averaged electron flow velocity profile at various times for $B_{00} = 0.0$ and $B_{00} = 1.0$ in subplots (a) and (b) respectively. The values of the other parameters have been chosen to be same as in Fig. 3.9. The flattening of shear profile is weaker for finite B_{00} case.	89
3.13	Evolution of average wave-numbers in different directions for $B_{00} = 0.0$. The values of the other parameters have been chosen to be same as in Fig. 3.9.	90
3.14	Evolution of average wave-numbers in three different directions has been shown in three different subplots in comparison for two cases $B_{00} = 0.0$ and $B_{00} = 1.0$. The values of the other parameters have been chosen to be same as in Fig. 3.9.	91
4.1	Representation of EMHD monopolar and dipolar solutions in the form of current pulses. Subplots (a) and (d) show the forms of typical monopole and dipole as lying in $x - z$ plane. The corresponding magnetic field and flow profiles are shown in subplots below to them (see subplots (b), (c) for monopole and subplots (e), (f) for dipole). Here, using the Maxwell's relation, the flow velocity is related to magnetic field as $v_0 = -dB_0/dx$. In subplots (c) and (e) we see that there are the regions of in flow and out flow that make the configuration as the sheared flow configuration.	97
4.2	The constant magnetic field contours of the monopole have been shown at various times in the $x - y$ plane.	102
4.3	The constant magnetic field contours of the monopole have been shown at various times in the $x - z$ plane. These times are similar to those of the subplots of Fig. 4.2.	103

- 4.4 The subplots show the plots of the magnetic field lines in the $x - y$ plane for $z = 0.0, 1.87, 3.68, 5.5, -2.06$ and 0.35 corresponding to times $t = 0.0, 359.561, 859.561, 1859.56, 3109.5$ and 4859.45 respectively. The z location at these times correspond to the location of the mid plane of the dipole structure as it propagates. The magnetic field lines which are initially straight as there is no dependence of equilibrium on y later due to the kink instability acquire y dependence. 104
- 4.5 The constant magnetic field contours of the dipole have been shown at various times in the $x - z$ plane. These times are similar to those of the subplots of Fig. 4.4. 105

Chapter 1

Introduction

The present thesis is devoted to the study of the current shear driven instabilities in plasmas in the context of Electron Magnetohydrodynamics (EMHD). This Chapter provides the objective and motivation for the studies compiled in the thesis. The EMHD model, a review of earlier work and plan of the thesis are also presented in this Chapter.

1.1 Objective and Motivation

Stability of sheared electron current configurations is a long standing topic in theoretical plasma physics. The typical sheared configurations of electron current are found to occur in many physical situations like, fast z-pinches [1, 2], fast ignition phenomena of laser fusion [3, 4, 5, 6], collisionless magnetic reconnections [7, 8, 9, 10, 11, 12, 13, 14, 15, 16, 17, 18, 19, 20], plasma opening devices [21, 22, 23], inter planetary current-carrying plasmas [24, 25] etc. These current configurations having equilibrium length scale smaller than the ion skin depth are amenable to various instabilities. These instabilities lead to the evolution of the current

Chapter 1: Introduction

configurations, sometimes to the point of complete destruction.

The equilibrium sheared electron current configurations are the characteristics of low density plasmas in which the current flows faster than the Alfvén velocity, where the Magnetohydrodynamic (MHD) model [26, 27, 28] is not applicable. In this scenario, we can ignore the ion dynamics and use a simplified Electron Magnetohydrodynamic (EMHD) model of plasmas in which the overall dynamics is governed by the motion of electron species only [29, 30, 31]. We shall provide description of EMHD model in the next section of this Chapter. The instabilities of current configurations considered here, are inertial scale instabilities driven by the gradient in equilibrium current in dissipation less, homogeneous plasma density regime. In EMHD, these current- gradient driven instabilities have been previously considered by Califano et al. [32], where they have been broadly categorized as tearing and bending instabilities. The first type of instability is the collisionless tearing instability [7, 33] of thin current-sheets which leads to the reconnection of magnetic field lines due to the effect of electron inertia. While, the second type of instability bends the flow lines and leads to the vortex structures. The mode has also been identified as the sausage mode [34]. Classification of these instabilities can be understood from Fig. 1.1.

Apart from these instabilities, a non-tearing, inertial scale instability is known which also falls in the category of current-gradient driven instabilities [35]. This mode is driven by perturbations similar to tearing mode [Fig. 1.1], but unlike the tearing mode it is a local mode and does not require reversed equilibrium magnetic field configuration. We depict this mode as kink mode. In our studies here, we focus only on the bending instability and the kink mode instability.

We note here that in EMHD, the electron flow velocity and the current velocity

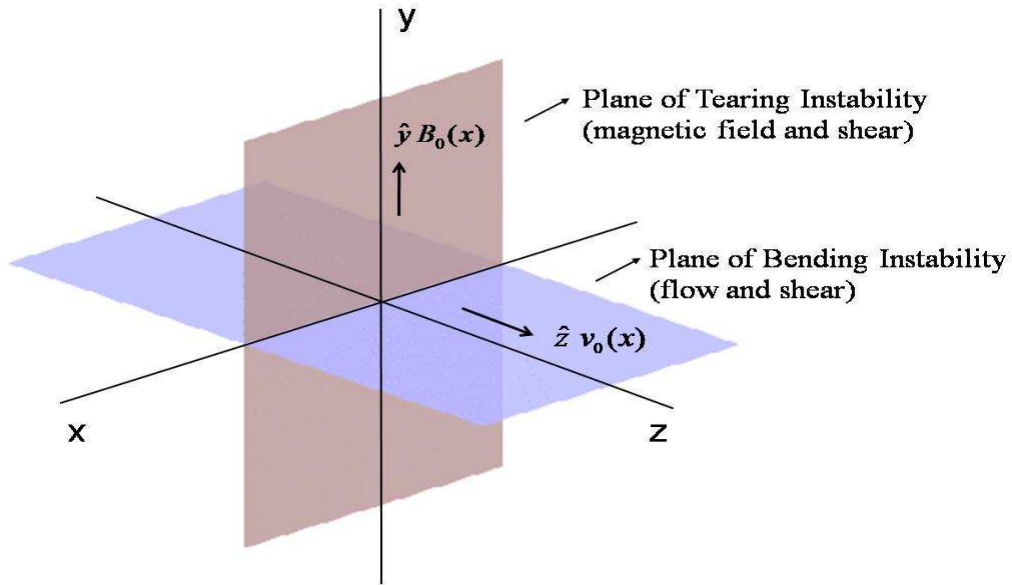


Figure 1.1: The schematic describes tearing and bending modes depending upon the orientation of perturbations relative to one dimensional equilibrium magnetic field $B_0(x)\hat{y}$. This magnetic field is created by an equilibrium electron flow $v_0(x)\hat{z}$ sheared along x direction. Perturbations lying in the vertical plane, containing magnetic field with a null-line, give rise to tearing instability. When the angle of perturbations is changed to lie in the horizontal plane of shear and flow, the instability changes from tearing type to bending type. Both the instabilities are driven by velocity shear or equivalently, current shear in system where electron dynamical response is only of relevance.

are same as the ions merely provide a stationary neutralizing background. In conventional MHD, the two are different. In view of this fact, the current gradient driven bending instability is similar to the velocity shear driven Kelvin Helmholtz (KH) instability of the electron fluid and vice versa. The KH instability destabilizes the interface of two fluids in relative motion. The development of instability may lead to turbulence, transport of energy and momentum and dissipation and mixing of fluids. The instability has been thoroughly discussed in literature for ordinary

Chapter 1: Introduction

hydrodynamic (HD) fluid [36, 37, 38] and MHD fluid [37, 39, 40, 41, 42]. The studies on KH instability in the context of EMHD have been presented by several researchers [34, 43, 44, 45, 46, 47, 48]. Many important features of the instability have been reported in these studies. In this thesis, we explore the instability further under certain additional considerations, which we shall discuss, in the later part of the thesis, after providing sufficient background.

1.2 Electron Magnetohydrodynamic (EMHD) Model

We provide here a discussion on the EMHD model which has been employed for our studies. First, we discuss the model in brief and its applicability to various phenomena of plasma physics. And then we discuss some of its aspects, relevant to the studies carried out in the thesis.

1.2.1 Brief Description of Model and Its Applicability

The EMHD model is a single fluid description of plasmas which considers electrons as the only species in motion and magnetized [29, 30]. In EMHD model, an incompressible electron fluid is considered to be flowing against static, neutralizing background of ions. The time scales are so fast that the inertial and magnetized response of ions are ignored and the overall dynamics is governed by the motion of electrons only. Thus, the model is valid only when the characteristic frequencies are large compared to the ion plasma frequency and gyro frequency, and are small compared to the electron plasma and gyro frequencies. The frequency range reads as follows:

$$\omega_{pi}, \omega_{ci} \ll \omega \ll \omega_{pe}, \omega_{ce}$$

Chapter 1: Introduction

Here, $\omega_{pj} = (4\pi ne^2/m_j)$ are ion plasma frequency and electron plasma frequency for $j = i, e$; respectively. Similarly, $\omega_{cj}(= eB/m_jc)$ are the gyro frequencies for ion and electron; m_j are the mass for two species, c in the speed of light, n and B are the typical values of plasma density and magnetic field respectively. Since the ion dynamics is completely ignored, one needs to deal with electron fluid equations only along with the Maxwell's equations to derive the EMHD equations. In our studies, electrons have been treated as a cold, incompressible electron fluid of uniform density. In the cold fluid (plasma) description, effects due to thermal motion of particles are neglected. This is valid when the phase velocities are much larger than the thermal velocities of particles. In this situation, the corresponding velocity distribution function may be approximately a Dirac delta function centered at the macroscopic fluid velocity.

In EMHD, displacement current term is also ignored under the assumption $\omega \ll \omega_{pe}, \omega_{pe}^2/\omega_{ce}$ which in turn gives an upper limit on characteristic frequencies. Under this assumption, the density perturbations in electron fluid can be discarded. The modified inequality can then be framed as,

$$\omega_{pi}, \omega_{ci} \ll \omega \ll \min(\omega_{pe}, \omega_{pe}^2/\omega_{ce})$$

In terms of spatial scales, the EMHD model is applicable to the scales which are shorter than the ion inertial scales and also the gyro-radius of ions. The spatial scales may fall below the electron inertial scale (skin depth) but remain larger than the Debye radius λ_D . Also, EMHD being a fluid description, the kinetic scales (particle orbit size of larmor radius) determine the lower bound of the length scale below which the model is again not applicable.

Since ions are stationary, the electron flow velocity \vec{v} is directly related to

Chapter 1: Introduction

current as, $\vec{J} = -ne\vec{v}$. In view of this definition and the assumptions discussed so far, the coupled fluid-Maxwell's equations lead to EMHD equations after some algebraic manipulations. The EMHD model for collisionless, homogeneous plasma is cast in terms of dimensionless equations, as follows¹,

$$\frac{\partial}{\partial t}(\nabla^2 \vec{B} - \vec{B}) = \vec{\nabla} \times [\vec{v} \times (\nabla^2 \vec{B} - \vec{B})] \quad (1.1)$$

$$\vec{v} = -\vec{\nabla} \times \vec{B} \quad (1.2)$$

Here, length has been normalized by electron skin depth $d_e (= c/\omega_{pe})$, magnetic field with some arbitrary value B_{00} , time with inverse of gyro frequency $\omega_{ce} (= eB_{00}/mc)$, and velocity field with electron Alfvén speed $\omega_{ce}d_e$. All the symbols retain their meanings described as earlier. The first equation is the evolution of the generalized vorticity $\Omega (= \nabla^2 \vec{B} - \vec{B})$ which implies that generalized vorticity is tied to the fluid flow, unlike the MHD, where it is magnetic field which is tied to the flow of fluid (plasma). The second equation is Ampere's relation, ignoring the displacement current, which relates the flow velocity to the magnetic field. In contrast to this, in MHD, flow velocity is related to magnetic field by an evolution equation.

The prescribed length and time scale windows of EMHD make the model applicable to physical systems comprising the fast time and short length scales like, astrophysical plasmas, earth's magnetosphere, and laboratory plasmas. The EMHD model has added much to the basic understanding of the phenomena of collisionless magnetic reconnection [8, 9, 7, 10, 11, 12, 13, 14], generation of large scale magnetic field, and rapid dissipation of magnetic field energy in the context of astrophysical

¹The thesis does not contain the mathematical derivation of EMHD model. For complete derivation of three dimensional EMHD equations and their reduction in two dimensions, reader may look into Refs. [48] and [56].

Chapter 1: Introduction

plasmas [49, 50]. The description of earth's plasma sheet and magneto tail region are other areas where the EMHD model has been applied [24, 25]. The model is further exploited to explain the anomalous stopping of energetic electrons in the fast ignition inertial confinement fusion scheme [47].

1.2.2 Natural Scales in EMHD

EMHD systems, unlike the ordinary hydrodynamic fluid systems, contain intrinsic length and time scales associated to the magnetized character of electron fluid. We discuss them as below.

Natural length scale: The EMHD systems contain the electron skin depth as the intrinsic length scale. This is defined as $d_e = c/\omega_{pe}$, where, c is the speed of light and ω_{pe} is the frequency of electron oscillations. The value of skin depth is finite if the mass of electron is finite. In the inertia less electron limit, the value of $d_e \rightarrow 0$ and in the case of neutral fluid $d_e \rightarrow \infty$. Owing to the presence of this intrinsic length scale, EMHD equations identify distinct spatial scale length regime *viz.* $kd_e \gg 1$ (hydrodynamic limit) and $kd_e \ll 1$ (magnetized fluid limit). In the first limit, the inertial terms dominate the electromagnetic force terms in the electron momentum equation and the system behaves hydrodynamically. In the other limit, the electromagnetic force terms dominate the inertial terms and the electromagnetic character of the electron fluid becomes important.

Natural time scale: In the presence of magnetic field, EMHD equations permit whistler waves as the normal excitation mode. This wave requires a finite component of the wave vector along the magnetic field. Whistler is a transverse circularly polarized electromagnetic wave. These waves are analogous to Alfvén waves in MHD, but unlike the Alfvén waves, are dispersive in nature. The natural time

Chapter 1: Introduction

scale in EMHD is associated to the time period of Whistler waves.

These natural scales have many interesting roles to play on various EMHD phenomena, some of those we discuss in this thesis. Role of these natural scales on velocity shear driven Kelvin Helmholtz (KH) instability has been studied as a major part of thesis work.

1.2.3 Nonlinear Solutions of EMHD

The EMHD system of equations closely resembles the ordinary HD fluid and hence is susceptible to the characteristic instabilities of ordinary HD, e.g., Kelvin-Helmholtz instability, Rayleigh-Taylor instability etc. The nonlinear features of ordinary HD fluids like, turbulence generation and coherent pattern formation are also displayed by EMHD systems. In a 2D system the conservation of energy and enstrophy leads to the process of inverse cascade by virtue of which coherent patterns are formed. The coherent structures have major role to play in determining the transport properties of a system. They are also believed to cause the intermittency in turbulence phenomena.

Coherent, nonlinear solutions of EMHD: In EMHD, the coherent structures manifest themselves in the form of magnetic islands, current sheets, vortices etc., and are found to be excited in various processes e.g., magnetic reconnections, Weibel instability, in laser plasma interaction studies, in tokamak plasmas during electron cyclotron resonant heating (ECRH) and laboratory experiments. Coherent structures can be best understood by finding the exact solutions of nonlinear equations. These solutions were obtained by Isichenko et al. [51] as localized vortices for 2D EMHD system. The vortices are stationary monopoles and traveling dipoles. Isichenko et al. obtained the analytical conditions for these solutions and also

studied their stability. The solutions being very robust and stable have important applications specially, the dipole solutions. The solutions contain the regions in which the electron current is significantly sheared. It is, therefore, of importance to know if these structures are susceptible to shear driven instability processes. We address this question in the thesis.

1.3 A Review of Earlier Work on Shear Driven Instabilities in EMHD Domain

The studies on shear driven instabilities in EMHD regime have a very rich literature. We present, in this section, some of the prominent work in this area relevant to the work carried out in the thesis.

Drake et al. [43, 44] have studied the stability of the current layers narrower than the ion skin depth. A dispersion relation was derived, which shows that the cross field gradient in current is required to drive the instability. It was also shown that for $\epsilon \leq d_e$, the KH instability is dominant over kink instability while for $\epsilon > d_e$, KH mode is stable and dominant instability is the kink instability. Here, ϵ is the shear width of current layer and d_e is the collisionless electron skin depth. In the 3D electromagnetic fluid simulations, the current layer breaks and evolves to a strongly turbulent nonlinear phase. Bulanov et al. have shown the KH instability of electron fluid vortices in their PIC simulation studies [52]. They have shown the existence of magnetic vortices in the electron fluid generated in the wake of an ultrashort, ultraintense laser pulse interacting with an underdense plasma. These vortices are unstable to the electron KH instability if the separation between two neighboring vortices is smaller than the electron skin depth. When the distance

Chapter 1: Introduction

between the vortices is larger than the electron skin depth, the instability becomes exponentially slow. The studies by Drake et al. and Bulanov et al., however, are incomplete. Drake et al. have derived just an approximate local dispersion relation which highlights very limited features of the kink instability. Moreover, in nonlinear fluid simulations, only the widening of shear layer has been reported and no discussion has been provided on issues like, saturation mechanism of instability, modification of mean flow profile, characterization of turbulence etc. In the work of Bulanov et al, the form of initial shear flow structure is not specific. Also, the saturation mechanism of sausage instability were discussed very qualitatively. We focus on some of these issues in our studies.

Das et al. [34] have carried out a systematic and detailed analytical study on sausage-like instability of electron current channels. In the local analysis of EMHD equations the configuration was found to be stable for sausage-like perturbations. In the nonlocal analysis, they have derived the dispersion relation for two choices of sheared flow profile: a step-function profile (zero shear width) and a piece-wise linear profile (finite shear width). In the short wavelength limit, the instability is essentially the KH instability of hydrodynamic fluid. However, in the long wavelength limit, the instability has growth rate substantially different from hydro fluids due to the magnetized character of electron fluid. The underlying physical mechanism for instability and hence the differences in two cases of MHD and EMHD was also discussed. Later, Jain et al. [45, 46, 47] carried out extensive numerical work on the sausage and kink instabilities in EMHD. Their studies can be summarized as follows. The development of sausage like structures is seen in 2D fluid simulations with growth rate agreeing with linear theory. The nonlinear state is found to be coherent due to the presence of two non-dissipative square

Chapter 1: Introduction

invariants namely, enstrophy and energy. The unstable modes cause the flattening of equilibrium shear profile and hence the directed electron flow is reduced which is related to the loss of electron kinetic energy. However, the reduction is not very efficient because the instability saturates easily. The saturation of instability can occur either by getting rid of curvature in equilibrium flow profile or by violating the instability criteria $k_z \epsilon_{eff} < 1$. Here, k_z is the wave vector along the flow and ϵ_{eff} is the increased effective shear width due to the back reaction of instability. The full three dimensional analysis shows that the instability criteria is much more relaxed. Unlike the 2D case, the local modes are also unstable and the instability is driven by the gradient rather than the curvature in equilibrium flow profile. Owing to the increased number of unstable modes and absence of two non-dissipative square invariants, the nonlinear evolution of instability leads to the turbulent state in 3D fluid simulations. The generation of turbulence leads to much more efficient reduction in directed flow of electrons. The relevance of these studies was shown in anomalous stopping of inward energetic electrons in fast ignition. The studies by Das et al. and Jain et al. are extensive and cover many important linear and nonlinear features of the shear driven instability. In our thesis, we further explore the instability in 2D and 3D under certain additional considerations. We shall discuss this in detail in the next section.

Califano et al. [32] have studied the linear dispersion equations and eigen structures of high frequency tearing-bending instabilities. These instabilities are driven by the electron current gradient in an inhomogeneous magnetic field of the tangent hyperbolic type. As the angle between the direction of propagation of perturbations and the inhomogeneous magnetic field lines is varied, perturbations change from tearing type (parallel propagation) to bending type (perpendicular propaga-

Chapter 1: Introduction

tion). The tearing instability acts across the magnetic null line and forms the chain of magnetic islands. However, the bending instability is similar to KH instability which bends the flow lines. At oblique propagation the tearing branch develops asymmetric magnetic island and complex velocity patterns with channel-like structure. A similar channel-like structure is seen in the bending instability at oblique propagation. The tearing instability appears to be dominant in equilibrium configuration with spatial scale-lengths longer than the skin depth. For shorter equilibrium scale-length, the tearing and bending branches have comparable growth rates. Lukin [35] has described a non-tearing inertial scale instability which does not fall in the category of the tearing-bending instabilities. But, the energy source of this instability also is the background current density gradient. It is a local mode with perturbations similar to tearing mode i.e., $\mathbf{k} \parallel \mathbf{B}_0 \perp \mathbf{J}_0$, and requires no background magnetic field reversal unlike the tearing mode. Here, \mathbf{k} is the wave vector of perturbations, \mathbf{B}_0 is the equilibrium magnetic field and \mathbf{J}_0 is the equilibrium current. An approximate analytical derivation of dispersion relation for the instability was obtained. Further, from quasilinear numerical calculations, the magnitude of the highest growth rate was shown to be independent of electron skin depth d_e and wave number k and to depend solely on the particular profile of $B_0(x)$, as long as $d_e^2 B_0''/B_0 \gg 1$. The occurrence of these modes has been shown in magnetic reconnection phenomena via simulations where the instability manifests itself as localized structures at the outflow side of magnetic separatrix. The tearing-bending modes and the non-tearing kink mode were also described earlier in section 1.1. The geometries can be understood from Fig. 1.1.

In EMHD, the electron flow shear driven instability has been identified as both the velocity shear driven KH instability and current- gradient driven sausage and

Chapter 1: Introduction

kink modes. This is because the electron flow velocity is related to the current as, $\vec{J} = -nev\vec{v}$. The gradient in current can be generated due to velocity shear or density gradient. However, Sita et al. [53] have shown that the free energy source for the flow shear driven KH like instability is the kinetic energy of the electron flow. The density gradient can not relax in a cold, collisionless plasma so there is no free energy available to excite the instability. Thus, the presence of current gradient due to density gradient alone is unable to excite the instability. We note here that in our studies, in homogeneous plasma (electron fluid) density limit, the current gradient driven bending instability is essentially the velocity shear driven KH instability.

Sharad et al. [54] have studied the KH destabilization of current pulses of finite extent formed at the density inhomogeneity layer. The instability leads to the coherent nonlinear state consisting of the circular vortices aligned along the contours of density profile. The vortices of alternating sign are arranged one after the other like beads in a wire. The current pulses considered in these studies are traveling dipole solution of EMHD obtained by Isichenko et al. [51]. These solutions are stable against sausage mode and propagate robustly in a homogeneous plasma medium [55, 56]. An understanding of stability of these current pulses to kink instability so far, is lacking.

1.4 Scope of the Thesis

The work presented in thesis focuses on the study of KH instability using EMHD model. As discussed already, unlike the hydrodynamic fluid model, the EMHD model contains natural length and time scales viz., electron skin depth and whistler time period respectively. Owing to the existence of natural scales, electron KH

Chapter 1: Introduction

may suffer major modifications from the KH instability in neutral fluid. In this thesis, we investigate the role of natural scales of EMHD on KH instability. Earlier studies, as reviewed in the last section, do not highlight this feature of instability.

In earlier 2D studies, the equilibrium as well as perturbed magnetic fields were directed along the symmetry direction. Hence, whistlers were clearly not supported. Whistler modes were supported in 3D studies. In those studies, however, the propagation direction of whistlers was orthogonal to the 2D plane in which KH action primarily takes place. To study the role of whistlers, we introduce a uniform external magnetic field along the flow direction (in the plane of KH). These studies would have relevance in ionosphere and magnetosphere, solar corona and pulsars [57, 58, 59] etc., where the counter streaming electron beams immersed in a magnetic field may exist. This kind of configuration is also quite likely in laboratory experiments [60, 61] where the plasma is confined with the help of an axial magnetic field.

In MHD, a uniform magnetic field parallel to flow is known to stabilize the fluid interface against the KH instability and it is ascribed to the tension generated to bend the magnetic field [37, 41, 62]. The reduction in growth rate is a function of field strength. The instability is fully suppressed if the Alfvén velocity exceeds the total velocity jump across the shear layer. Whistlers are the normal oscillatory mode of EMHD akin to Alfvén modes in MHD. One expects that oscillations set up at whistler time scale would give similar effects on instability as Alfvén modes do in MHD. The presence of magnetic field also largely affects the nonlinear evolution of instability in MHD [42, 63, 64, 65, 66, 67, 68]. Even a weak magnetic field potentially changes the nonlinear state. The magnetic field caught in vortices formed due to KH instability gets amplified and then relaxes through the process

Chapter 1: Introduction

of magnetic reconnections [66, 67]. Magnetic reconnection leads to the disruption of flow vortex. Once the vortex is destroyed, the flow relaxes into a broadened, laminar and marginally stable shear layer. In even weaker (very weak) field case the magnetic reconnection leads primarily to the expulsion of field line from inside the vortex and to enhance the dissipation of kinetic energy. This is well known flux expulsion phenomena [69]. We also try to understand the nonlinear phase of EMHD instability in the presence of in-plane magnetic field.

Earlier studies on EMHD KH instability show that in 3D regime kink mode is also present in addition to the KH mode [46]. The kink mode lies in the plane of magnetic field and shear and unlike the KH mode it is a local mode. We investigate the interplay of the two modes, KH and kink, with and without external magnetic field in a considerable detail. In 3D, the evolution of shear driven instabilities leads to the self consistent generation of turbulence in the nonlinear state [43, 47]. The generation of electromagnetic turbulence due to the action of shear driven instabilities has been shown to have important implications. This leads to the anomalous stopping of energetic electrons moving towards core in Fast Ignition, which are known to eventually create the ignition spot by dumping their energy to the core [47]. Also, in collisionless magnetic reconnections [43], the generation of turbulence may alter the mechanism by which the frozen in field condition breaks in the dissipative regime. The reconnections may also be facilitated by the anomalous viscosity and anomalous resistivity associated to the turbulence generation. In our thesis, we analyze the spectral cascade features of the turbulence generated in three dimensional simulations, with and without an external magnetic field along the flow direction. The nonlinear cascade develops the anisotropy mediated by the normal oscillatory modes; Alfvén in MHD [70, 71] and whistlers in EMHD

Chapter 1: Introduction

[72, 73]. In view of this, nonlinear cascade is expected to show the anisotropy in the presence of whistlers; which we have quantified.

We also address in this thesis, the question of stability of coherent nonlinear solutions of the EMHD equations from the perspective of the aforementioned modes, KH and kink. Isichenko et al. [51] obtained exact, nonlinear solutions of two dimensional EMHD equations in the form of localized rotating electron currents, giving rise to monopolar and dipolar magnetic field. These solutions have regions where electron flow velocity/current is significantly sheared and hence can be susceptible to the flow shear driven instabilities. These solutions were shown to be very robust and stable against the sausage instability, in the earlier 2D studies [55, 56, 54]. In these studies, the kink mode was not supported, and hence the stability of the solutions against this mode has remained unknown. We make an attempt to investigate this issue in the present thesis.

The scope of the thesis can be summarized as follows. We discuss the role of natural length and time scale on KH instability, in Chapter 2. The interplay of KH and kink modes under various physical conditions is discussed in Chapter 3. In Chapter 4, shear driven KH and kink modes are investigated for Isichenko solutions.

1.5 Summary of Chapters

The Chapter-wise summary of the thesis is given below.

Chapter 2: Role of Natural Length and Time Scales on Electron Magnetohydrodynamic Kelvin Helmholtz Instability: 2D Studies

In Chapter 2, we investigate the role of natural scales on velocity shear driven KH instability in the context of 2D EMHD. The perturbations lie in the plane of flow and shear, in which the major action of KH lies, variations along the equilibrium magnetic field are neglected. The role of electron skin depth has been discussed in comparison with the KH instability of neutral hydrodynamics fluid. To understand the role of whistlers we introduce a uniform external magnetic field B_0 along the flow direction. Presence of this magnetic field excites the whistlers in the system, unlike the previous 2D studies [34, 45]. In those studies, a single equation describing the evolution of the magnetic field component along the symmetry direction was sufficient to describe the instability. But here, we need to solve a set of coupled equations in two scalar fields. This is essentially due to the fact that whistler waves couple the in-plane magnetic field perturbations to the magnetic perturbations along the symmetry direction. The instability problem is solved as the eigen value problem analytically, for step profile and numerically, for *tanh* profile of equilibrium flow velocity. The eigen values are obtained as the growth rate of instability. The role of B_0 has been to reduce the instability growth rate. Further, the growth rate curves show that the instability is nonlocal even in the presence of in-plane magnetic field B_0 .

Nonlinear simulations have been carried out to understand the role of whistlers in the nonlinear regime of instability. For this purpose we have developed a nonlinear fluid code which uses flux corrected transport algorithm [74, 75]. The code

Chapter 1: Introduction

solves 2D EMHD equations for tangent hyperbolic profile of equilibrium velocity. In the absence of B_0 , the nonlinear state is a coherent vortex formed as a consequence of inverse cascade. However, in the presence of B_0 , the nonlinear state is significantly changed from the ordered state of $B_0 = 0$ case. The long scale structures are formed only along the direction of B_0 and there is hardly any extension in structures along the transverse direction. This induces the anisotropy in the system. We provide a quantitative estimate of anisotropy in the Fourier spectrum of two fields. The observed anisotropy is a characteristics of the nonlinear cascade mediated by whistlers. The anisotropic cascade has an adverse effect on the KH instability induced mixing of the fluids flowing in two directions around the shear layer. Consequently, the flattening of shear layer is weaker in the presence of whistlers, which we have also measured.

Chapter 3: Interplay of Kelvin Helmholtz and Kink Modes: 3D Studies

When the variations along the direction of self-consistent equilibrium magnetic field (generated due to sheared flow) are also allowed, a new local mode exists in the plane of the magnetic field and shear. The mode requires finite electron inertia and is driven by the gradient in the equilibrium velocity unlike the KH mode which is driven by the curvature in equilibrium velocity. We note that due to similarity in current and flow velocity in EMHD, velocity shear driven KH is often termed as the current-gradient sausage mode. In Chapter 3, we investigate the interplay of the two modes, sausage and kink, under various physical conditions determined by: (a) the value of shear width in comparison to the electron skin depth, (b) a uniform magnetic field (B_{00}) present along the flow direction and (c) a uniform

Chapter 1: Introduction

magnetic field (C_0) employed along the direction of self-consistent magnetic field. For sharper shear width, the dominant mode is sausage mode while for broader shear width, the dominant instability is kink instability. The presence of B_{00} has been shown to reduce the pure sausage growth rate. We show here that the pure kink mode remains uninfluenced by this magnetic field. Also, the presence of C_0 has no effect on sausage growth rate [34], but has been shown by us to alter the growth rate of pure kink mode. Therefore, one mode can dominate over the other in the given conditions.

We also carry out the simulations of the 3D instability with the help of a nonlinear fluid code. The growth rates of instabilities calculated in the linear regime of simulations match with the linear theory. The nonlinear state is strongly turbulent in these simulations unlike the 2D case. The spectrum of turbulence is found to be anisotropic. We have observed that the spectral cascade is inhibited both along the direction of flow as well as the direction of magnetic field. Thus, the shortest scales are generated along the shear direction. In the presence of B_{00} , the scales along the shear direction are more or less unchanged while along other two directions, the scales turn out to be longer than the case for $B_{00} = 0$. These observations are consistent with the anisotropic feature of whistler mediated cascade. The broadening of shear layer occurs much more slowly for this case as the kink mode being the dominant mode governs the evolution of system. During the linear phase the kink instability does not alter the 2D flow configuration. Thus, the broadening occurs at later nonlinear phase when the other modes also grow. This shows that it is important to understand the interplay of two modes under various physical conditions, as the evolution would be different when governed by the different modes.

Chapter 4: Stability of Isichenko Solutions of Electron Magnetohydrodynamic Model Against Shear Driven Modes

In section 1.2.3, we pointed out that the EMHD system permits certain exact, nonlinear solutions. Isichenko and Marnachev [51] obtained these solutions as the stationary monopoles and propagating dipoles of localized electron flow structure. The dynamical properties of these solutions have been studied in considerable detail by many researchers [55, 56, 76, 77]. Among these structures, dipoles are of practical importance. The dipoles carrying energy and momentum with them propagate stably and may prove to be useful in phenomena like, fast ignition concept of laser fusion [3, 5, 6], fast magnetic field transport [49, 50], laser plasma interaction studies [78] etc.

The electron flow pattern in these EMHD structures, monopoles and dipoles, is significantly sheared and hence they could be unstable to the shear driven modes namely, sausage and kink [34, 46]. The structures are known to be stable to the 2D sausage perturbations as the unstable wavelengths are longer than the structure size, an explanation provided by Sharad et al. [54]. For kink mode, however, wavelengths smaller than the structure size are also unstable. Stability of structures against this mode is not known so far; we investigate this in Chapter 4. For this, we carry out a 3D nonlinear simulations with monopoles and dipoles as the initial conditions. We observe that the structures are unstable in our simulations. The unstable behaviour of structures has been attributed to the presence of kink mode.

Chapter 1: Introduction

Chapter 5: Summary and Future Scope

Finally, in Chapter 5, conclusions of the thesis work have been drawn and the prospects for future work have been outlined.

Chapter 2

Role of Natural Length and Time

Scales on Electron

Magnetohydrodynamic Kelvin

Helmholtz Instability: 2D Studies

The Electron Magnetohydrodynamic (EMHD) model represents an incompressible electron fluid moving against static, neutralizing background ion species. In contrast to ordinary hydrodynamic fluids, the EMHD model contains intrinsic length (electron skin depth) and time (whistler period) scales. In this Chapter, we investigate the role of skin depth and existence of whistlers on velocity shear driven Kelvin Helmholtz instability in the context of two dimensional EMHD. Numerical simulations are also carried out to understand the role of whistlers in nonlinear regime of instability.

2.1 Introduction

Electron Magnetohydrodynamics (EMHD) is a fluid model to describe the plasmas in which the electrons dynamics is of importance. The ions are static and provide a neutralizing background to the electrons. The EMHD system closely resembles an incompressible hydrodynamic fluid system and hence the characteristics neutral fluid instabilities are present here as well. One of the prominent neutral fluid instability is Kelvin Helmholtz instability in which the interface of two fluids in relative motion (parallel to interface) is unstable under certain conditions. The Kelvin Helmholtz instability of neutral hydrodynamic fluid is thoroughly discussed in the literature [37, 38]. In the context of EMHD also, the instability has been investigated in certain detail and has often been termed as sausage and kink like modes [34, 46]. Besides due similarities, the EMHD system also has certain differences with neutral fluids due to the magnetized character of the electron fluid. The electromagnetic character of the system manifests as the existence of intrinsic natural scales. In the context of EMHD, the electron skin depth is such a length scale arising due the inertia of electrons. In the the presence of external (and/or strong self consistent) magnetic field, whistler waves are the normal modes of the system and hence the whistler periods appear as the natural time scale. A neutral hydrodynamic fluid system, in contrast, is devoid of any specific scales. In this Chapter, we discuss the role of these natural length and time scales on the velocity shear driven Kelvin Helmholtz instability in the context of 2D EMHD. And the comparison with the neutral hydrodynamic fluid instability are presented.

In these studies the spatial variations in perturbations are confined in the plane comprising the flow and shear directions, the variations in the direction normal to

this plane (which is also the direction of self-consistent magnetic field generated due to the shear flow) have been neglected. The EMHD set of equations reduces to the Navier-Stoke's equations of hydrodynamic fluid in the short wavelength limit. To understand the role of skin depth, the shear width of the system is varied in comparison to the electron skin depth. We show that by appropriate rescaling the KH growth rate curve plotted with respect to the excitation wave number (along the flow direction) reduces to a universal curve for the neutral fluid hydrodynamics system (see Fig. 2.1). This, however, does not happen for the EMHD system for which the growth rate diminishes as the shear width becomes broader in comparison to the electron skin depth parameter. The KH instability in EMHD is prominent only when the shear in electron flow velocity is sharper than the skin depth, a fact which has been outlined in our earlier studies also [34, 45].

We also study in detail the role of whistler waves on this particular instability. In previous 2D EMHD studies of KH like mode [34, 45], the equilibrium and also the perturbed magnetic fields arising as a result of the 2D electron current flow, was directed along the symmetry direction. Since the variations were confined in the two dimensional plane orthogonal to the equilibrium magnetic field, the configuration clearly did not support the normal oscillatory whistler wave mode associated with EMHD phenomena. The 3D study of the instability in subsequent work [46, 47] does support the whistler mode. However, in the 3D case one is not able to isolate the role of whistlers from effects arising due to the three dimensionality of the problem. Furthermore, in those studies [46, 47] the propagation direction of the whistler waves being primarily along the equilibrium magnetic field, was orthogonal to the 2D plane defined by the equilibrium shear and the fluid flow direction. For the KH instability major action is confined to this plane. We, there-

fore, choose here to study a 2D case of the instability with an additional uniform magnetic field in the flow direction. For this case whistlers are permitted even in the 2D limit. This configuration is thus markedly different from both the previous 2D and 3D studies carried out by us. For this case, we would see in the next section that the evolution is governed by a set of coupled equations in two scalar fields. This is unlike the previous 2D studies where the magnetic field component along the symmetry direction was sufficient for the description. This is essentially due to the fact that the whistler wave perturbations couple the in-plane magnetic field perturbations to the magnetic perturbations along the symmetry direction¹. We wish to point out here that Califano *et al.* [32] also considered an instability of a sheared electron flow configuration. The 2D plane of perturbations in their case is inclined with respect to the electron flow direction. Such a geometry has been termed by us as a 3D kink mode. Angle between the 2D plane of perturbations and the flow direction is changed through a dimensionless parameter α by choosing its values between 0 and 1. The choice of $\alpha = 1$ (2D plane of perturbations lying along the flow direction) in their work reduces the configuration to the 2D case that we discuss here. Furthermore, the studies by Califano *et al.* have been restricted to the case for which the shear width is comparable or broader than the electron skin depth. We have considered in our studies shear width, which are sharper than the electron skin depth. We assume that the kinetic scales are much shorter than the electron skin depth and the shear width for the applicability of the fluid EMHD model.

In section 2.3, we discuss the role of the natural length scale ($d_e = c/\omega_{pe}$) that

¹For description of geometry, see Fig. 1.1 in Chapter 1. The $x - z$ plane in the figure is the 2D plane of flow and shear that we consider here. The external uniform magnetic field lies in this plane along the flow direction. y is the symmetry direction.

appears in EMHD. We compare the KH instability in neutral hydrodynamic fluid with that of EMHD. In section 2.4, the role of whistler waves on the instability is discussed. An interesting observation is that in 2D, even in the presence of whistler waves, the instability continues to be nonlocal. The growth rate is finite only for those modes with scales longer than the original shear width. This is in contrast to the 3D case where the local modes were also found to be unstable. Thus, the three dimensional character of the mode (and not the existence of whistler waves) is essential for the destabilization of local modes for the electron velocity shear driven instability. In section 2.5, a numerical study of the shear driven instability in the presence of in-plane magnetic field is presented. The role of whistler waves in the nonlinear regime is outlined. Section 2.6 contains the discussion and summary of our observations.

2.2 Governing Equations

In the 2D $x - z$ plane, the EMHD equations (1.1) and (1.2), given in Chapter 1, can be written in terms of evolution of two scalar fields, which define the total magnetic field as $\vec{B} = b\hat{y} + \hat{y} \times \nabla\psi$. The electron velocity can then be expressed in terms of these two scalar fields as $\vec{v}_e = -\nabla \times \vec{B} = \hat{y} \times \nabla b - \hat{y} \nabla^2 \psi$ [55],

$$\begin{aligned} \frac{\partial}{\partial t}(\nabla^2 b - b) + \hat{y} \times \nabla b \cdot \nabla \nabla^2 b - \hat{y} \times \nabla \psi \cdot \nabla \nabla^2 \psi &= 0 \\ \frac{\partial}{\partial t}(\nabla^2 \psi - \psi) + \hat{y} \times \nabla b \cdot \nabla (\nabla^2 \psi - \psi) &= 0 \end{aligned} \quad (2.1)$$

Here, \hat{y} denotes the symmetry direction. The equation has been expressed in normalized variables. Magnetic field has been normalized by a typical amplitude of B_{00} , the time by the corresponding electron gyro-period $\omega_{ce}^{-1} = (eB_{00}/m_e c)^{-1}$

and length by the electron skin depth $d_e = c/\omega_{pe}$. The limit of $k^2 d_e^2 \gg 1$ along with $\psi = 0$, reduces the coupled set Eq.(2.1) to the Navier Stokes equations in 2D for an incompressible neutral fluid hydrodynamics,

$$\frac{\partial}{\partial t} \nabla^2 b + \hat{y} \times \nabla b \cdot \nabla \nabla^2 b = 0 \quad (2.2)$$

here, b can be identified with the velocity potential.

The equilibrium sheared electron flow velocity in the presence of in - plane magnetic field can be described by a choice of $b_0 = b_0(x)$ and $\psi_0 = -B_0 x$. This choice of ψ_0 ensures that the in - plane magnetic field is oriented along the flow direction. The total equilibrium magnetic field can thus be represented by $\vec{B}_{eq} = \hat{y} b_0(x) + \hat{z} B_0$. The field b_0 is an equilibrium magnetic field directed along the symmetry direction \hat{y} and is dependent on x . The in - plane magnetic field B_0 is directed along \hat{z} and is chosen to be a constant. The equilibrium electron velocity profile is defined by $\vec{v}_0 = -\hat{z} db_0/dx$. A specific form of the electron velocity shear profile can be chosen by an appropriate choice of the functional form for $b_0(x)$. The dynamical evolution of a small perturbation in the two fields, viz., b_1 and ψ_1 around this equilibrium can be analyzed with the help of linearized EMHD model Eqs.(2.1),

$$\begin{aligned} \frac{\partial}{\partial t} (\nabla^2 b_1 - b_1) + v_0 \frac{\partial}{\partial z} \nabla^2 b_1 - v_0'' \frac{\partial b_1}{\partial z} - B_0 \frac{\partial}{\partial z} \nabla^2 \psi_1 &= 0 \\ \frac{\partial}{\partial t} (\nabla^2 \psi_1 - \psi_1) + v_0 \frac{\partial}{\partial z} (\nabla^2 \psi_1 - \psi_1) + B_0 \frac{\partial b_1}{\partial z} &= 0 \end{aligned} \quad (2.3)$$

It should be noted that for the case of $B_0 = 0$, the equations reduce to the form analyzed in the earlier work [34]. In this case the field ψ_1 is merely convected by the equilibrium flow velocity due to the velocity potential b_0 and plays no active

role in evolution. The evolution of the field b_1 gets entirely decoupled from the field ψ_1 for the linear problem. The linear stability problem is reduced to that of the study of the evolution of the single scalar field of b_1 . The presence of finite B_0 couples the evolution of b_1 and ψ_1 fields in the linear limit through whistler like perturbations and its influence on the instability is a topic of our investigation. Fourier analyzing Eq.(2.3) in z and time we obtain,

$$\begin{aligned} \frac{d^2 b_1}{dx^2} - (1 + k_z^2) b_1 - \frac{k_z(v_0 - v_0'')}{(\omega - k_z v_0)} b_1 + \frac{k_z B_0}{(\omega - k_z v_0)} \left(\frac{d^2 \psi_1}{dx^2} - k_z^2 \psi_1 \right) &= 0 \\ \frac{d^2 \psi_1}{dx^2} - (1 + k_z^2) \psi_1 - \frac{k_z B_0}{(\omega - k_z v_0)} b_1 &= 0 \end{aligned} \quad (2.4)$$

For $v_0 = 0$, one obtains the whistler wave dispersion relation from Eq.(2.4). The coupled set of Eqs.(2.4) can also be expressed in a fashion which eliminates the second derivative of ψ_1 from the first equation of the set [Eqs.(2.4)] by substituting for it from the second equation,

$$\begin{aligned} \frac{d^2 b_1}{dx^2} - (1 + k_z^2) b_1 - \frac{k_z(v_0 - v_0'')}{(\omega - k_z v_0)} b_1 + \frac{k_z B_0}{(\omega - k_z v_0)} \psi_1 + \frac{k_z^2 B_0^2}{(\omega - k_z v_0)^2} b_1 &= 0 \\ \frac{d^2 \psi_1}{dx^2} - (1 + k_z^2) \psi_1 - \frac{k_z B_0}{(\omega - k_z v_0)} b_1 &= 0 \end{aligned} \quad (2.5)$$

This set of coupled linearized equations we shall use for the linear instability calculations. The equations shall be analyzed analytically and numerically to be solved as the eigen value problem.

2.3 Role of Skin Depth

In this section we choose to study the role of electron skin depth on the KH instability and thereby offer a comparison amidst the KH mode in a Navier Stokes

Chapter 2: Role of natural length and time scales ...

(NS) (the limit of $d_e^{-1} \rightarrow 0$) and an EMHD fluid (d_e is finite and taken to be unity). To avoid any role of whistlers we confine ourselves to the choice of $B_0 = 0$ (the in-plane component of equilibrium magnetic field) in this section. This reduces the equilibrium configuration to the case studies earlier. We would see in next section that a finite value of in-plane component of B_0 introduces the magnetic tension, causes whistler excitations, and reduces the KH growth rate. The linearized equations in the NS limit,

$$\frac{d^2 b_1}{dx^2} - k_z^2 b_1 + \frac{k_z v_0''}{(\omega - k_z v_0)} b_1 = 0 \quad (2.6)$$

and in the EMHD limit, in the absence of B_0 ,

$$\frac{d^2 b_1}{dx^2} - (1 + k_z^2) b_1 - \frac{k_z (v_0 - v_0'')}{(\omega - k_z v_0)} b_1 = 0 \quad (2.7)$$

We consider here a tangent hyperbolic shear profile for the equilibrium flow,

$$v_0(x) = V_0 \tanh\left(\frac{x}{\epsilon}\right) \quad (2.8)$$

The growth rate for the hydrodynamic case is a universal curve shown by the thick line in Fig.2.1. The growth rate has been plotted here as a function of $k_z \epsilon$. Here, ϵ is the shear width of the flow as can be seen from the above equation. In the hydrodynamic case there is no special scale in the system. Hence, a change in the shear width ϵ can always be accommodated by an appropriate length scale rescaling, which would mean a readjustment in the value of V_0 as well. We indeed observe that the plot of growth rate for the hydrodynamic case collapses on a single curve for differing values of ϵ when the velocity V_0 is adjusted to accommodate

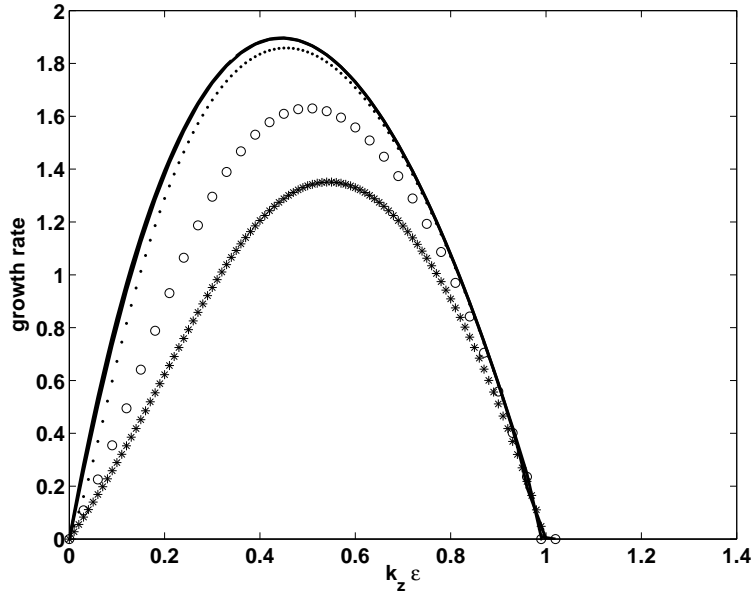


Figure 2.1: The plot of growth rate vs. $k_z \epsilon$ for the hydrodynamic case (thick curve). The growth rate has been obtained for a shear flow profile $v_0 = V_0 \tanh(x/\epsilon)$. The curve for the hydrodynamic case is universal for the choice of $\epsilon = 0.1f$ and $V_0 = 1.0f$. The curves with dots, circles and stars show the growth rate for an EMHD system for $f = 1, 3, 5$ respectively.

for the length rescaling. The thick line representing the hydrodynamic case in Fig.2.1 corresponds to several choices of shear width, e.g. $\epsilon = 0.1f$ along with $V_0 = 1.0f$, obtained by varying the parameter f . This can also be demonstrated from Eq.(2.6), which is invariant under the transformation $\epsilon_n = \epsilon f$, $k_{zn} = k_z/f$, $d/dx_n = (1/f)d/dx$ and $v_{0n} = v_0 f$. The value of ω thus remains the same. The growth rate curve when plotted against $k_z \epsilon = k_{zn} \epsilon_n$ has an identical form. It can be seen that Eq.(2.7) does not remain invariant under this transformation.

Hence, for the EMHD fluid case, where the skin depth exists as a special scale ($d_e = 1$ has been chosen as a normalizing scale), the growth rate curves are no longer universal. For each value of f a different growth rate curve results. For finite d_e the growth rate deviates from the universal curve for the NS system predominantly

at lower k_z values (i.e. at longer scales). With increasing f as the shear width increases in comparison with the skin depth and the growth rate keeps reducing. It becomes negligible when the shear width is much broader than the electron skin depth.

Another striking feature of the growth rate curve is the fact that it has a bell shaped character with a single maxima for both NS as well as the EMHD cases. For a tangent hyperbolic shear flow it is zero at $k_z = 0$ and also at $k_z\epsilon = 1.0$. For all values of the wavenumber beyond $k_z\epsilon = 1$ the growth rate continues to remain zero. The unstable wavenumbers for the tangent hyperbolic profile thus exist only in the domain of $0 \leq k_z\epsilon \leq 1.0$, irrespective of the values of V_0 . Thus as the shear width parameter ϵ is increased, the threshold condition on $k_z\epsilon$ being unity, diminishes the range of unstable k_z modes. Though the exact value of the upper limit on $k_z\epsilon$ is dependent on the specific form of the shear profile, the cut off value for unstable wavenumbers is constrained by $k_z\epsilon$ of the order of unity. For instance, for a piecewise linear profile the growth rate vanishes beyond a smaller value of k_z , viz., $k_z\epsilon = 0.639$ [34]. In another publication [79] an analytical proof was given to show that the growth rate is zero for $k_z\epsilon = 1$ for the tangent hyperbolic equilibrium shear profile.

The fairly general constraint can, however, be understood on physical grounds. The mode which is driven unstable due to a shear scale length of ϵ , has an eigenstructure which itself is like a sheared flow pattern orthogonal to the original flow direction having a typical shear scale length of k_z^{-1} as depicted in Fig.2.2. Since the free energy for the instability is provided by the sheared flow configuration, the unstable eigen functions themselves cannot have sharper shear flow structure. This is responsible for the threshold on the wavenumber k_z . Thus, the KH instability

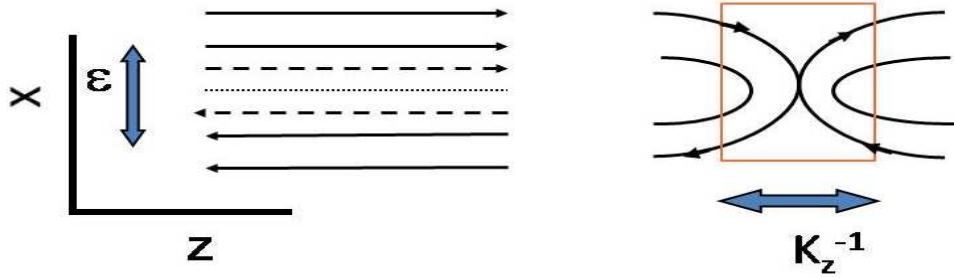


Figure 2.2: A schematic showing the flow configuration after KH destabilization in 2D. It can be seen that the destabilized flow configuration results in a sheared flow orthogonal to the original shear flow, with a shear width given by k_z^{-1} .

in 2D always generates velocity shear scales which are longer than the original equilibrium shear scale. This is responsible for the threshold condition of the unstable wavenumbers a $k_{zth}\epsilon \sim \mathcal{O}(1)$. The instability is therefore nonlocal in 2D. In the next section we would see that even in the presence of whistler wave like excitations, the threshold condition on the unstable modes continues to hold.

2.4 Role of Whistler Waves

In this section we study the influence of whistler waves on the shear driven instability of EMHD model and choose B_0 to be finite. For this purpose, we choose two kinds of equilibrium fluid shear flow profiles. A step velocity profile for which the shear width $\epsilon \rightarrow 0$ is used for analytical simplicity. A tangent hyperbolic shear profile is then studied to investigate the influence of finite shear width of the flow profile.

2.4.1 Step Velocity Profile

We choose a step electron velocity shear profile of the form $v_0(x) = -V_0 + 2V_0\Theta(x)$. Thus in region I ($-\infty \leq x \leq 0$), $v_0(x) = -V_0$ and for region II ($0 \leq x \leq \infty$) we have $v_0(x) = V_0$. We choose to depict the perturbed fields by $b_1 = b_{I,II}$ and $\psi_1 = \psi_{I,II}$ in the two regions. For a finite jump in the equilibrium flow velocity it can be shown by using Eq.(2.4) that the following functions of the perturbed fields should be continuous at $x = 0$ the location of velocity discontinuity,

$$\begin{aligned} f_1 &= (\omega - k_z v_0) \frac{db_1}{dx} + k_z v_0' b_1; & f_2 &= \frac{b_1}{(\omega - k_z v_0)} \\ f_3 &= \frac{d\psi_1}{dx}; & f_4 &= \psi_1 \end{aligned} \quad (2.9)$$

In the two regions, the Eq.(2.5) can be written as,

$$\begin{aligned} \frac{d^2}{dx^2} b_{I,II} + \alpha_{I,II} b_{I,II} + \beta_{I,II} \psi_{I,II} &= 0 \\ \frac{d^2}{dx^2} \psi_{I,II} + \eta \psi_{I,II} - \beta_{I,II} b_{I,II} &= 0 \end{aligned} \quad (2.10)$$

Here, $\eta = -(1 + k_z^2)$ and the coefficients α, β are defined in the two regions as,

$$\begin{aligned} \alpha_{I,II} &= \eta + \frac{k_z^2 B_0^2}{(\omega \pm k_z V_0)^2} \pm \frac{k_z V_0}{(\omega \pm k_z V_0)} \\ \beta_{I,II} &= \frac{k_z B_0}{(\omega \pm k_z V_0)} \end{aligned}$$

Since the wave functions should vanish at $\pm\infty$, we choose the solution of Eq.(2.10) as,

$$b_I = A_b \exp(p_I x); \quad b_{II} = C_b \exp(-p_{II} x)$$

Chapter 2: Role of natural length and time scales ...

$$\psi_I = A_\psi \exp(p_I x); \quad \psi_{II} = C_\psi \exp(-p_{II} x)$$

where, $p_{I,II}$ are those roots which have a positive real part. They are obtained by substituting for $b_{I,II}$ and $\psi_{I,II}$ in Eq.(2.10). We thus have,

$$p_{I,II}^2 = -\frac{(\alpha_{I,II} + \eta)}{2} \pm \frac{1}{2} \sqrt{(\alpha_{I,II} + \eta)^2 - 4(\alpha_{I,II}\eta + \beta_{I,II}^2)}$$

Thus, there are two roots each for p_I^2 and p_{II}^2 corresponding to the \pm sign before the square root. Upon substituting for η , $\alpha_{I,II}$ and $\beta_{I,II}$ the roots are,

$$p_{I\pm}^2 = \left\{ 1 + k_z^2 - \frac{k_z V_0}{2\Omega_+} - \frac{k_z^2 B_0^2}{2\Omega_+^2} \right\} \pm \frac{1}{2} \left\{ \left(\frac{k_z V_0}{\Omega_+} + \frac{k_z^2 B_0^2}{\Omega_+^2} \right)^2 - \frac{4k_z^2 B_0^2}{\Omega_+^2} \right\}^{1/2}$$

$$p_{II\pm}^2 = \left\{ 1 + k_z^2 + \frac{k_z V_0}{2\Omega_-} - \frac{k_z^2 B_0^2}{2\Omega_-^2} \right\} \pm \frac{1}{2} \left\{ \left(\frac{k_z V_0}{\Omega_-} - \frac{k_z^2 B_0^2}{\Omega_-^2} \right)^2 - \frac{4k_z^2 B_0^2}{\Omega_-^2} \right\}^{1/2}$$

Here $\Omega_\pm = \omega \pm k_z V_0$ and the \pm sign in the suffix denotes the two roots corresponding to the positive and negative sign before the square root. In the limit of $B_0 = 0$ one recovers the expression obtained in earlier studies by choosing appropriate sign of the square root in the two regions. In addition there is another value $p_{I,II}^2 = 1 + k_z^2$ corresponding to the evolution equation for ψ (which gets decoupled from b in this limit). The earlier studies [34] had then shown that upon using the matching conditions one finds a purely imaginary value for ω for all finite values of k_z and V_0 . This has shown that a sheared electron velocity configuration with zero shear width is always unstable.

In the present case, the other limit of $V_0 = 0$, leads to $p_I^2 = p_{II}^2 = -k_x^2$ (the wave number along x) and yields the dispersion relation of whistler wave mode for which ω is real. Clearly, in the general case when both V_0 and B_0 are finite, a

Chapter 2: Role of natural length and time scales ...

complex value of ω can be expected. Using Eq.(2.10) we can find a relationship,

$$A_{\psi\pm} = \frac{\beta_I}{p_{I\pm}^2 + \eta} A_{b\pm}; \quad C_{\psi\pm} = \frac{\beta_{II}}{p_{II\pm}^2 + \eta} C_{b\pm}.$$

This leaves us with four unknown coefficients $A_{b\pm}$ and $C_{b\pm}$. The matching conditions are then utilized to eliminate these coefficients, which yields the value of ω from $\det||M|| = 0$ where the matrix M is defined as follows:

$$\begin{vmatrix} 1/\Omega_+ & 1/\Omega_+ & -1/\Omega_- & -1/\Omega_- \\ \Omega_+ p_{I+} & \Omega_+ p_{I-} & \Omega_- p_{II+} & \Omega_- p_{II-} \\ 1/[(p_{I+}^2 + \eta)\Omega_+] & 1/[(p_{I-}^2 + \eta)\Omega_+] & -1/[(p_{II+}^2 + \eta)\Omega_-] & -1/[(p_{II-}^2 + \eta)\Omega_-] \\ p_{I+}/[(p_{I+}^2 + \eta)\Omega_+] & p_{I-}/[(p_{I-}^2 + \eta)\Omega_+] & p_{II+}/[(p_{II+}^2 + \eta)\Omega_-] & p_{II-}/[(p_{II-}^2 + \eta)\Omega_-] \end{vmatrix}$$

The roots, ω for $\det || M || = 0$, for various values of B_0 and k_z have been obtained. We show in Fig. 2.3 the plot of the variation of the real and imaginary part of ω as a function of the in - plane magnetic field B_0 . The plots clearly show that as the value of B_0 is increased the growth rate of the KH mode decreases. This is because the perturbations associated with the instability cause bending of the equilibrium magnetic field which requires energy.

An interesting feature of the plot is a sudden fall of the growth rate in the neighborhood of a particular value of the B_0 . A closer look reveals that this fall occurs at the location when the KH growth rate $\gamma = k_z V_0 \sqrt{(1 + 4k_z^2)/(3 + 4k_z^2)}$ of the unmagnetized electron fluid for $B_0 = 0$ matches with the typical whistler

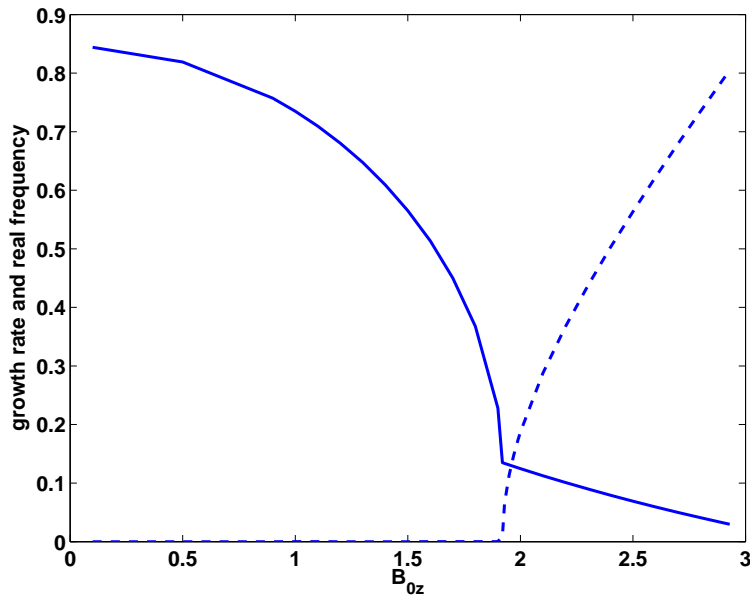


Figure 2.3: The growth rate (solid line) and the real frequency (dashed line) for the KH mode as a function of the in-plane magnetic field B_0 for a step electron velocity profile.

frequency of the system. The flow perturbations transverse to the shear flow in the KH mode grow at the typical time scale of $\sim (k_z V_0)^{-1}$. In EMHD prescription it is well known that $\vec{B} - d_e^2 \nabla^2 \vec{B}$ is tied to the fluid flow velocity. Since the equilibrium field B_0 is homogeneous, the flow perturbations carry the equilibrium field lines with themselves. Thus, the flow perturbations due to the KH instability distort the equilibrium straight magnetic field to a sheared configuration. The tension due to this distortion tries to restore the magnetic field line to its original configuration, causing oscillations at the whistler frequency. When the whistler period becomes comparable to the growth time of the KH mode, the phase reversal of the transverse perturbations occur at the time scale at which the shear instability grows, resulting in considerably reducing the growth rate. The whistler frequency increases with B_0 and at higher B_0 thus it becomes more and more difficult for the KH instability to

get excited. The growth rate subsequently at higher B_0 falls to zero as illustrated from the plots of the Fig.2.3. The variation of real part of ω with B_0 shows deviation from the whistler frequency at the lower value of B_0 . However, at large B_0 it asymptotically matches with the whistler frequency.

The step velocity profile is an extreme choice made for the sake of simplified analytical treatment. In the realistic case the velocity would vary in a continuous manner. The width of the sheared electron flow profile plays an important role for the instability. In earlier 2D studies [34] (with no in-plane equilibrium magnetic field and hence no whistlers) it was observed that only those modes which satisfy $k_z \epsilon < 1$ condition were unstable. The typical scale length of the eigen mode structure along the shear direction is similar to $p_{I,II}^{-1}$ for the step profile considered in this section. The expression for $p_{I,II}$ in the absence of B_0 shows a monotonic dependence on k_z . For shear profile with finite width, similar of proportionality of eigen function scales along the shear direction x with k_z can be expected. Thus the condition $k_z \epsilon < 1$ for instability translates to the fact that the 2D instability is essentially nonlocal, and arises only when the mode structure is broader than the shear width. In the next section, we investigate the role of finite shear width of the velocity profile on this particular instability in the presence of whistler modes.

2.4.2 Velocity Profile with Finite Shear Width

In this section, we consider the instability in the presence of B_0 when the shear of the equilibrium electron flow has a finite width. For this purpose, we choose tangent hyperbolic form of the velocity profile shown in Eq.(2.8). We use the coupled set of Eq.(2.5) with this form of v_0 to evaluate the eigen value ω numerically. The results have been shown in Fig.2.4, which show that the maximum growth rate

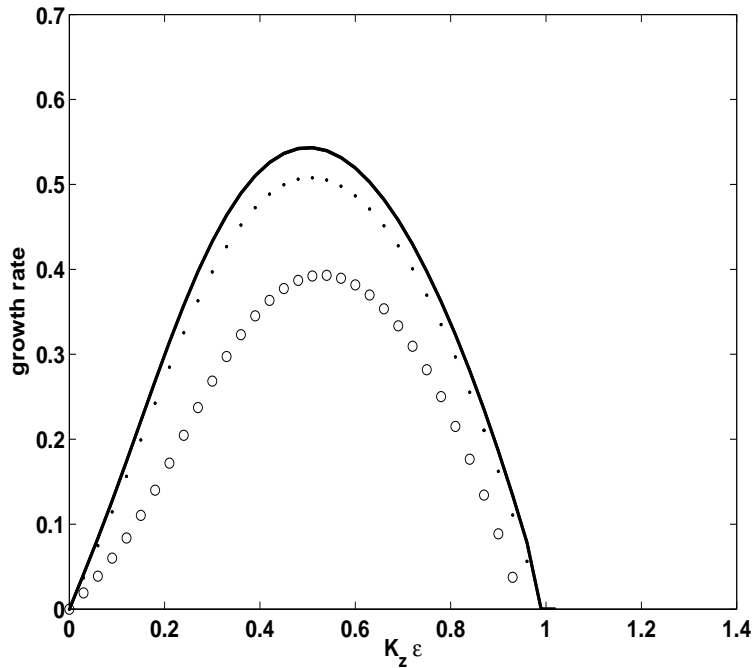


Figure 2.4: The KH growth rate as a function of $k_z \epsilon$ for a tangent hyperbolic shear flow profile. Here the solid, dotted and the curve with circles correspond to $B_0 = 0$, 0.5 and 1.0 respectively.

reduces in the presence of a magnetic field. This feature is same as that observed in the context of step velocity profile in the previous section. The transverse fluid motion associated with the unstable KH mode generates transverse magnetic field perturbations as it carries with itself the equilibrium B_0 magnetic field. The consequent tension of the magnetic field perturbation provides the restoring force (responsible for the whistler wave oscillations) and opposes the growth of the KH mode. The creation of magnetic field perturbations costs energy and hence the KH growth does not remain as energetically favourable as for the case when $B_0 = 0$.

It should be noted that the growth rate curve of Fig.2.4 is again confined to $0 < k_z \epsilon < 1.0$. This feature, therefore, is a universal aspect of the KH instability in 2D. The physical interpretations provided in the previous section holds good

even in the presence of in - plane equilibrium magnetic field B_0 .

2.5 Nonlinear Simulations

In this section, we simulate the coupled set of Eq.(2.1) using the flux corrected algorithm developed by Boris *et al.* [74]. A tangent hyperbolic form for the initial shear flow configuration for which the linear growth rates have been evaluated in the previous section, has been considered here also. This is to understand the behaviour of the additional in - plane equilibrium magnetic field in the nonlinear regime of the KH instability. The shear flow equilibrium configuration along with the in-plane magnetic field is chosen as the initial state for the b and ψ fields. A low amplitude arbitrary perturbation is purposely added initially to hasten the growth of the instability, which otherwise would take long to emerge from the very low amplitude numerical noise.

In Fig.2.5 we show the evolution of the perturbed energy of the system for $B_0 = 0.0, 0.5$ and 1.0 . During the initial phase of the simulation the total perturbed energy increases exponentially. In the semilog plot of Fig.2.5 this can be seen initially where the curve is a straight line. The slope of this line matches closely with twice the maximum growth rate γ obtained analytically in the previous section for each of the distinct values of B_0 . The dashed line shown alongside the simulation curve has twice the slope corresponding to the analytical value of the maximum growth rate. Thus the simulations also confirm that the presence of B_0 reduces the maximum growth rate. As the amplitude of the perturbed field increases, the nonlinear effects become important in the simulation resulting in the saturation of the perturbed energy seen at the later stage.

In Fig.2.6 and Fig.2.7 we show the contour plot of the field b at various times

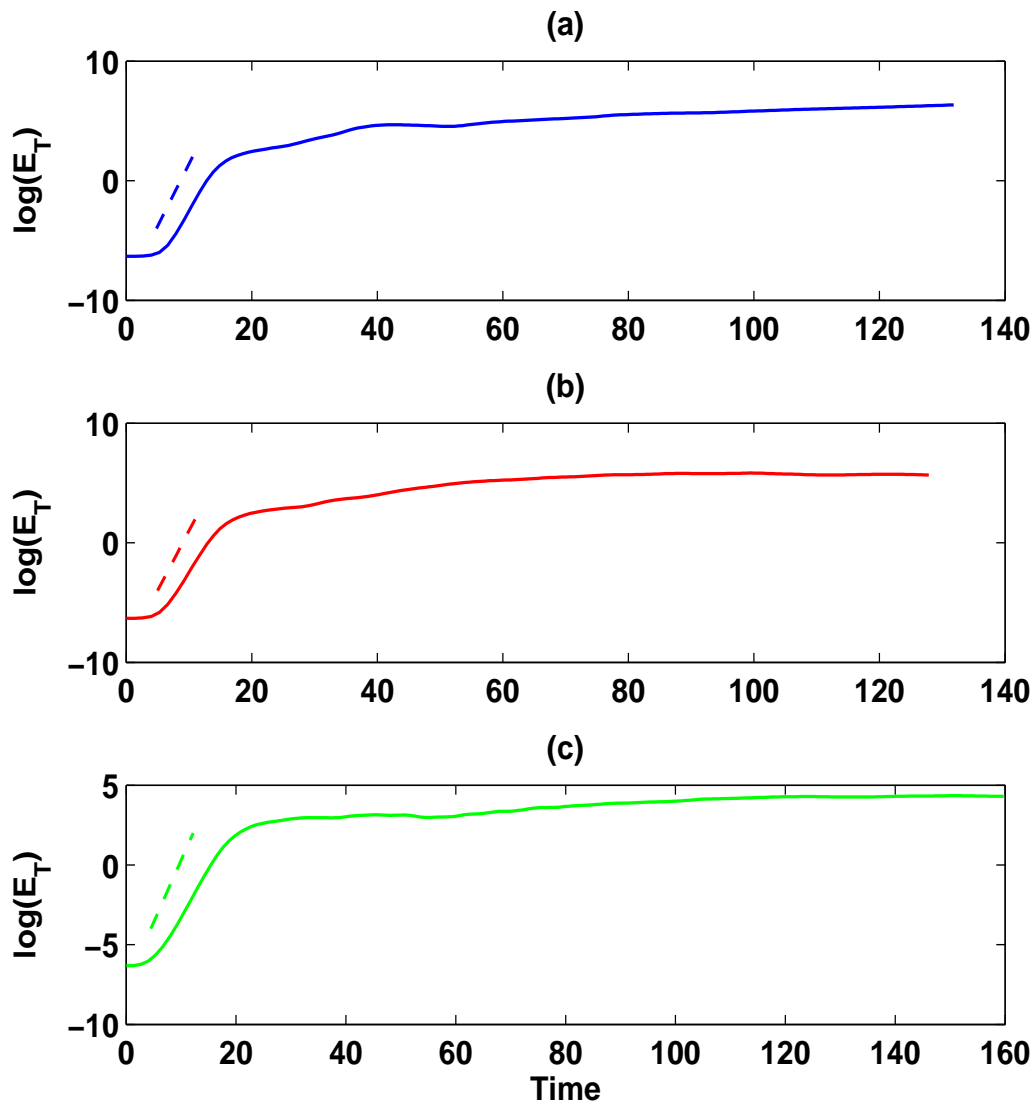


Figure 2.5: The evolution of perturbed energy for $B_0 = 0, 0.5, 1.0$ in subplots (a), (b) and (c) respectively.

(both during linear and nonlinear phases) for two cases of $B_0 = 0$ and $B_0 = 1$. These plots are for the total b field corresponding to the sum of equilibrium as well as the perturbations. Fig.2.8 and Fig.2.9 on the other hand show similar plots for

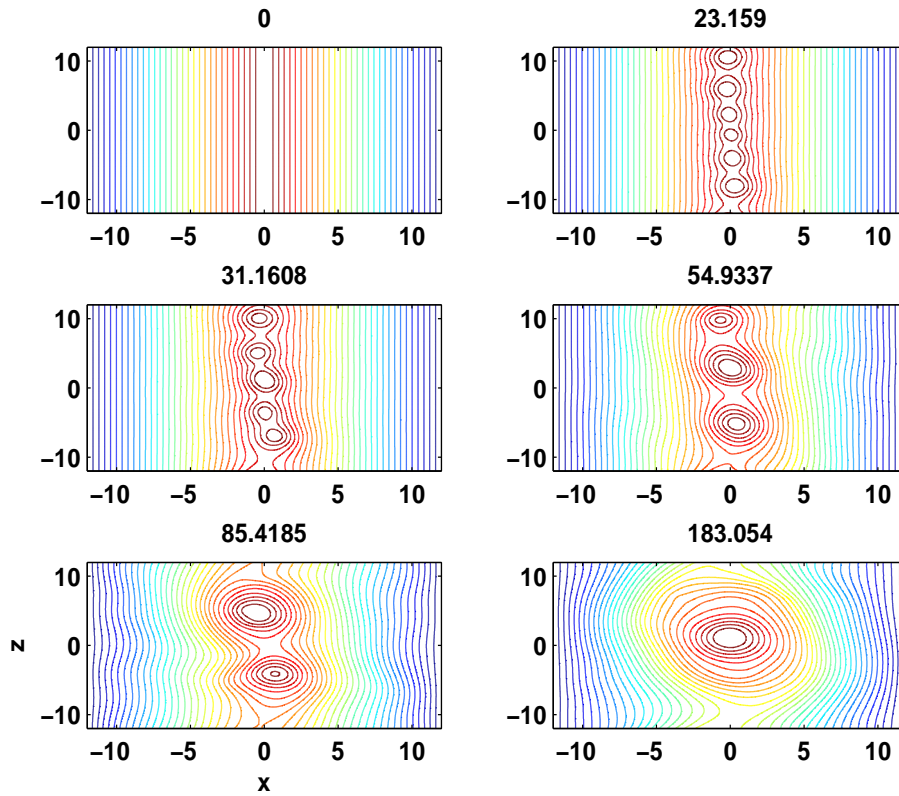


Figure 2.6: Contour plots for the field b at various times for the nonlinear simulation of $B_0 = 0.0$ case.

the perturbed field $\tilde{\psi} = \psi - \psi_0$. The equilibrium contribution to the field, namely $\psi_0 = -B_0x$ has not been included in the plots. The field $\psi = \tilde{\psi}$ for the case in Fig.2.8 where $B_0 = 0$.

For this simulation the maximally growing mode has a wavenumber $k_z = 1.67$. This corresponds to a wavelength of $\lambda = 3.77$. The simulation box length being $L_z = L_x = 24.0$ can accommodate 6 number of wavelengths for this particular mode along the periodic z direction. Indeed, we observe that during the initial state there appears 6 structures. The structures, however, coalesce later. For $B_0 = 0$, the final state in b field shows one large structure fitting the box size.

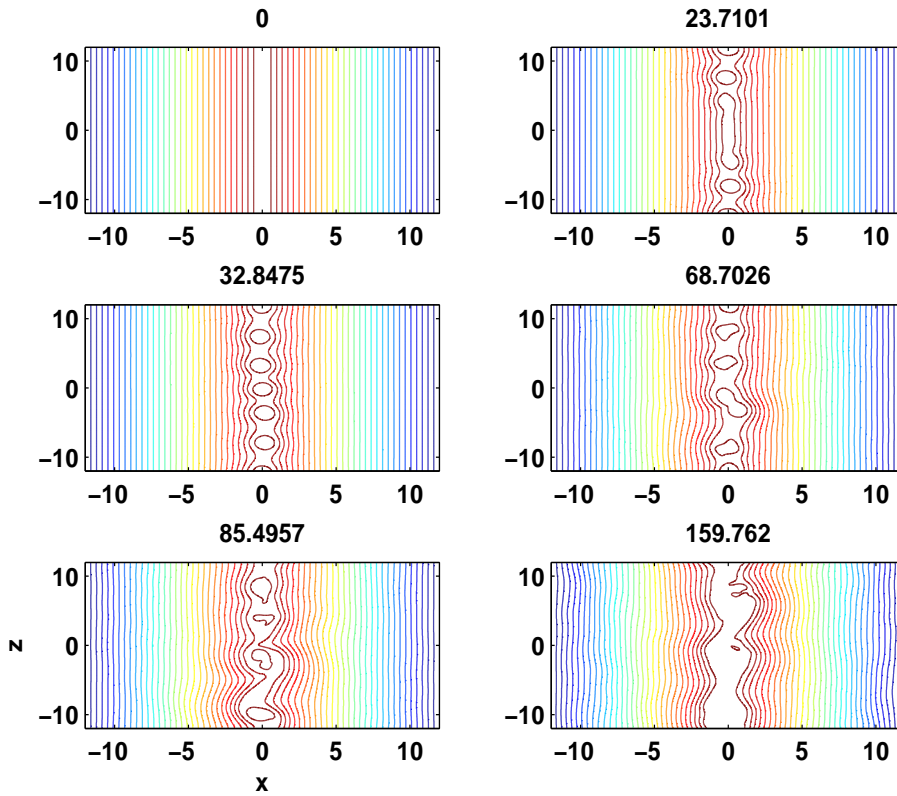


Figure 2.7: Contour plots for the field b at various times for the nonlinear simulation of $B_0 = 1.0$ case.

When $B_0 = 0$ the field b gets decoupled from the field ψ . The evolution of the field b in this case supports two square integral invariants in the non-dissipative limit. The existence of two square integral invariants is responsible for the inverse spectral cascade and formation of long scale patterns in b field.

It should also be noted that when $B_0 = 0$ the field ψ gets merely convected by the field b . We had for these simulations chosen an initial small perturbation in ψ , as is evident from the $t = 0$ contours of ψ in Fig.2.8. The field ψ merely gets convected by the electron flow. There is no growth of energy content of this field in this case. The field ψ thus continues to have a low amplitude and behave

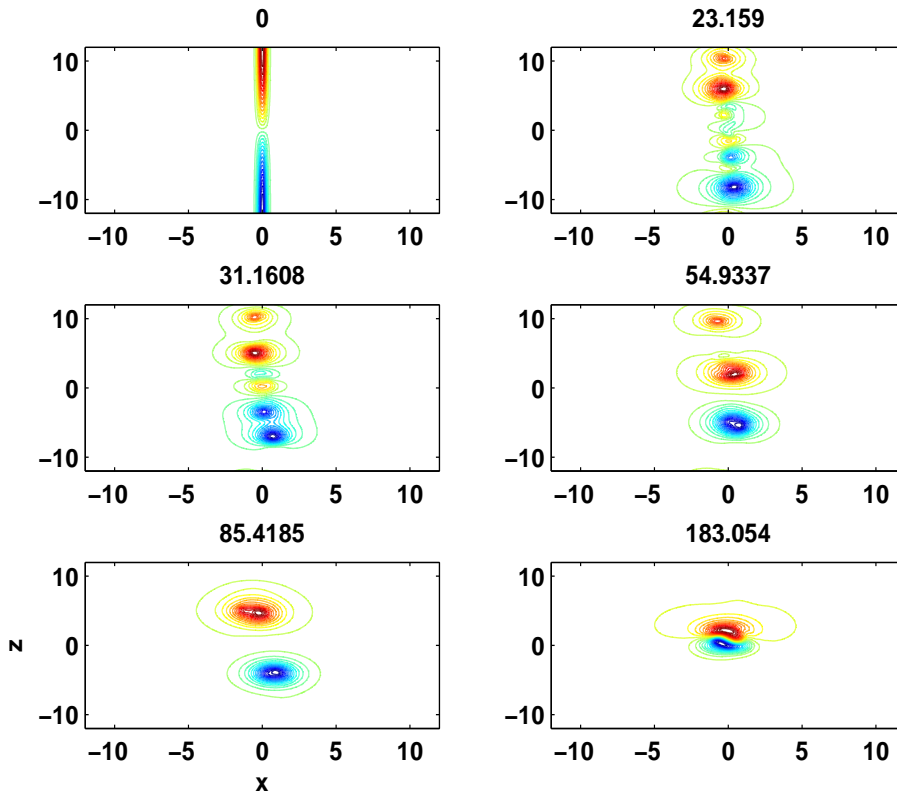


Figure 2.8: Contour plots for the field $\tilde{\psi}$ at various times for the nonlinear simulation of $B_0 = 0.0$ case.

as a passive scalar in this particular case. It should be noted from the plots for simulations with $B_0 = 0$ that even though there is a distinction between the flow direction (z axis) and the shear direction (x) the evolved structure in both b and ψ field is typically isotropic.

When B_0 is chosen to be finite the contours of b during the linear phase are quite similar to the case of $B_0 = 0$. The structure corresponding to the maximally growing mode emerges during this period. However, during the nonlinear phase the structures in b field seem to be preferentially elongated along the z direction (the direction of in-plane magnetic field). The structures hardly get extended

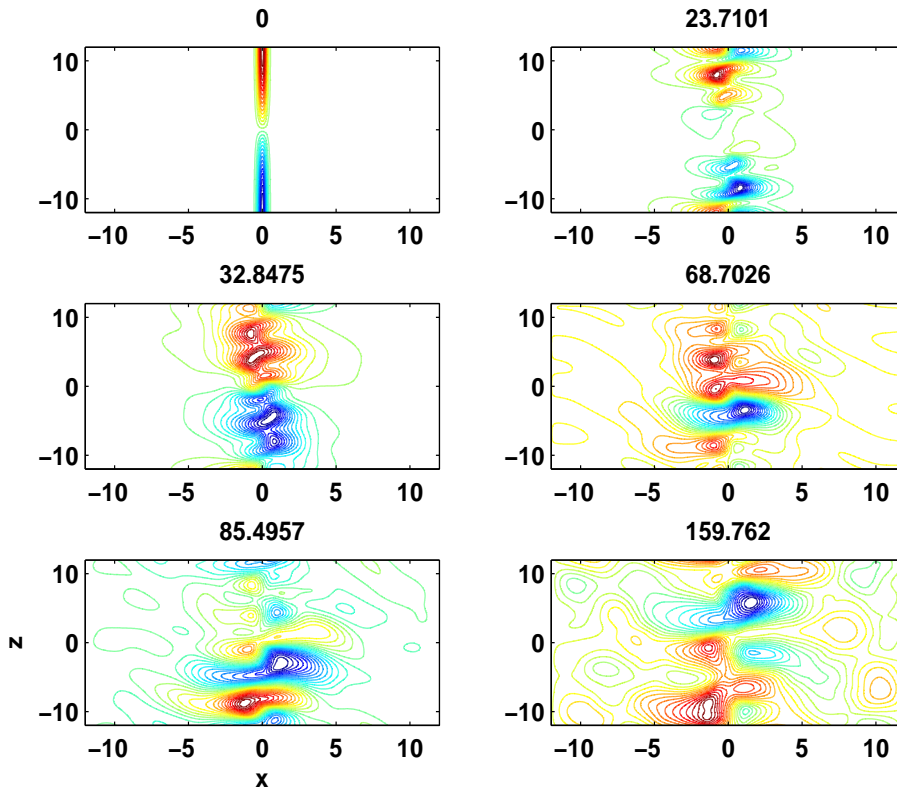


Figure 2.9: Contour plots for the field $\tilde{\psi}$ at various times for the nonlinear simulation of $B_0 = 1.0$ case.

along the transverse dimension. Thus, in the presence of the in-plane magnetic field the inverse cascade in b gets limited to the direction of the in-plane magnetic field. This can be explained by realizing that the whistler wave mediated cascade is anisotropic [72, 73]. The nonlinear interaction of whistler wave produces diminishing wave numbers parallel to B_0 . The perpendicular wavenumber on the other hand increases as the result of these interactions. The contour plots of the field $\tilde{\psi}$ for B_0 finite shows considerable randomness as compared to the case of $B_0 = 0$. The field is now no longer passively convected. It couples actively to the b field through whistler wave excitations. However, the structures in ψ field do not seem

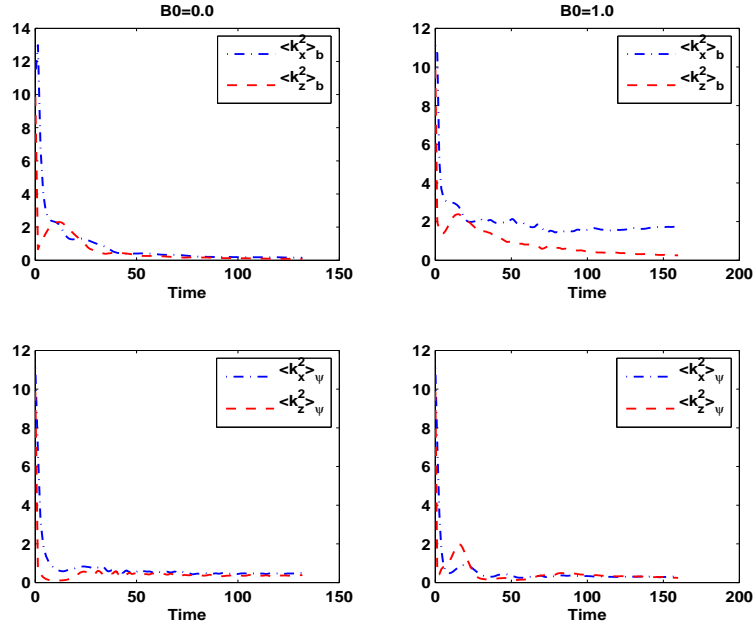


Figure 2.10: The evolution of mean square wavenumbers for the b and ψ fields in the x and z directions.

to exhibit any anisotropy (Fig. 2.9).

The smaller scale generation in the transverse direction for b field and a relatively isotropic structures of ψ in the presence of B_0 can be quantitatively observed from Fig.2.10 which shows the evolution of mean square wavenumbers defined as follows,

$$\langle k_{x,z}^2 \rangle_A = \frac{\int \int k_{x,z}^2 |A(k_x, k_y)|^2 dk_x dk_z}{\int \int |A(k_x, k_y)|^2 dk_x dk_z} \quad (2.11)$$

Here $A(k_x, k_z)$ represents the Fourier transformed fields (b or ψ). The plot in Fig.2.10 clearly shows that $\langle k_x^2 \rangle$ for the field b asymptotes at a comparatively higher value than $\langle k_z^2 \rangle$ in the presence of B_0 . However, for the ψ field the mean square wavenumbers along both the directions are almost identical. This is a characteristic feature of the anisotropy exhibited by the whistler wave mediated

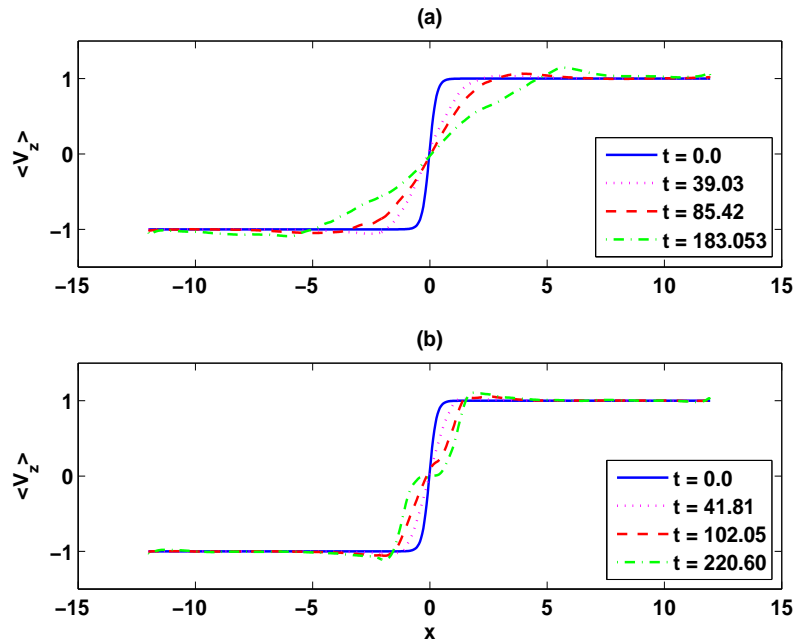


Figure 2.11: The plot of z averaged electron flow velocity profile at various times for $B_0 = 0$ and $B_0 = 1$ in subplot (a) and subplot(b) respectively.

cascade in the nonlinear regime for the EMHD system as observed in previous studies [72, 73].

This decrease in the transverse extent of the perturbations in the presence of B_0 has an adverse effect on the KH instability induced mixing of the fluid flowing in the two directions around the shear layer. This can be observed from the plot of z averaged flow shown for the two cases in Fig.2.11. The flattening of the shear layer is considerably weaker in the presence of B_0 .

2.6 Summary

We have in this work investigated the role of the existence of natural length scales (skin depth) and time scale (whistler wave) in EMHD phenomena on a prominent

velocity shear driven fluid Kelvin - Helmholtz instability in 2D. The growth rate of the instability decreases as the shear width is increased in comparison to the electron skin depth.

The magnetic field corresponding to a 2D shear flow in EMHD is directed orthogonal to this plane. For 2D KH instability studies the perturbation scales are also confined in this plane. The lack of variations along the magnetic field essentially rules out the whistler excitations in this case. To study the role of whistler in the 2D KH instability we have considered an additional homogeneous magnetic field B_0 directed along the flow direction in the equilibrium. This kind of configuration is quite likely in laboratory experiments on EMHD [60, 61] where the plasma is confined with the help of an axial magnetic field. Also the presence of electron beams in plasma threaded by a magnetic field is ubiquitous in nature. For instance in ionosphere and magnetosphere [57], the solar corona [58] and pulsars [59] etc., the equilibrium configuration considered here might exist.

We observe that the growth of the KH instability reduces in the presence of a homogeneous magnetic field directed along the flow configuration. This is primarily due to the whistler wave excitations that exist for such system. This has been illustrated explicitly analytically by evaluating the growth rate for a step velocity shear configuration, and has also been demonstrated for a tangent hyperbolic shear flow profile by numerical eigen value evaluation. The tangent shear flow profile shows that the 2D KH mode is nonlocal with perturbation scales always being longer than the original shear flow. A physical understanding of this has been provided.

The nonlinear simulation studies highlight another aspect. For $B_0 = 0$, the 2D EMHD model represented solely in terms of the magnetic field component

along the symmetry direction b conserves two non-dissipative square integrals. This constrains the evolution in the nonlinear regime for b field towards long scale inverse spectral cascade. In this case there are no whistler wave excitations in the system and the nonlinear cascade is governed entirely due to interactions amongst the eddies. For the case when B_0 is finite the system excites whistler waves. The nonlinear cascade mediated through these whistler waves cause an anisotropic spectral cascade [72, 73]. This anisotropy is dominant for the field b , for which preferentially longer scales get formed only along the direction of the in-plane magnetic field. The transverse spectrum for b has considerably shorter scales. As a result of this feature considerably reduced mixing of forward and reverse electron flows occurs in the presence of B_0 . The effective viscous coefficient arising due to the KH induced turbulence is thus significantly smaller in the presence of in-plane magnetic field.

Chapter 3

Interplay of Kelvin Helmholtz and Kink Modes: 3D Studies

In the previous Chapter, we have studied velocity shear driven Kelvin Helmholtz (KH) instability, which lies in the two dimensional plane of flow and shear. Perturbations were confined in this plane with no spatial variations along the normal direction which is also the direction of magnetic field (generated due to 2D sheared flow). However, in three dimensional regime of instability, in addition to KH mode, a new mode also exists in the plane of magnetic field and shear. This is a local mode, known as kink mode. In this Chapter, the interplay of these two modes has been studied for simple sheared flow case, as well as for the case when an external magnetic field also exists. The studies have been carried out extensively in linear and nonlinear regimes.

3.1 Introduction

As we know that the EMHD model closely resembles the behaviour of neutral incompressible hydrodynamic fluid, with the additional characteristic traits associated with the magnetized electron fluid flow dynamics. The magnetized character of the electron fluid essentially introduces (i) intrinsic natural length scales, e.g. electron skin depth and (ii) an oscillatory dispersive whistler mode in the system. The EMHD model thus provides an interesting paradigm for studying spectral cascade and turbulent features, associated with nonlinearity, in a medium which contains special scales as well. For instance, the presence and/or absence of whistler effect on spectral cascade have continued to be debatable in this regard. It should be noted that the flow of electrons automatically has associated with it an ambient magnetic field. Thus, the possibility of whistler mode excitation exists, if one permits variations along the direction of such a magnetic field. For a sheared electron velocity flow, the associated magnetic field is directed orthogonal to the 2D plane of shear and flow. The study of velocity shear instability, with variations confined in the 2D plane of shear and flow, therefore, does not get plagued by the whistler modes. In the previous Chapter, we had specifically added an external magnetic field along the flow direction and had studied its implication due to whistlers on the 2D mode (with variations confined in the plane of flow and shear termed as the pure sausage mode, see Fig. 3.1(a)) of the velocity shear driven instability. The study showed the reduction and complete vanishing of the growth rate of the instability with increasing strength of the external magnetic field aligned along the flow direction. The flow perturbations associated with the sausage mode had to overcome the whistler oscillatory mode for growth. Basically

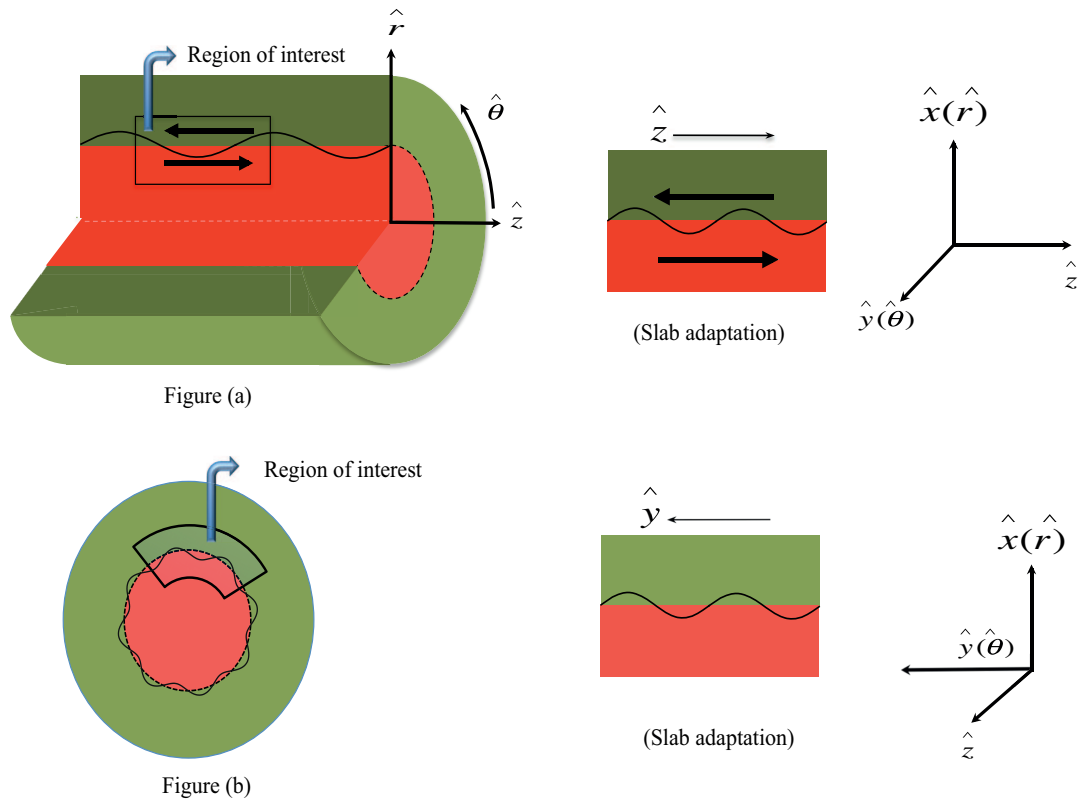


Figure 3.1: A schematic diagram showing the pure sausage (subplot (a)) and pure kink (subplot (b)) perturbations.

the flow perturbations had to bend the magnetic field lines which becomes difficult with its increasing strength. Thus, in the 2D case, there exists a threshold magnitude of the external magnetic field beyond which the sheared electron flow was unable to excite the instability. When perturbations perpendicular to the plane of flow and shear are permitted, but with no variation along the flow direction, a new mode turns up which we term as the pure kink mode as shown in Fig. 3.1(b).

In our studies presented in this Chapter, we permit full three dimensional perturbations that would include both the modes i.e. sausage and kink in the

Chapter 3: Interplay of Kelvin Helmholtz and ...

system (modes having general perturbations are termed as mixed modes). The interplay of these two modes under various physical conditions has been extensively studied here. The pure kink mode having no variations along flow direction may not be affected by the addition of an external magnetic field along the flow direction. We investigate and confirm this with our 3D studies here. However, the magnetic field along the flow direction may change the growth rate of mixed modes. In addition, we also employ an external magnetic field along the direction normal to plane of flow and shear. This magnetic field may change the growth rate of pure kink mode and may not affect the pure sausage mode. We try to understand the role of this magnetic on the two modes of instability. The nonlinear state of instability in three dimensions is strongly turbulent due to the direct cascade of power, unlike the inverse cascade in 2D. We also carry out the simulations to understand the spectral cascade features with and without an external magnetic field present along the flow direction in the nonlinear regime of instability. The spectral cascade is expected to be anisotropic due to the presence of whistlers and the flow along the preferred directions.

The Chapter has been organized as follows. In section 3.2 we briefly introduce the model and the equilibrium configuration of the system. Section 3.3 contains linear instability analysis for specific equilibrium flow profiles (a step profile and a tangent hyperbolic profile) for our studies in the presence of external magnetic field. Section 3.4 contains the results of the nonlinear simulations. We provide the comparisons of the growth rates from linear theory with the growth rates measured in the linear regime of the simulations. We also briefly comment on the spectral power cascade features in the presence of external magnetic field. Section 3.5 summarizes the studies presented in the Chapter.

3.2 Model and Governing Equations

We rewrite the normalized EMHD equations (1.1) and (1.2) as below,

$$\begin{aligned}\frac{\partial}{\partial t}(\nabla^2 \vec{B} - \vec{B}) &= \vec{\nabla} \times [\vec{v} \times (\nabla^2 \vec{B} - \vec{B})] \\ \vec{v} &= -\vec{\nabla} \times \vec{B}\end{aligned}\tag{3.1}$$

These equations have been obtained from the combined set of electron fluid equations and Maxwell's equations under the approximation of ions being static and providing a neutralizing background and ignoring the displacement current and electron density fluctuations, which would occur at the electron plasma period. The first equation represents the evolution of generalized vorticity $\vec{\nabla} \times \{\vec{v} - \vec{A}\} = \nabla^2 \vec{B} - \vec{B}$ and is obtained by taking the curl of electron momentum equation and making use of Faraday's law. Second equation is Ampere's law in which displacement current has been ignored (under EMHD assumption). Here, the length scale has been normalized by electron skin depth $d_e = c/\omega_{pe}$, magnetic field by a typical magnitude concerning any problem, e.g. B_N , the time has been normalized by the electron cyclotron period corresponding to the normalizing magnetic field B_N .

We consider an equilibrium electron flow velocity with a sheared configuration of the form, $\vec{v}_0(x) = v_0(x)\hat{z}$. This electron flow, directed along \hat{z} axis, is sheared along the x axis. The 2D $x - z$ plane forms the flow-shear plane of the equilibrium electron velocity distribution. Since the electron flow also constitutes a current in the system, corresponding to this flow, there exists an equilibrium magnetic field along \hat{y} , the third dimension, which can be obtained by integrating the relationship $dB_0/dx = -v_0(x)$ (thus $B_0(x) = -\int^x v_0(x)dx + C_0$). In addition to this

self consistent magnetic field, in our studies we have also considered the presence of an external homogeneous magnetic field $B_{00}\hat{z}$ along the flow direction for our equilibrium. We now linearize Eqs. (3.1) around this equilibrium to study its stability. The Fourier transform along y and z coordinates and time variable of the linearized set of equations leads to the following coupled set of equations,

$$\frac{d^2 B_{x1}}{dx^2} - (1 + k^2)B_{x1} = \frac{k_y(v_0' + B_0)v_{x1}}{\bar{\omega}} + \frac{k_z B_{00}v_{x1}}{\bar{\omega}} \quad (3.2)$$

$$\frac{d^2 v_{x1}}{dx^2} - (1 + k^2)v_{x1} + \frac{B_{x1}}{a} + \frac{k_z(v_0'' - v_0)}{\bar{\omega}}v_{x1} + \frac{(k_y B_0 + k_z B_{00})}{\bar{\omega}a}v_{x1} = 0 \quad (3.3)$$

Here, $a = \bar{\omega}/[k_y(v_0' + B_0) + k_z B_{00}]$, $\bar{\omega} = \omega - k_z v_0$ and $k^2 = k_y^2 + k_z^2$. It should be noted that in Eqs. (3.2) and (3.3), v_0 and B_0 are functions of x , whereas B_{00} appears as a constant parameter. The instability of the equilibrium has been analyzed in the next section by evaluating the eigen value ω for the combined set of Eqs. (3.2,3.3) for given specific forms of the equilibrium flow profiles.

3.3 Linear Instability

In this section, we analyze the coupled linearized Eqs. (3.2) and (3.3) obtained in the previous section to understand the role of the presence of the external B_{00} on the 3D instability. We mention here that we would term modes with finite k_y and with $k_z = 0$ as the pure kink modes. Those with finite k_z , and with $k_y = 0$ as the pure sausage modes of the system. Modes with both k_y and k_z as finite are the mixed modes. The terms sausage and kink used here are in analogy with the perturbations of a cylindrical plasma column in the context of MHD. The form of

perturbations for two modes in cylindrical geometry and their representation in the slab geometry has been shown with the help of a schematic diagram in Fig. 3.1. We first present the local stability analysis by assuming that the perturbation length scales are smaller than the shear scale length.

3.3.1 Local Analysis

Assuming that the perturbation scales are smaller than the equilibrium scales, we take the Fourier transform of Eqs. (3.2) and (3.3) also along x direction and obtain the dispersion relation as follows:

$$2\bar{\omega}(1 + k_0^2) = (v_0'' - v_0)k_z \pm \{(v_0'' - v_0)^2 k_z^2 - 4[k_y(v_0' + B_0) + k_z B_{00}][k_y v_0' - k_0^2(k_y B_0 + k_z B_{00})]\}^{1/2} \quad (3.4)$$

Here $k_0 = (k_x^2 + k_y^2 + k_z^2)^{1/2}$. The above dispersion relation predicts the possibility of instability when the discriminant $D = -4[k_y(v_0' + B_0) + k_z B_{00}][k_y v_0' - k_0^2(k_y B_0 + k_z B_{00})] + (v_0'' - v_0)^2 k_z^2 < 0$. It is clear that for $v_0' = 0$ and/or $k_y = 0$, D is always positive. It shows that the variations perpendicular to the plane of flow and shear (*i.e.* k_y finite) along with a finite value of v_0' is essential for any local instability to exist. Furthermore, the existence of a finite in-plane magnetic field B_{00} does not influence the growth rate of pure kink modes for which $k_z = 0$. When both k_y and k_z are finite, the growth rate diminishes with increase in B_{00} as the expression for the discriminant clearly suggests.

It can be shown that in various simplified limits, the local dispersion relation reduces to well known forms:

Chapter 3: Interplay of Kelvin Helmholtz and ...

- Case (i): Choosing $B_{00} = 0$ the dispersion relation reduces to,

$$2\bar{\omega}(1 + k_0^2) = (v_0'' - v_0)k_z \pm \{(v_0'' - v_0)^2 k_z^2 - 4k_y^2(v_0' + B_0)(v_0' - k_0^2 B_0)\}^{1/2} \quad (3.5)$$

This matches with the dispersion relation of Jain *et al.* [46] obtained earlier.

- Case (ii): For $k_y = 0$ and $B_{00} = 0$, the dispersion relation reduces to the local dispersion relation obtained by us earlier [34] in the context of 2D sausage modes.
- Case (iii): For $v_0 = v_0' = v_0'' = 0$ we obtain,

$$\omega = \frac{(k_y B_0 + k_z B_{00})k_0}{(1 + k_0^2)} \quad (3.6)$$

the dispersion relation for the whistler waves.

It is clear that in the presence of 3D perturbations, local unstable modes exist for a sheared electron flow configuration.

3.3.2 Nonlocal Analysis: tanh-profile

We now consider the general case where the perturbation scales can be extended. In this case it will not be possible to take the Fourier transform along the sheared direction of x . The eigen modes in this case sense the extended profile of the velocity shear. The growth rate of instability has to be obtained as an eigen value of the solution of ordinary differential equation. We have considered a specific tangent hyperbolic shear flow profile for the purpose of our studies *i.e.*, $v_0(x) = V_0 \tanh(x/\epsilon)$, where 2ϵ is typically the width of shear region around $x = 0$ and

$|V_0|$ is the asymptotic magnitude of the fluid flow far from the shear region. The corresponding equilibrium magnetic field can be obtained by integrating Ampere's law,

$$B_0(x) = -V_0\epsilon \log \cosh(x/\epsilon) + C_0 \quad (3.7)$$

Here, C_0 is the constant of integration and represents a uniform magnetic field along \hat{y} direction. We have made use of two coupled linearized Eqs. (3.2) and (3.3) to evaluate the eigen values numerically. The magnitude of the external magnetic field B_{00} along the flow direction as well as the value of C_0 has been varied to study their role on the instability.

Our linear studies indicate that the dominance of pure sausage and/or kink mode gets determined by the following three factors, (i) the comparison of shear scale ϵ of the flow with the electron skin depth. For sharper shear scales, the sausage growth rates are higher. (ii) the addition of B_{00} along the flow direction reduces the sausage growth rate as for the sausage configuration extra energy is now required to bend the field lines of B_{00} . This field, however, does not influence the kink growth rates. (iii) The addition of C_0 , a uniform magnetic field along the third dimension (perpendicular to the plane of flow and shear), similarly reduces the kink growth rate and has no influence on sausage mode.

In Fig. 3.2(a), we show the surface plot of the growth rate as a function of $k_z\epsilon$ and $k_y\epsilon$ for $B_{00} = 0$ and $C_0 = 0$. This plot corresponds to $\epsilon = 0.3$, *i.e.* the shear scale is about 1/3 of the skin depth. For this particular value of skin depth, the maximum growth rate of the sausage mode is almost comparable with that of the maximum growth rate of the kink mode. This has been clearly illustrated in the line plots of Fig. 3.2(b) for which the growth rate plot as a function of $k_z\epsilon$ is shown

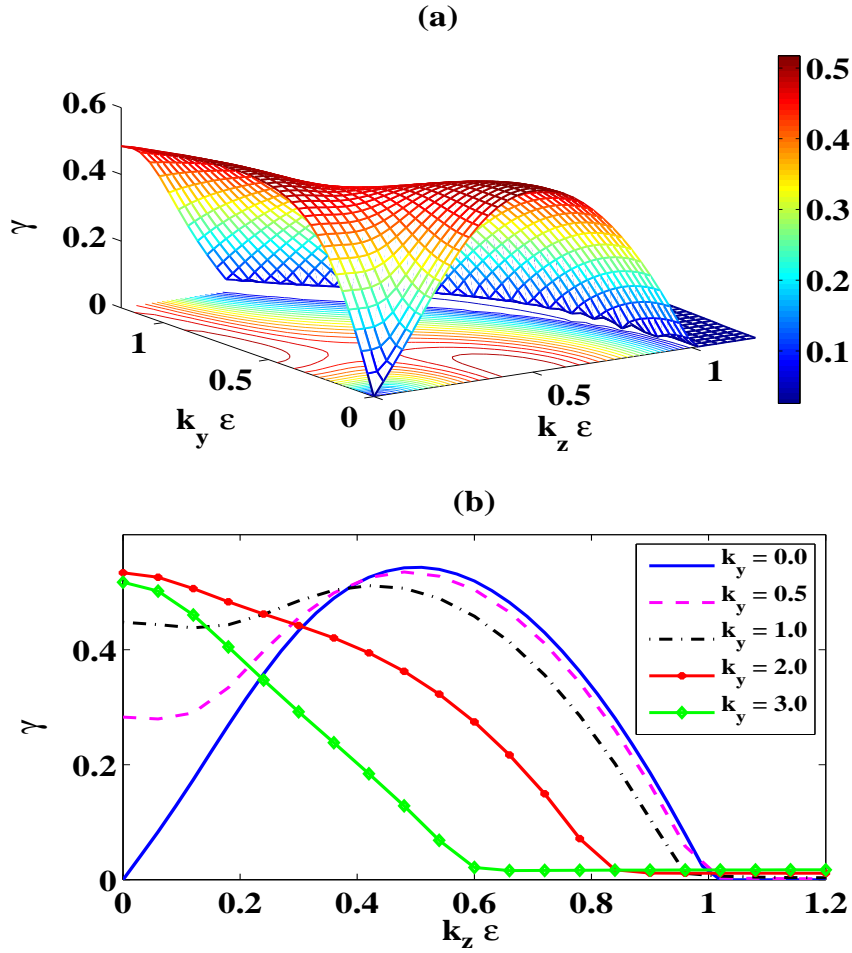


Figure 3.2: The subplot (a) shows the surface plot of the growth rate for the tangent hyperbolic velocity shear profile $\vec{v}_0(x) = \hat{z}V_0 \tanh(x/\epsilon)$ as a function of $k_z \epsilon$ and $k_y \epsilon$ for $B_{00} = 0$ and $C_0 = 0$. For this case $V_0 = 1.0$ and $\epsilon = 0.3$. In subplot (b) of the figure the same data for growth rate has been shown as a function of $k_z \epsilon$. The various curves show different values of k_y . For this case the kink growth rate for $k_y = 2, k_z = 0$ (equal to 0.52) is almost identical to the maximum growth rate of the sausage mode at $k_z \epsilon = 0.5, k_y = 0$ (equal to 0.54).

for various values of k_y . It should be noted that for this case, the maximum of the kink growth rate occurring for $k_y = 2, k_z = 0$ is almost identical to the maximum growth rate of the sausage mode at $k_z \epsilon = 0.5, k_y = 0$. When ϵ is decreased below

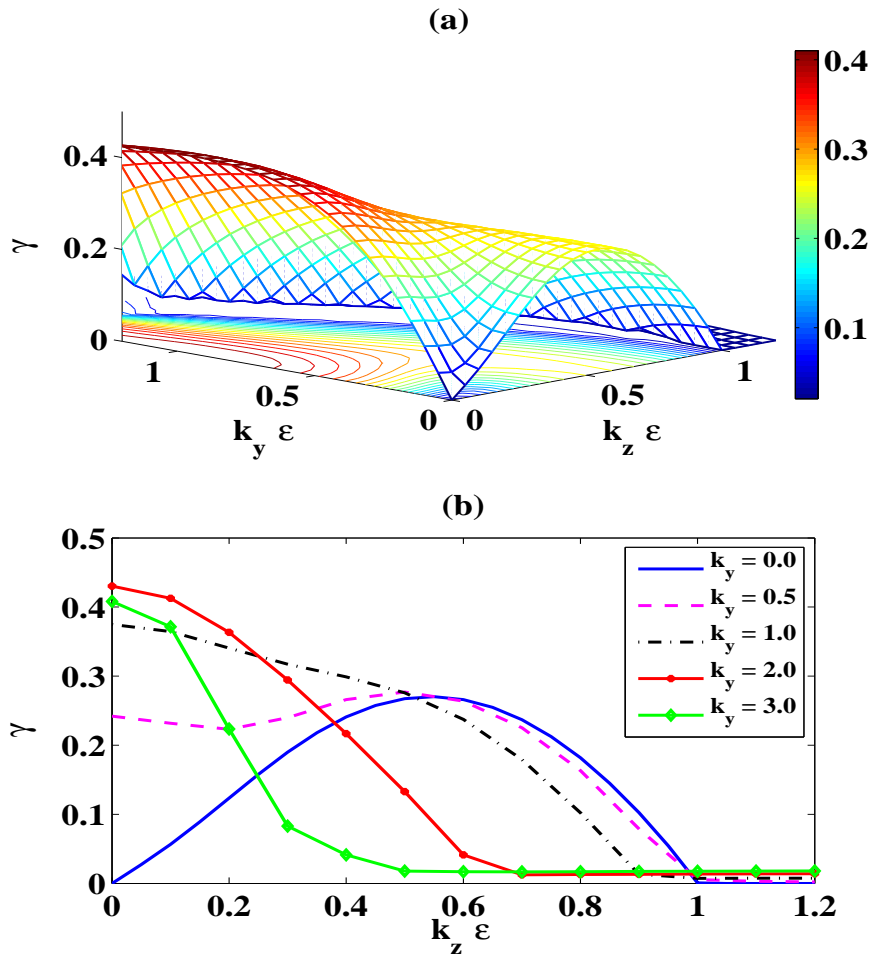


Figure 3.3: The subplot (a) shows the surface plot of the growth rate for the tangent hyperbolic velocity shear profile $\vec{v}_0(x) = \hat{z}V_0 \tanh(x/\epsilon)$ as a function of $k_z \epsilon$ and $k_y \epsilon$ for $B_{00} = 0$ and $C_0 = 0$. For this case $V_0 = 1.0$ and $\epsilon = 0.5$. In subplot (b) of the figure the same data for growth rate has been shown as a function of $k_z \epsilon$. The various curves show different values of k_y . For this case the kink growth rate for $k_y = 2, k_z = 0$ (equal to 0.43) is higher than the maximum growth rate of the sausage mode at $k_z \epsilon = 0.5, k_y = 0$ (equal to 0.27). The pure kink mode clearly dominates for this case.

the value of 0.3 we observe that the sausage growth rate dominates. However, for a higher value of ϵ , say $\epsilon = 0.5$, the growth rate corresponding to the kink modes dominate the system as can be seen from the plots of Fig. 3.3.

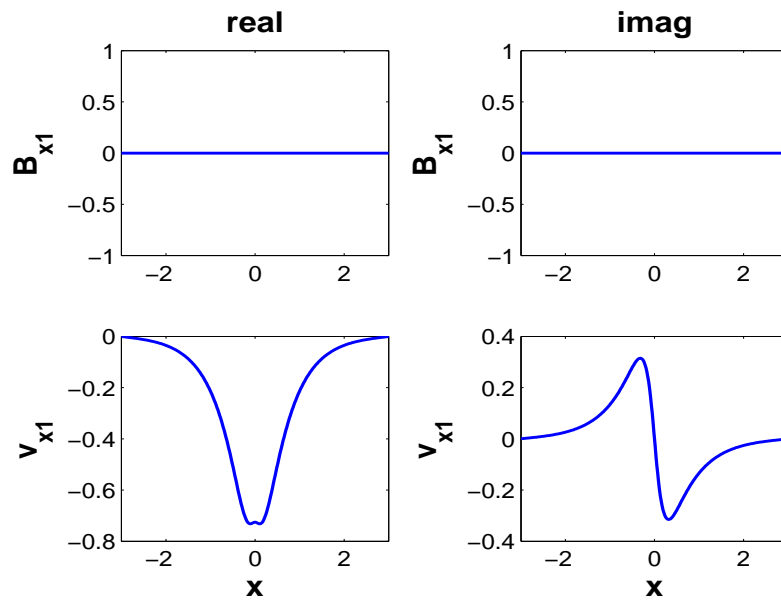


Figure 3.4: Plot of the eigen functions of pure sausage mode ($k_y = 0$). The other parameter values are $V_0 = 1.0$, $\epsilon = 0.3$, $k_z = 1.7$, $B_{00} = 0.0$ and $C_0 = 0.0$.

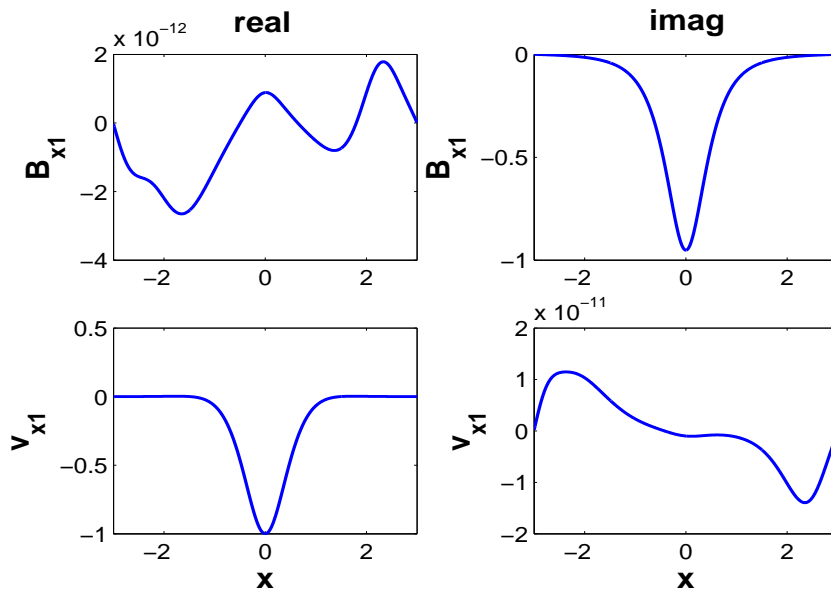


Figure 3.5: Plot of the eigen functions of pure kink mode ($k_z = 0$). The other parameter values are $V_0 = 1.0$, $\epsilon = 0.3$, $k_y = 2.0$, $B_{00} = 0.0$ and $C_0 = 0.0$.

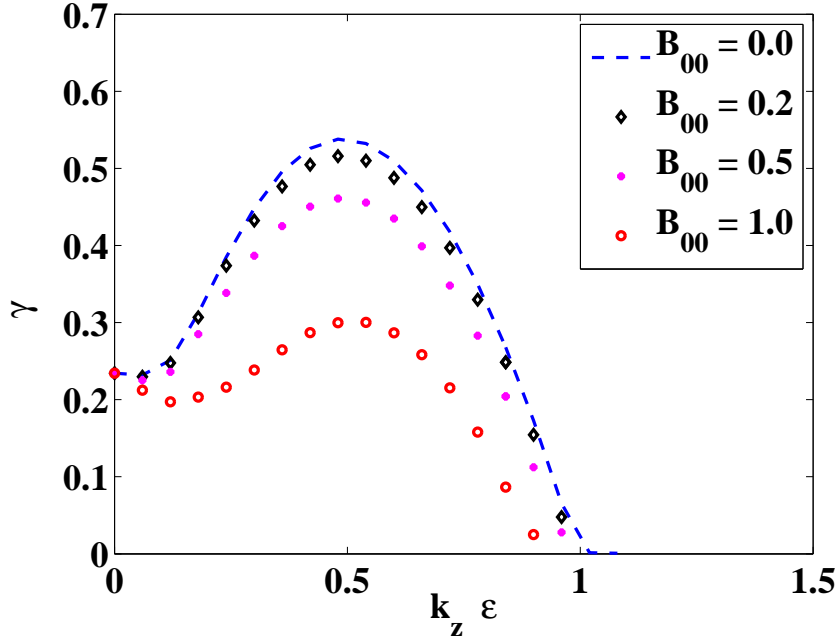


Figure 3.6: Variation of growth rate with $k_z \epsilon$ for different values of uniform magnetic field B_{00} along flow direction. The various parameters for this case are $V_0 = 1.0$, $C_0 = 0$, $\epsilon = 0.3$ and $k_y = 0.4$. The growth rate decreases as the value of B_{00} increases.

The eigen functions for pure sausage mode (*i.e.* $k_y = 0$ and k_z finite) are shown in Fig. 3.4. We can see that there is no structure in B_{x1} while, v_{x1} has a localized structure in x . The two linearized equations get decoupled in this case for $B_{00} = 0$ and the field B_{x1} assumes a trivial solution. Whereas, for pure kink mode (k_y finite and $k_z = 0$), both B_{x1} and v_{x1} are finite as can be observed in Fig. 3.5.

We next study the case when a uniform magnetic field B_{00} along the flow direction is added. It can be observed from Fig. 3.6 that for increasing values of B_{00} the sausage growth rate decreases consistently. However, the growth rate of the kink mode $k_z = 0$, and finite k_y does not get influenced by this magnetic field. It is clear from this figure (Fig. 3.6) as well as from Fig. 3.7, where the growth

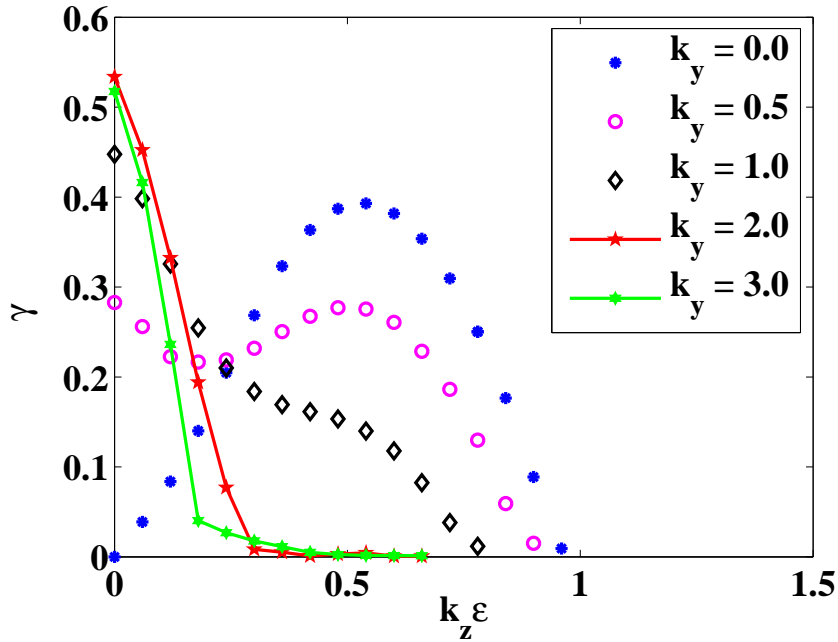


Figure 3.7: Variation of growth rate as a function of $k_z \epsilon$ for the case $B_{00} = 1.0$ with $V_0 = 1.0$, $C_0 = 0$ and $\epsilon = 0.3$. The various curves correspond to different values of k_y . For this case the kink growth rate for $k_y = 2, k_z = 0$ (equal to 0.52) is higher than the maximum growth rate of the sausage mode at $k_z \epsilon = 0.5, k_y = 0$ (equal to 0.39). The pure kink mode clearly dominates in this case.

rate plots for various k_y has been shown, that the kink growth in this case can significantly dominate the sausage growth. This is physically understandable as the 3D kink related perturbations do not cause the bending of the magnetic field lines associated with B_{00} , whereas the sausage perturbations do have to bend these lines. Thus, from energy point of view the kink perturbations can dominate even though the shear scale length ϵ is sharp when the value of B_{00} is increased. On the other hand when C_0 , which corresponds to a uniform magnetic field along the \hat{y} , is chosen to be finite, the growth rate of kink mode reduces significantly. Whereas, the sausage mode thrives irrespective of the value of C_0 . This can be seen from the plots of Fig. 3.8.

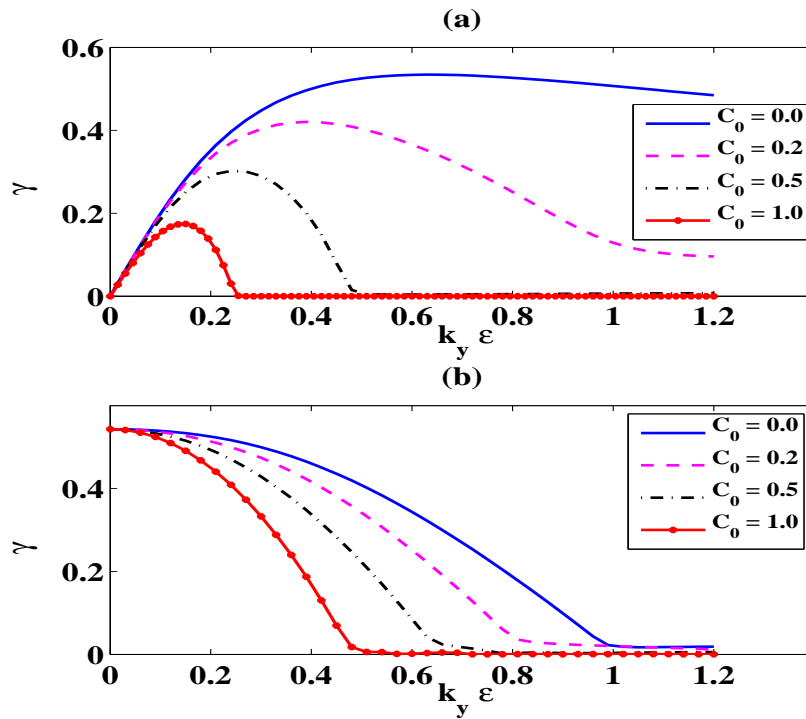


Figure 3.8: The variation of growth rate as a function of $k_y \epsilon$ has been shown in subplot (a) for $k_z = 0$ *i.e.* pure kink modes and in subplot (b) for the value of $k_z = 1.7$. The different curves correspond to the different values of C_0 in two subplots. The other parameters are $V_0 = 1.0$ $B_{00} = 0$ and $\epsilon = 0.3$. It is clear from the two subplots that as the value of C_0 is increased the growth rate of kink consistently drops down whereas the pure sausage growth rate is not influenced by this field.

It would be interesting to see how these factors (predominance of one mode over the other in various situations) figure in the nonlinear evolution of a 3D system. We present the results of the nonlinear evolution in the next section.

3.4 Nonlinear Simulations

The components of the evolution Eqs. (3.1) can be expressed in the form of generalized continuity equations with source terms. The components have been evolved

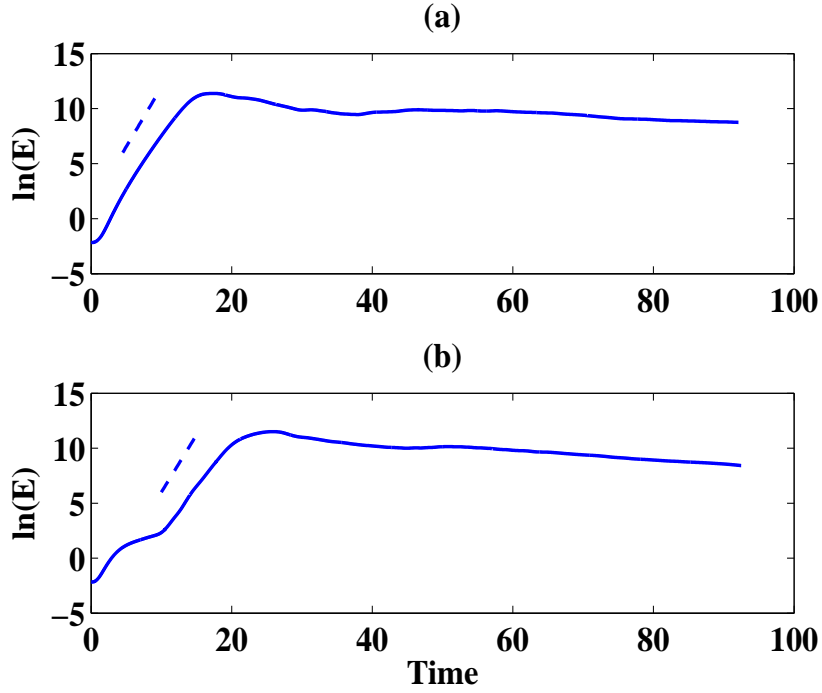


Figure 3.9: The evolution of perturbed energy with $V_0 = 1.0$, $C_0 = 0$ and $\epsilon = 0.3$ for $B_{00} = 0.0$ and $B_{00} = 1.0$ has been shown in subplots (a) and (b) respectively. The dashed lines shown alongside are having the slope equal to $2\gamma_i$, where γ_i is the growth rate of the maximally growing mode in the system. In subplot (a) the slope corresponds to growth rate of pure sausage mode (with $\gamma_i = 0.54$) whereas, in subplot (b) the slope corresponds to the growth rate of pure kink mode (with $\gamma_i = 0.52$) which is the maximally growing mode in the system for this case.

in slab geometry using the flux corrected scheme of Boris *et. al.* [75]. A suite of subroutine for solving such generalized continuity equations are available as a package known as LCPFCT [74]. This has been adapted suitably for our system of equations. At each time step one evolves $\nabla^2 \vec{B} - \vec{B}$ first and then employs a Helmholtz solver to solve for \vec{B} at the updated time. The updated electron velocity is obtained from the relationship $\vec{v} = -\nabla \times \vec{B}$, which is then used to evolve $\nabla^2 \vec{B} - \vec{B}$ at the next step. The evolution of total energy was tracked throughout the time of evolution to ascertain the accuracy. We observe that the numerical

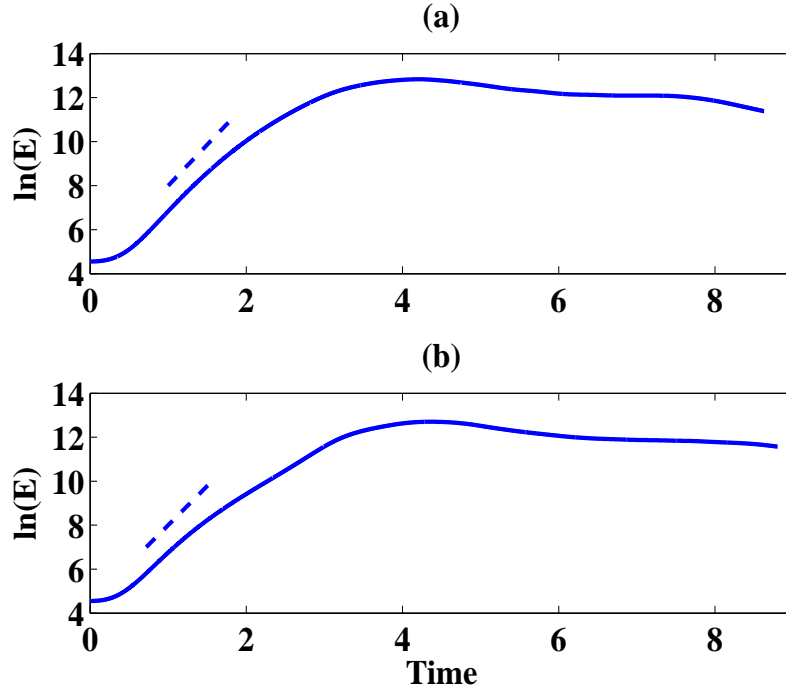


Figure 3.10: The evolution of perturbed energy with $V_0 = 1.0$, $C_0 = 0$ and $\epsilon = 0.1$ for $B_{00} = 0.0$ and $B_{00} = 1.0$ has been shown in subplots (a) and (b) respectively. The dashed lines shown alongside are having the slope equal to $2\gamma_i$, where γ_i is the growth rate of the maximally growing mode in the system. For two cases the values of γ_i are equal to 1.85 and 1.78 for subplots (a) and (b) respectively. The maximally growing mode for two cases is pure sausage mode.

variation of total energy is $(\Delta E_{tot}/E_{tot}) \sim \mathcal{O}(10^{-6})$ in the linear regime whereas the change in the perturbed energy $(\Delta E_p/E_{tot}) \sim \mathcal{O}(10^{-3})$. The initial condition was chosen as the sheared electron velocity flow equilibrium of the tangent hyperbolic form, $\vec{v}_0 = \hat{z}V_0 \tanh(x/\epsilon)$. This translates to the initial condition for the magnetic field of the form,

$$\vec{B}_0 = -V_0\epsilon \log [\cosh(x/\epsilon)] \hat{y} + C_0\hat{y} \quad (3.8)$$

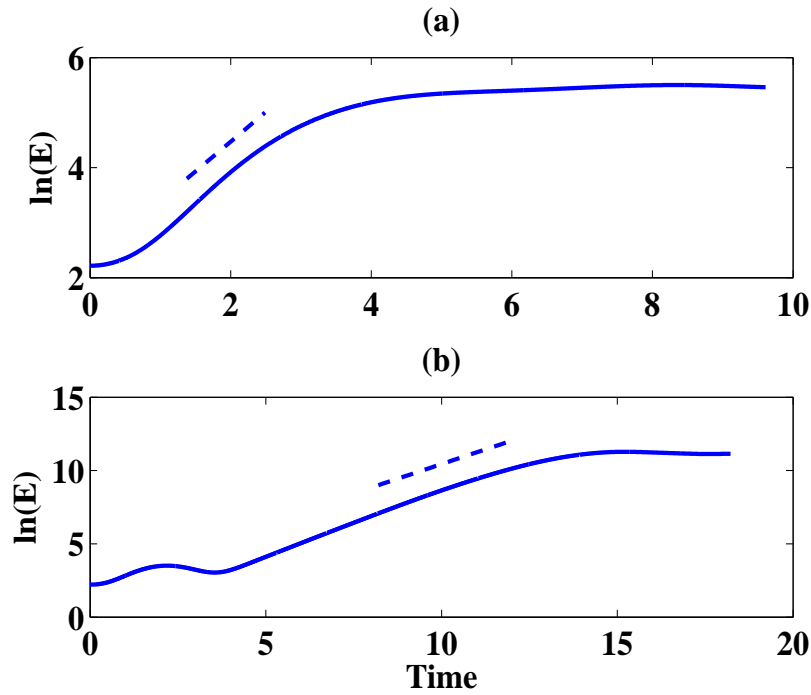


Figure 3.11: The evolution of perturbed energy with $V_0 = 1.0$, $C_0 = 1.0$ and $\epsilon = 0.3$ for $B_{00} = 0.0$ and $B_{00} = 1.0$ has been shown in subplots (a) and (b) respectively. The dashed lines shown alongside are having the slope equal to $2\gamma_i$, where γ_i is the growth rate of the maximally growing mode in the system. For two cases the values of γ_i are equal to 0.54 and 0.39 for subplots (a) and (b) respectively. Here again the maximally growing mode for two cases is pure sausage mode.

We have also often chosen an additional uniform magnetic field $B_{00}\hat{z}$ along the flow direction. The presence of this magnetic field does not disturb the equilibrium flow. However, a finite $B_{00}\hat{z}$ influences the linear growth rate of the system as we saw in our linear analysis. Here, we have studied the role of this magnetic field along with C_0 on the nonlinear state.

The evolution of perturbed energy has been shown in Fig. 3.9 for the case of $\epsilon = 0.3$ and $C_0 = 0$ in subplot (a) for $B_{00} = 0.0$ and in subplot (b) for $B_{00} = 1.0$ respectively, depicted by the solid lines. The perturbed energy shows a linear rise in the semilog plot initially. This corresponds to the linear growth rate regime.

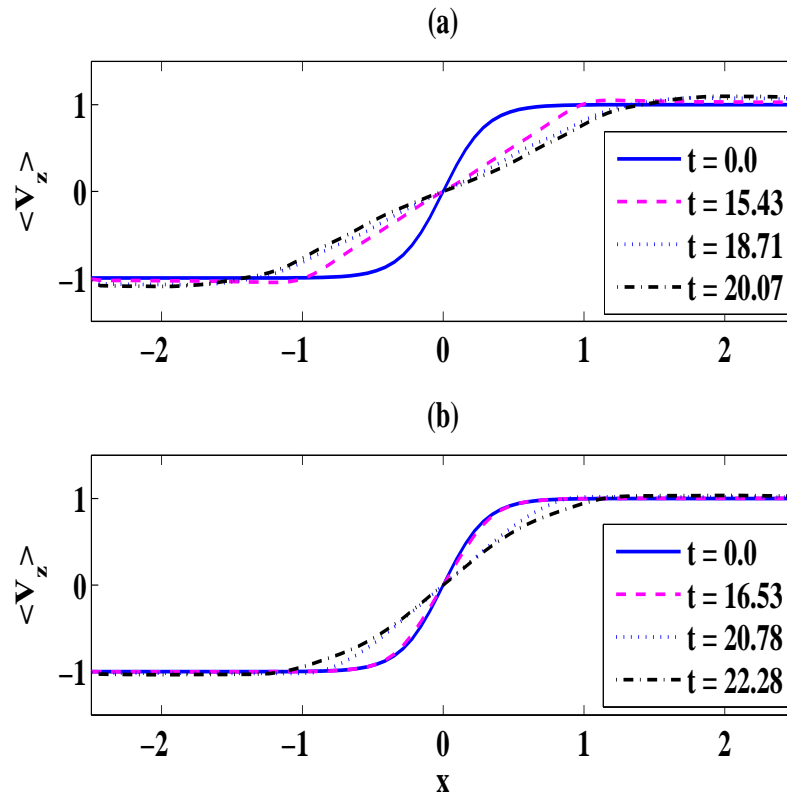


Figure 3.12: The plot of averaged electron flow velocity profile at various times for $B_{00} = 0.0$ and $B_{00} = 1.0$ in subplots (a) and (b) respectively. The values of the other parameters have been chosen to be same as in Fig. 3.9. The flattening of shear profile is weaker for finite B_{00} case.

We observe that the slope of the dashed lines drawn along side for the two cases matches with twice of the maximally growing mode corresponding to it. While for (a) the sausage mode has the maximum, for (b) it is the kink mode. The energy is observed to saturate subsequently when the perturbations acquire a nonlinear amplitude. Further, it is interesting to see that for another plot in Fig. 3.10 with $\epsilon = 0.1$, the sausage mode dominates in both cases of $B_{00} = 0.0$ and $B_{00} = 1.0$. In addition, in Fig. 3.11, C_0 is chosen to be finite for the case of $\epsilon = 0.3$. Here again the sausage mode dominates for both cases of $B_{00} = 0.0$ and $B_{00} = 1.0$.

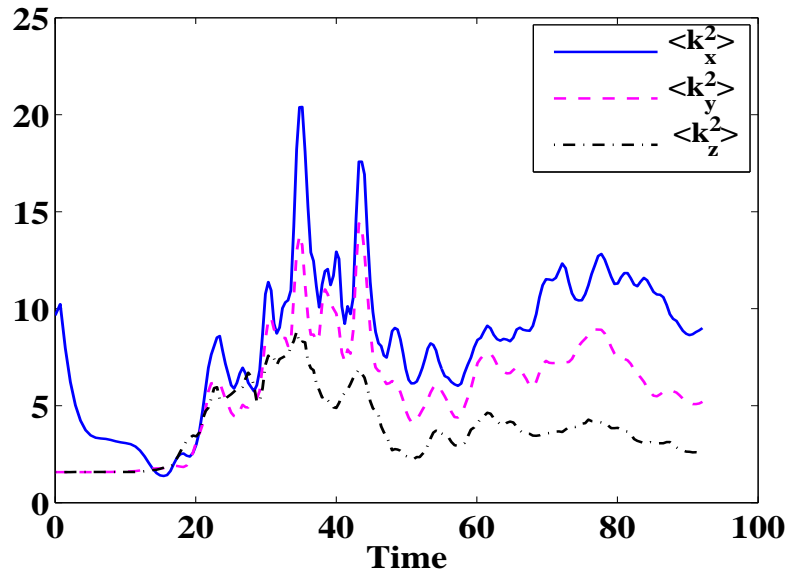


Figure 3.13: Evolution of average wave-numbers in different directions for $B_{00} = 0.0$. The values of the other parameters have been chosen to be same as in Fig. 3.9.

It is often of importance to know the process of nonlinear broadening of the shear layer in the presence of these unstable modes. The nonlinear broadening of the shear layer provides the information on the effective anomalous viscosity for the system in the nonlinear regime of the instability. We show the evolution of the mean flow profile with time in Fig. 3.12 for the two cases (a) and (b) of Fig. 3.9. It is observed that the broadening occurs much more slowly when the system evolution is governed by the kink like mode than that of the sausage mode. This can be understood by realizing that during the linear phase, the kink mode does not alter the 2D flow structure. Thus, the broadening occurs for this case only at a later phase when the nonlinear phase sets in and energy starts to trickle in the other modes as well. This is corroborated by studying the time at which the profile gets broadened in the two subplots.

For a 2D EMHD system, typically, one encounters inverse cascade of energy

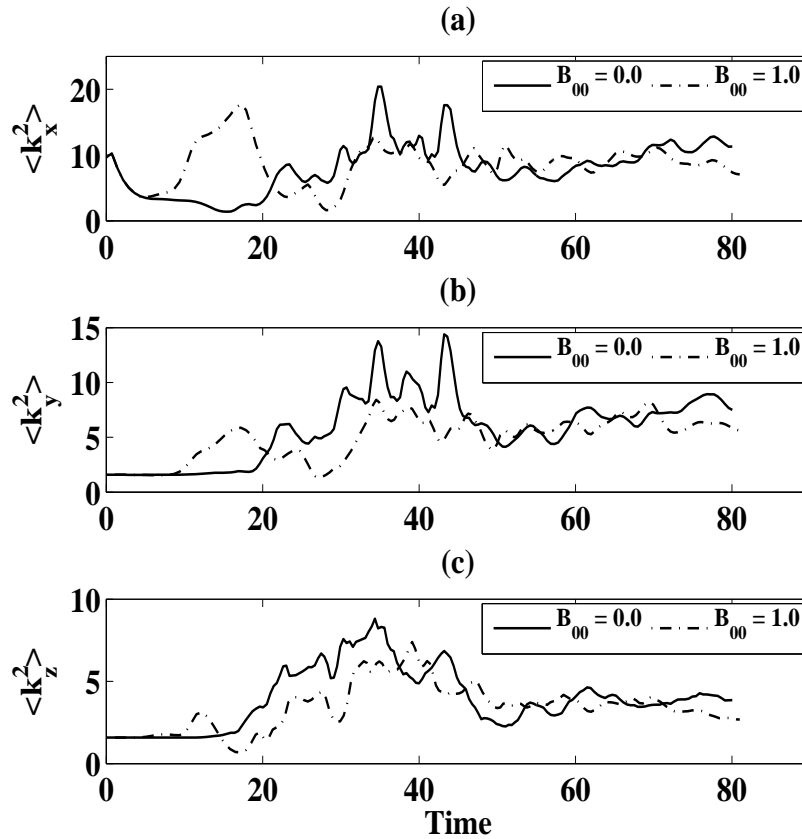


Figure 3.14: Evolution of average wave-numbers in three different directions has been shown in three different subplots in comparison for two cases $B_{00} = 0.0$ and $B_{00} = 1.0$. The values of the other parameters have been chosen to be same as in Fig. 3.9.

and the final state comprises of ordered vortex flow patterns. However, in the presence of additional external uniform fields, short scale structures were observed to get formed in 2D [80]. Here, we investigate the behaviour of the spectrum in the nonlinear regime of the KH instability in 3D with and without external magnetic field. The plot of Fig. 3.13 shows the evolution of the average wavenumber along the three directions. The evolution of average wavenumber, along all the three directions, shows a sudden rise and then a steady slow decay which eventually

shows a saturation. It is observed that the average value of the wavenumber is typically highest along the direction of shear \hat{x} ; along \hat{z} , the directions of flow and \hat{y} , the direction of the magnetic field associated with flow, the scales are in general longer in the nonlinear regime. It appears, therefore, that both the presence of flow and magnetic field inhibits the process of direct cascade of spectrum towards higher wavenumbers. This leads to significant anisotropization of the spectrum.

In the presence of B_{00} , we observe that the evolution of the typical scale along the \hat{x} (shear direction) remains more or less unaltered. This can be seen from the plot of Fig. 3.14. However, the scales along the other two directions turn out to be longer when B_{00} is finite than when it is chosen to be zero. These results are in conformity with the whistler wave mediated spectral cascade features presented in references [72, 73].

3.5 Summary

The study of electron velocity shear driven instability in EMHD (Electron Magnetohydrodynamics) regime in three dimensions has been carried out. The instability is non - local in the plane defined by the flow direction and that of the shear and is the familiar Kelvin - Helmholtz (KH) mode which has often been termed as the sausage mode in the context of Electron Magnetohydrodynamics flows. On the other hand a local instability with perturbations in the plane of shear and the magnetic field exists which has been referred as kink mode. The addition of an external magnetic field along the shear flow direction has been shown earlier to stabilize the sausage modes in 2D. We have shown here that the kink modes remain uninfluenced by this magnetic field and hence can be the pertinent fastest growing mode in such a scenario. It is also shown that the addition of external

Chapter 3: Interplay of Kelvin Helmholtz and ...

magnetic field along the ambient magnetic field direction generated by the flow (e.g. perpendicular to shear and flow direction) reduces the kink mode but the sausage growth remains unaltered by it. The nonlinear evolution confirms these observations.

We also observe that the spectral cascade towards shorter scales in 3D gets inhibited both along the flow as well as along the direction of magnetic field. Thus the shortest scales are found along the shear direction, while in the other two directions, one observes scales which are typically longer. This is consistent with an earlier work where it was shown that the spectral cascade is typically mediated by the whistler wave.

Chapter 4

Stability of Isichenko Solutions of Electron Magnetohydrodynamic Model Against Shear Driven Modes

The studies on velocity shear driven Electron Magnetohydrodynamics (EMHD) instability in the previous Chapters, have shown that the instability is nonlocal, if the variations lie in the plane of flow and shear. This is usual Kelvin Helmholtz mode, often termed as sausage mode in EMHD. Besides the KH mode, a local mode with perturbations in the plane of magnetic field and shear is also known to exist, which is termed as the kink mode. In this Chapter, we analyze these instability processes for the exact nonlinear solutions of EMHD equations in the form of monopolar and dipolar magnetic field structures obtained by Isichenko et al. [51].

4.1 Introduction

The coherent structures play an important role in governing transport properties of a system. The presence of these structures is believed to be the cause of phenomena of intermittency in turbulence. The coherent structures can be described as the exact solutions of the nonlinear fluid equations. The studies on transport, stability and interaction processes of these structures provide an understanding of their role in the turbulence. The EMHD equations in 2D permits certain exact, nonlinear electron flow solutions. These solutions were obtained by Isichenko and Marnachev as the isolated, coherent structures [51]. The first variety of solutions are the rotating electron currents giving rise to monopolar magnetic fields. These monopolar solutions are radially symmetric and stationary solutions. The other variety includes the electron currents producing bipolar magnetic fields. These dipolar solutions are radially non-symmetric and propagate with constant speed in their axial direction.

In their work, Isichenko et al. have obtained analytical conditions for the existence of exact nonlinear localized solutions of EMHD equations in two dimensions. They also carried out the stability analysis and have shown that the solutions are stable. The propagation and interaction characteristics of such EMHD solutions in a homogeneous plasma have been studied by Das [55] and later by Dastgeer [56] in 2D. They observe structures to be fairly robust and stable. Various interaction processes amidst monopoles and dipoles have also been studied by them and a qualitative understanding of the observations has been provided on the basis of point vortex model (PVM). Subsequent studies in 2D by Sharad et al. [76] on propagation of such structures in an inhomogeneous plasma illustrate interesting

adjustments in shapes. However, the overall integrity of the structures is found to remain preserved in such simulations.

While the monopolar solutions represent static electron current pulse in plasma, the dipolar solutions can be looked upon as propagating current pulses. They thus mock up a translating current pulse in which the central region carries a forward current (along the direction of propagation) and the outer region carries a reverse current surrounding the forward current, a situation of practical relevance in various scenarios. For instance, in the case of fast ignition scenario [5, 6], the hot electrons generated by the lasers at the critical density surface move towards the dense core and generate the return shielding current in background electrons to maintain the charge neutrality. This configuration is subjected to the Weibel and tearing instabilities. Due to these processes the current filaments are formed which self-organize through the coalescence process and finally result in few cylindrical current channels in which the return current surrounds the central forward current. The electrons constituting the forward current are good source for heating the core and produce the hot spot for ignition by dumping their energy to the background plasma through various processes. Sharad et al. [77] have shown in their studies a novel mechanism, the formation of current shock, through which these dipoles dissipate their energy and have discussed the implications of their study to the fast ignition. The similar current pulses are also formed in other phenomena such as fast magnetic reconnections [7, 10, 11, 12, 13, 14, 33], fast magnetic field transport [49, 50], laser plasma interactions [78], etc.

The EMHD solutions have an electron flow configuration which is significantly sheared (Fig. 4.1). Since the simulations in 2D show the structures to be robust and stable. It is, thus, of importance to understand why the structures are not

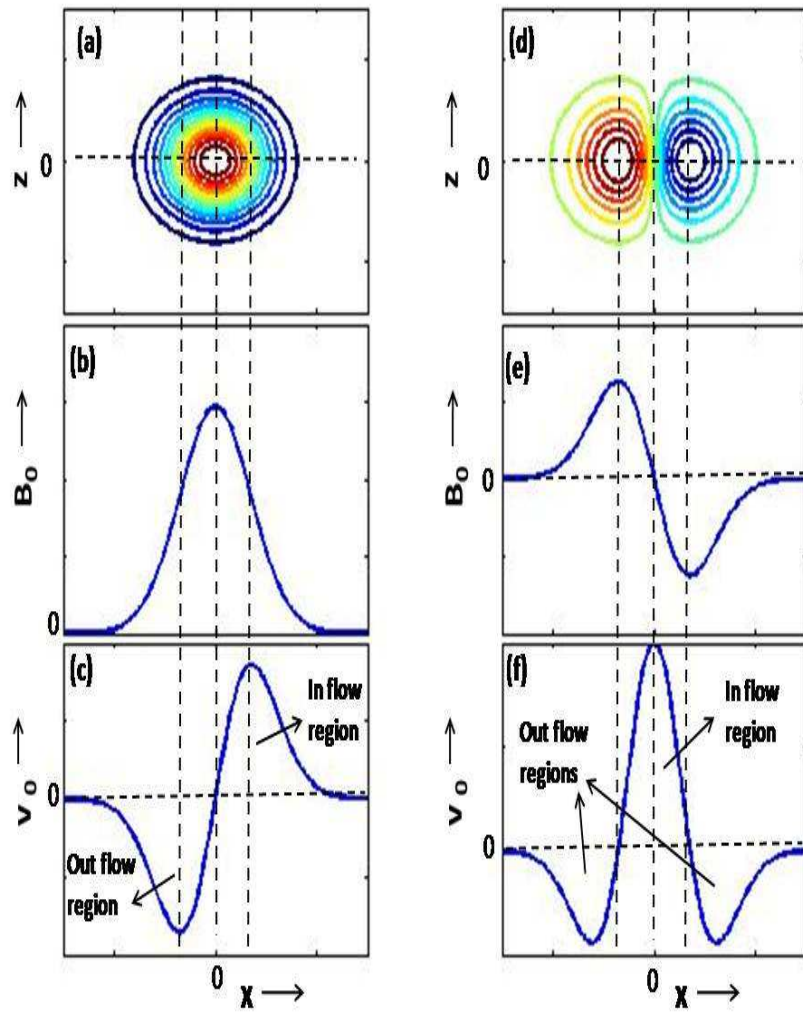


Figure 4.1: Representation of EMHD monopolar and dipolar solutions in the form of current pulses. Subplots (a) and (d) show the forms of typical monopole and dipole as lying in $x-z$ plane. The corresponding magnetic field and flow profiles are shown in subplots below to them (see subplots (b), (c) for monopole and subplots (e), (f) for dipole). Here, using the Maxwell's relation, the flow velocity is related to magnetic field as $v_0 = -dB_0/dx$. In subplots (c) and (e) we see that there are the regions of in flow and out flow that make the configuration as the sheared flow configuration.

Chapter 4: Stability of Isichenko solutions ...

susceptible to the 2D instabilities discussed in earlier Chapters. An explanation of this was provided by Sharad et al. [54], where they suggest structure size being comparable to the shear scale, nonlocal 2D sausage mode, having a cut off wavelength of the order of shear scale, can not be excited. A 3D evolution of these solutions has not been carried out so far where the kink mode, being local mode, has no such cut offs. In this Chapter we study the 3D evolution numerically and show explicitly the destabilization of these solutions.

The Chapter has been organized as follows. In section 4.2 we briefly describe the nonlinear solutions of EMHD equation. In section 4.3, we present the results of numerical simulations in 3D carried out with monopole and dipole structures as the initial conditions in a homogeneous plasma medium. In section 4.4, the stability of structures against flow shear driven modes has been discussed. Finally, in section 4.5, we summarize the outcome of our study.

4.2 Solutions of 2D EMHD

We recall the two dimensional EMHD equations (Eqs. 2.1 in Chapter 2),

$$\begin{aligned} \frac{\partial}{\partial t}(\nabla^2\psi - \psi) + \hat{y} \times \nabla b \cdot \nabla(\nabla^2\psi - \psi) &= 0 \\ \frac{\partial}{\partial t}(\nabla^2b - b) + \hat{y} \times \nabla b \cdot \nabla\nabla^2b - \hat{y} \times \nabla\psi \cdot \nabla\nabla^2\psi - \psi &= 0 \end{aligned} \quad (4.1)$$

Here b and ψ are two scalars which represent the total magnetic field as, $\vec{B} = b\hat{y} + \hat{y} \times \nabla\psi$, y is the symmetry direction. Using the property $\hat{y} \times \nabla A \cdot \nabla B = [A, B]$,

the above set of equations (Eqs. 4.1) could be cast in the following form,

$$\begin{aligned}\frac{\partial \mathcal{F}}{\partial t} + [b, \mathcal{F}] &= 0 \\ \frac{\partial \mathcal{G}}{\partial t} + [b, \mathcal{G}] &= [\psi, \mathcal{F}]\end{aligned}\tag{4.2}$$

Here $\mathcal{F} = \psi - \nabla^2 \psi$ and $\mathcal{G} = b - \nabla^2 b$. The Eqs. (4.2) are in Hamiltonian form in terms of non-canonical Poisson brackets [81] with energy functional,

$$\mathcal{H} = \frac{1}{2} \int [b^2 + (\nabla \psi)^2 + (\nabla b)^2 + (\nabla^2 \psi)^2] dx dz,$$

which is the total energy (sum of the magnetic energy and the kinetic energy) of the system. In Eqs. 4.2 the field b acts as a stream function which advects the quantities \mathcal{F} and \mathcal{G} . The quantity \mathcal{F} is advected as a Lagrangian invariant which represents the conservation of generalized momentum along y direction. The quantity \mathcal{G} , in addition to advection, has a source term in the evolution equation, and is not a Lagrangian invariant.

The Poisson bracket in Eqs. (4.2) vanishes for radially symmetric forms. Hence the symmetric structures i.e. monopoles are exact, stationary solutions of these equations. Any collection of monopoles separated by a distance much larger than their spatial extent such that there is no spatial overlap among them, is also a solution. Two monopoles when placed sufficiently close to each other influence the dynamics of each other. The another interesting solution which is a traveling dipole, is indeed a manifestation of this interaction. A dipole can be imagined as a combination of two monopoles of equal strength but opposite polarity placed in the vicinity of each other. The net results of interaction is the translation of the combined structure. These solutions were obtained analytically by Isichenko et al. [51] by seeking the stationarity in a moving frame. The solutions are the

Chapter 4: Stability of Isichenko solutions ...

combination of Bessel functions of various kinds.

Consider the case that the currents lie in the $x - z$ plane only i.e. $\psi = 0$. For this, Eqs. (4.2) reduce to,

$$\frac{\partial}{\partial t}(b - \nabla^2 b) + [b, b - \nabla^2 b] = 0 \quad (4.3)$$

Stationary monopolar solutions can be obtained for $[b, b - \nabla^2 b] = 0$ which suggests $\nabla^2 b = f(b)$. Here, f is a function of b . For instance, a localized b of the following form can be one such solution,

$$b = A_0 \exp \left\{ -\frac{(x - x_0)^2 + (z - z_0)^2}{\sigma^2} \right\} \quad (4.4)$$

Here, A_0 and σ are constants which decide the strength and spatial extent of the structure, respectively. The other constants x_0 and z_0 fix the location of centre of the structure in the 2D space. This form we have used in our studies as the initial conditions for monopole.

The propagating dipole solutions are obtained by transforming the coordinates to a frame moving with uniform velocity U along z direction. Stationarity in this frame yields,

$$[\nabla^2 b - b, b - Ux] = 0 \quad \Rightarrow \quad \nabla^2 b - b = f_b(b - Ux) \quad (4.5)$$

Here, f_b is an arbitrary function of $(b - Ux)$. Isichenko et al. [51] have obtained the analytical solutions which are localized within a finite spatial extent a_0 . In the inner region ($r \leq a_0$), the vorticity source function is chosen to be a linear function of its argument as, $f_b(= \beta(b - Ux))$. For localization, the function f_b is chosen to

vanish (i.e. $\beta = 0$) in the outside region ($r > a_0$). Solutions are obtained in the cylindrical coordinates as given below,¹

$$\begin{aligned} b &= [d_1 J_1(kr) + d_2 r] \cos(\theta); & r \leq a_0 \\ b &= d_3 K_1(r) \cos(\theta); & r > a_0 \end{aligned} \tag{4.6}$$

Here, d 's and k are unknown constants which are determined from the matching of field b and its derivatives at $r = a_0$. The above solutions of b form the dipole structure for a set of free parameters (U, β, a_0). These solutions with the known constants are then used as initial state in our studies.

4.3 Nonlinear Simulations

To study the evolution of the EMHD structures (monopole and dipole) against 3D perturbations we have carried out 3D nonlinear simulations. The simulation scheme is the same as adapted in Chapter 3. The initial conditions chosen are monopole and dipole structures. Boundary conditions are chosen to be periodic in all the three directions. The values of various parameters have been mentioned wherever required. We have checked for the conservation of total energy in our simulation run(s) to ascertain that there is no numerical instability.

Evolution of Monopole:

The monopole structure has been chosen to lie in the $x - z$ plane. The monopole magnetic field is along y - direction. We show the contour lines showing the magnetic field of the monopole in the $x - y$ plane at various times in Fig. 4.2. The

¹Detailed mathematical derivation of solutions can be seen in Ref. [82].

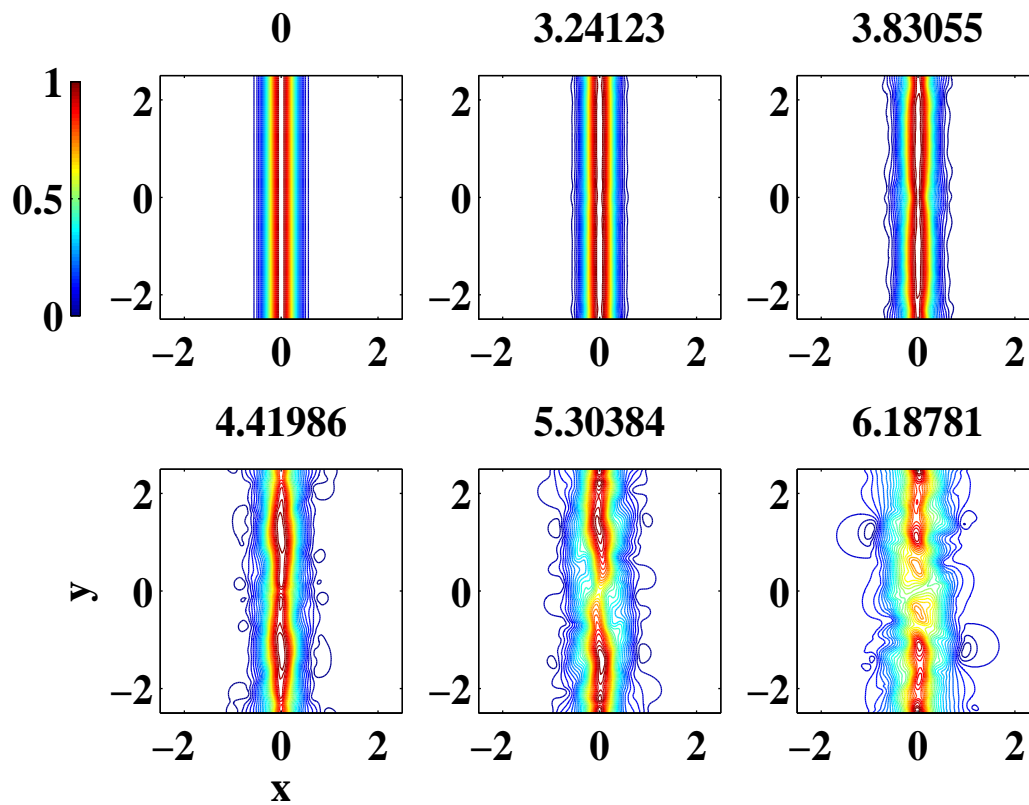


Figure 4.2: The constant magnetic field contours of the monopole have been shown at various times in the $x - y$ plane.

contour lines which are straight initially (as the equilibrium is independent of y) evolve to show the development of instability (at $t = 3.24123$). The instability becomes more pronounced at later time, say at $t = 3.83055$. Up to this time the monopole continues to maintain its identity and remains stable, although its shape gets somewhat distorted. This can be seen from the subplots of Fig. 4.3 at the corresponding times. This figure shows the contour structures of monopoles in the $x - z$ plane. In the later subplot of Fig. 4.2, short scale patterns are seen and the monopole at corresponding times (in Fig. 4.3) shows considerable disintegration.

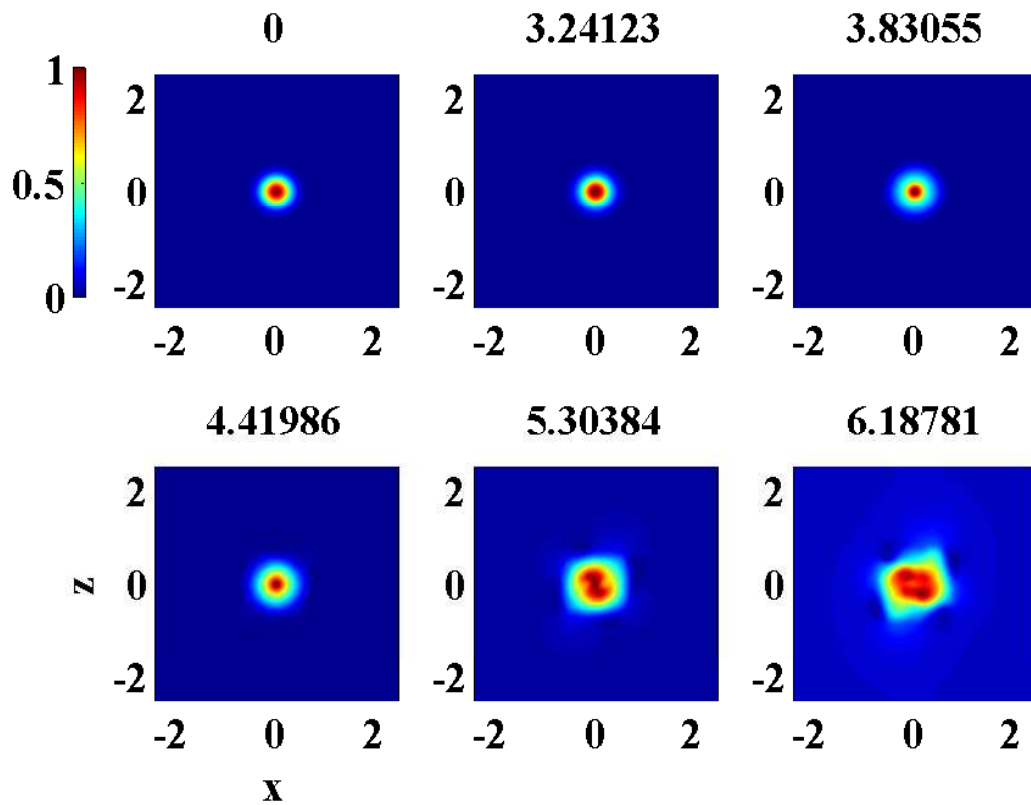


Figure 4.3: The constant magnetic field contours of the monopole have been shown at various times in the $x-z$ plane. These times are similar to those of the subplots of Fig. 4.2.

Evolution of Dipole:

In another simulation, we study the evolution of dipole structure as given in Eq. 4.6. The dipole structure has been chosen to lie in the $x-z$ plane and propagating along z -direction. The dipole magnetic field is along y -direction. We show the contour lines showing the magnetic field of the dipole in the $x-y$ plane at various times in Fig. 4.4. As the dipole propagates with an axial speed z , the z location of the chosen $x-y$ plane in the figure corresponds to the central region of the dipole. The contour lines which are straight initially (as the equilibrium is independent of

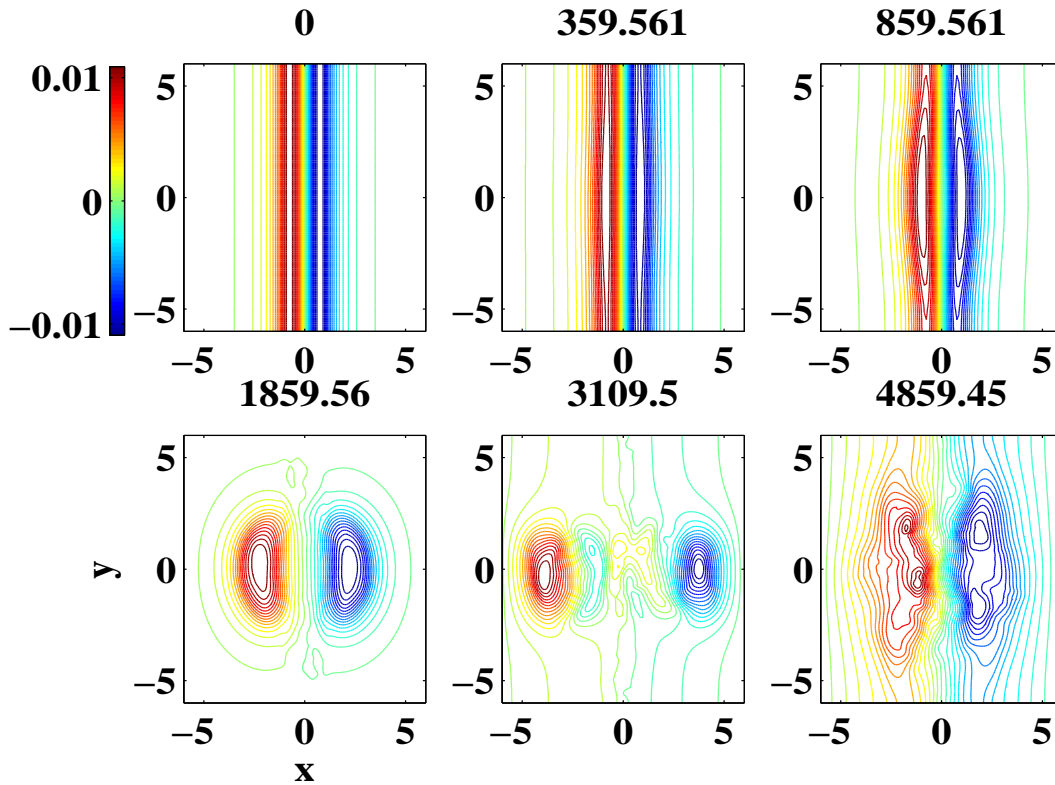


Figure 4.4: The subplots show the plots of the magnetic field lines in the $x - y$ plane for $z = 0.0, 1.87, 3.68, 5.5, -2.06$ and 0.35 corresponding to times $t = 0.0, 359.561, 859.561, 1859.56, 3109.5$ and 4859.45 respectively. The z location at these times correspond to the location of the mid plane of the dipole structure as it propagates. The magnetic field lines which are initially straight as there is no dependence of equilibrium on y later due to the kink instability acquire y dependence.

y) evolve to show the development of instability (at $t = 359.561$). The instability becomes more pronounced at later time, say at $t = 859.561$. Up to this time the dipole continues to maintain its identity and continues to propagate stably, although its shape gets somewhat distorted. This can be seen from the subplots of Fig. 4.5 at the corresponding times. This figure shows the contour structures of dipoles in the $x - z$ plane at $y = 0.0$. Later, the magnetic field lines of the plot in Fig. 4.4 develop a wider bulge and form an island structure (at $t = 1859.56$). At

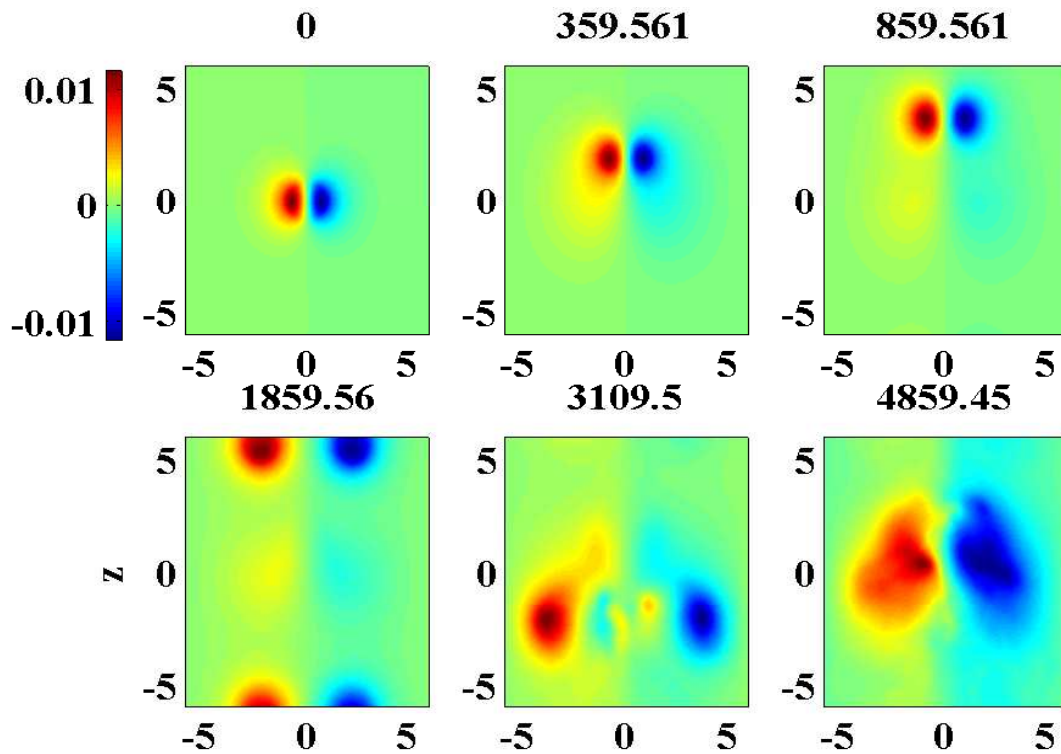


Figure 4.5: The constant magnetic field contours of the dipole have been shown at various times in the $x - z$ plane. These times are similar to those of the subplots of Fig. 4.4.

these later times the dipole shows considerable disintegration. At subsequent times the dipole structure disintegrates completely and small scale structure formation can be observed.

4.4 Discussion

The structures both monopoles and dipoles, in our simulations, are found to be unstable. These structures, however, were stable against sausage mode in their 2D evolution, where kink mode was not supported. The stability of structures against

Chapter 4: Stability of Isichenko solutions ...

sausage mode had been argued by Sharad et al. [54] on the following basis. For these structures, the shear layer width as well as the total extent of shear flow both have an extent of typical electron skin depth size. The sausage mode can only be excited if a scale length along the flow direction is longer than the shear width, e.g., referred to as $k_z \epsilon < 1$ (k_z being the wavenumber along the flow direction and ϵ being the typical shear width) in earlier work. The total extent of the shear flow being limited in size permits no wavenumber to satisfy the criteria of $k_z \epsilon < 1$, hence the structures remain stable to the sausage mode. The kink mode, however, is free from this kind of restriction. Hence, in our simulations, where kink mode is also operative, the structures show destabilization.

The unstable behaviour of the structures raises the question of their relevance in various phenomena described in earlier studies. One needs to compare the instability growth rate along with the time scales involved in the phenomena to investigate the relevance of the structures. We choose to discuss here the study by Sharad et al. [77]. In their study, the dipoles, while moving in an inhomogeneous plasma medium, are shown to dissipate their energy through the mechanism of current shock formation. Implications of the study were shown in the fast ignition phenomena. The study, being two dimensional, does not support the kink mode. However, in real 3D situation the dipoles would become kink unstable as shown by us. We need to compare here, the time scale at which dipoles dissipate their energy with the growth rate of kink instability to see the relevance of dipoles.

As obtained by Sharad et al. [77], the rate of energy dissipation in the shock structure is,

$$Q = \frac{b_0^2 a^2}{2} K L v_e \quad (4.7)$$

Chapter 4: Stability of Isichenko solutions ...

Here, b_0 is the typical value of magnetic field in dipole, v_e is the typical incoming velocity of dipoles and a is the system length along the transverse directions. L is the typical shock length and K is the inverse of the normalized density scale length. The time scale T at which the dipole energy gets dissipated is obtained as,

$$T = \frac{\frac{b_0^2}{2} a^2 L}{Q} \sim \frac{1}{K v_e} \quad (4.8)$$

This suggests that the dissipation would occur fast for the sharp density gradients.

Let us now recall the local dispersion relation for the kink mode obtained as Eq. (3.5) in Chapter 3,

$$2\bar{\omega}(1 + k_0^2) = (v_0'' - v_0)k_z \pm \{(v_0'' - v_0)^2 k_z^2 - 4k_y^2(v_0' + B_0)(v_0' - k_0^2 B_0)\}^{1/2} \quad (4.9)$$

The above dispersion relation predicts the local instability when the discriminant $D = -4k_y^2(v_0' + B_0)(v_0' - k_0^2 B_0) + (v_0'' - v_0)^2 k_z^2 < 0$. It is clear that k_y and v_0' need to be finite for the instability to exist. However, finite values of k_z and B_0 , make the task of exciting kink mode difficult. Choosing $k_z = 0$ and also $B_0 = 0$, the growth rate of instability yields,

$$\gamma = \frac{2k_y v_0'}{2(1 + k_0^2)} \sim \frac{k_y v_0}{\epsilon(1 + k_0^2)} \quad (4.10)$$

Here, ϵ is the shear width or size of the dipole. For $k \sim 1$, the $\gamma \sim v_0/2\epsilon$. This suggests that the instability growth rate diminishes as the shear width increases, as known.

The two time scales T and γ^{-1} would compete with each other to tell which process is dominant. For dipoles to be of relevance i.e. when dissipative process

is dominant, the condition $\gamma T < 1$ should be satisfied. This means that dipoles dissipate their energy before the instability destroys them. Since the finite value of k_z and B_0 reduce the instability growth rate, the condition $\gamma T < 1$ may be favourable in this parameter regime. Hence the dissipative process may be important. In the other limit i.e. $\gamma T > 1$, the dipoles decay due to instability before the dissipation phenomena takes place and hence may not be of relevance. One, thus, needs to look into the parameter space of kink growth rate and compare it with the dissipation time scale T to establish the usefulness of the dipole structures. The expression for growth rate of kink mode Eq. 4.9 is only approximate one and is valid only in the local limit. For more accurate and detailed discussion the nonlocal analysis of the instability needs to be taken into account; the study is underway.

4.5 Summary

In this Chapter, we have investigated the stability of Isichenko solutions of 2D EMHD against the three dimensional perturbations. The solutions are the coherent, localized structures in the form of stationary monopoles and traveling dipoles which propagate with constant speed in their axial direction. The electron flow configuration is significantly sheared in these structures and hence are susceptible to the velocity shear driven instability processes. It is known that for 2D perturbations (variations confined in the plane of flow and shear only), the unstable mode is sausage mode which is a nonlocal mode. When the variations along the third dimension are also allowed, another mode exists, which is a local mode and termed as the kink mode.

The EMHD structures are known to be very robust and stable against the

Chapter 4: Stability of Isichenko solutions ...

2D sausage mode perturbations. However, in our three dimensional nonlinear simulations, we observe that they get destabilized due to the kink mode. The puzzling behavior of structures (stability for sausage and instability for kink mode) can be understood from the following argument. The structure size does not permit the wavenumber to satisfy the instability criteria of sausage mode for which the wavelength should be broader than the shear width, and hence the structures are stable to sausage mode. However, for kink mode which is local in nature, the wavelengths sharper than the shear width are also unstable. Hence the structures become unstable due to the presence of this mode.

Chapter 5

Summary and Future Scope

This Chapter presents the summary and conclusion of the work carried out in the thesis. The Chapter also provides the discussion on possible future research problems in continuation to the work presented in the thesis.

5.1 Summary and Conclusions

The work in the thesis has been focused on the studies of shear driven EMHD instabilities in plasmas. Here, we present summary of the work carried out in previous Chapters with a brief discussion on the important results obtained therein.

- **Role of natural length and time scales of EMHD on 2D Kelvin Helmholtz instability**

Kelvin Helmholtz (KH) instability is one of the prominent fluid instabilities in which interface of two fluids in relative motion is unstable under certain conditions. In the context of EMHD, the instability has been studied in considerable detail [34, 45, 46, 47]. In this thesis, we explore the instability

Chapter 5: Summary and future scope

further under certain additional considerations. Due to its electromagnetic character, the EMHD model exhibits natural length (electron inertia) and time (whistler period) scales. We have studied the role of these natural scales of EMHD on KH instability in 2D, in Chapter 2. Here, 2D refers to the case when the perturbations are confined in the 2D plane consisting of flow and shear directions. The self consistent magnetic field arising due to 2D sheared flow of electrons, is directed along the symmetry direction. A linear analysis solves the problem as matrix eigen problem and obtains the eigen values as the growth rate of the instability. It is observed that the growth rate decreases as the shear width is increased in comparison to the electron skin depth. The instability is prominent only when the shear in the electron flow velocity is sharper than the electron skin depth.

In order to understand the role of whistlers on the instability, a uniform magnetic field (B_0) is imposed along the direction of flow. This magnetic field, being tied to the fluid flow, gets distorted to a sheared configuration due to the action of KH. The tension caused by this distortion tries to restore the magnetic field lines to its original configuration and sets up the oscillations at whistler frequency. The process of exciting whistlers costs energy and opposes the growth of KH mode. Consequently, KH growth rate is found to reduce with increasing B_0 . Nonlinear fluid simulations were carried out to understand the role of whistlers in the nonlinear regime of instability. The instability growth rates with and without B_0 in simulations match with linear theory, this validates the simulation code. In the absence of B_0 , the 2D EMHD model is known to conserve two non-dissipative square integrals namely, energy and enstrophy. This constrains the power transfer in the

nonlinear regime towards longer scale due to the process of inverse cascade. As a result, in simulations for the case of $B_0 = 0$, the final nonlinear state is a coherent pattern occupying the box size. However, in the presence of B_0 , the nonlinear cascade is governed by the interactions among whistlers and exhibits strong anisotropic character [72, 73]. In the final nonlinear state the structures are seen preferentially elongated along the direction of magnetic field. There is hardly any extension along the transverse direction. As a result, the mixing of the fluids flowing in two directions induced by KH instability gets considerably reduced. Hence, the effective viscous coefficient is found to be significantly smaller for this case.

- **Interplay of Kelvin Helmholtz and kink modes**

In Chapter 3, we carried out linear and nonlinear studies of velocity shear driven 3D EMHD instability. In these studies, we permit the spatial variations along the direction of self-consistent magnetic field generated due to sheared flow. In addition to the sausage mode (KH mode), a local mode with perturbations in the plane of shear and the magnetic field exists which is termed as the kink mode [35, 46]. The interplay of these modes with and without external magnetic field has been studied extensively in the linear and nonlinear regimes. The studies indicate that the dominance of one mode over the other is mainly determined by the following three factors: (i) The value of shear width in comparison with electron skin depth. For sharper shear width the sausage growth rate is higher. (ii) The external magnetic field (B_{00}) along the flow direction. The presence of B_{00} stabilizes the sausage mode and does not affect the kink mode. So, kink may be the dominant mode for this case. (iii) The external magnetic field (C_0) along the direc-

Chapter 5: Summary and future scope

tion of magnetic field generated by the flow. The presence of C_0 reduces the growth rate of kink mode and does not affect the sausage growth rate. So, sausage can dominate in these conditions.

Nonlinear simulations of 3D instability were also carried out. The linear growth rates obtained from various simulation runs are in agreement with the linear results. Unlike the 2D case, the nonlinear state is found to be strongly turbulent [43, 47]. This is due to the non existence of two non-dissipative square invariants and also the larger number of unstable modes in 3D. We have analyzed the spectral cascade features of the turbulence generated in the nonlinear state with and without external magnetic field along the flow direction. It is observed that the spectral cascade towards shorter scales is inhibited along the direction of flow as well as the direction of magnetic field. The shortest scales are thus found to generate along the shear direction while, in other two directions the scales are typically longer. This induces significant anisotropy in the spectrum. In simulations with the external magnetic field (B_{00}) present along the flow direction, we observe that the scales along the shear directions are more or less unchanged. However, along the other two directions, the scales are longer in comparison to the case when this magnetic field is not present. These results are in conformity with the whistler mediated spectral cascade features [72, 73]. We have also measured the nonlinear broadening of shear layer which provides the information on the effective viscous coefficient. The broadening of shear layer occurs much slowly for the case when magnetic field is present along the flow directions. In that case the system evolution is governed by the kink mode which in the linear phase does not alter the 2D flow structure. The broadening occurs

only at later nonlinear phase when the energy starts to trickle in other modes as well.

- **Stability of Isichenko solutions against sausage and kink modes**

The 2D EMHD system has exact stationary monopole and propagating dipolar solutions of localized electron flow structures, obtained by Isichenko et al. [51]. The 2D evolution of these structures has been studied in considerable details by several authors [55, 56, 76, 77, 54], where they have been found to be stable. The dipole solutions are of practical importance as they can be imagined as propagating current pulses carrying energy and momentum. They may be employed for the purpose of hot spot generation in Fast Ignition scenario by dumping their energy to the core through collision less processes [77]. The electron flow configuration is significantly sheared in these structures and hence could be susceptible to various flow shear driven instability processes (sausage and kink modes, studied by us in Chapters 2 and 3). In Chapter 4, we have investigated these instability processes for EMHD structures. For this purpose, we have carried out 3D nonlinear simulations to see the evolution of the monopole and dipole in a homogeneous plasma medium. As mentioned above, the EMHD structures, monopole and dipole, are known to be very robust and stable in their 2D evolution [55, 56, 76, 77, 54]. In 2D, kink mode is not supported and the structures are stable to sausage mode. Stability of structures against sausage mode can be understood by the following argument, as provided by Sharad et al. [54]. The structure size does not permit the wave number to satisfy the instability criteria of sausage mode viz., $k_z \epsilon < 1$; here, ' k_z ' is the wavenumber along the flow direction and ' ϵ ' is the shear width. Hence, the structures are stable to sausage mode.

However, kink mode, being a local mode, does not have to follow such kind of criteria and the structures could go unstable due to this mode. In fact, in our three dimensional simulations, where kink mode is also in action, we observe that the structures get destabilized. The unstable behaviour of structures raises a question of their relevance in various phenomena as described earlier [55, 56, 77]. The magnitude of instability growth rate needs to be taken into consideration along with the time scales involved in various phenomena to investigate the relevance of these structures. A discussion on this has been provided in the thesis.

5.2 Future Scope

We discuss here the possible future research problems as an extension of the work presented in the thesis.

- In Chapter 2, we have employed an external magnetic field parallel to flow in order to understand the role of whistlers on KH instability. In the absence of this magnetic field, nonlinear state is a coherent vortex. However, with the magnetic field present, such vortex is not seen in the later nonlinear phase in simulations. Strength of the magnetic field applied is typically of the order of self-consistent magnetic field. For weak and very weak magnetic field cases, “Disruptive” and “Dissipative” phenomena of vortex, as seen in MHD studies, could be investigated.
- In Chapter 4, we have studied the stability of dipole solution obtained for the case when $\psi = 0$ i.e., currents lie in 2D plane of dipoles. Stability of dipoles for ψ finite case against kink mode can also be carried out.

Chapter 5: Summary and future scope

- In our studies, the kink mode is shown to exist in the plane containing the direction of self-consistent magnetic field and of shear (see Fig. 1.1). The magnetic field profile considered has a definite sign i.e. does not have a null-line. In the same configuration (perturbations confined in the plane of magnetic field and shear), another unstable mode may also be present, but for a reversed magnetic field configuration. This is the well-known tearing mode which leads to the reconnection of field lines in the presence of electron inertia [33, 7]. The two instabilities, tearing and kink, can be investigated simultaneously for an equilibrium magnetic field.
- A general three dimensional study can then follow by allowing the variations along the flow direction as well, that would include the Kelvin Helmholtz (KH) mode also in the system.
- We have modeled our studies using slab coordinate system. However, the current configurations, described in various phenomena, are cylindrical in shape. It is, thus, important to carry out the studies in cylindrical geometry for more realistic description.
- There are typical situations e.g., fast ignition, where the sheared flow configurations of electrons moving at relativistic speeds exist. It is, thus, of importance to understand the role of relativity on the flow shear driven instability.

Bibliography

- [1] A. A. Chernov and V. V. Yan'kov, *Soviet Journal of Plasma Physics* **8**, 522 (1982).
- [2] D. D. Ryutov, M. S. Derzon, and M. K. Matzen, *Reviews of Modern Physics* **72**, 000167 (2000).
- [3] M. Tabak, J. Hammer, M. E. Glinsky, W. L. Kruer, S. C. Wilks, J. Woodworth, E. M. Campbell, M. D. Perry, and R. J. Mason, *Phys. Plasmas* **1**, 1626 (1994).
- [4] S. Hain and P. Mulsar, *Physical Review Letters* **86**, 1015 (2001).
- [5] R. Kodama, P. A. Norreys, K. Mima, A. E. Dangor, R. G. Evans, H. Fujita, Y. Kitagawa, K. Krushelnik, T. Miyakoshi, N. Miyanga, T. Norimatsu, S. J. Rose, T. Shozaki, K. Shigemori, A. Sunahara, M. Tampo, K. A. Tanaka, Y. Toyama, T. Yamanaka, and M. Zepf, *Nature (London)* **412**, 798 (2001); R. Kodama, H. Shiraga, K. Shigemori, Y. Toyama, S. Fujioka, H. Azechi, H. Fujita, H. Habara, T. Hall, Y. Izawa, T. Jitsuno, Y. Kitagawa, K. M. Krushelnik, K. L. Lancaster, K. Mima, K. Nagai, M. Nakai, H. Nishimura, T. Norimatsu, P. A. Norreys, S. Sakabe, K. A. Tanaka, A. Youssef, M. Zepf, and T. Yamanaka, *ibid.* **418**, 933 (2002); M. H. Key, *ibid.* **412**, 775 (2001).

Bibliography

- [6] K. A. Tanaka, R. Kodama, K. Mima, Y. Kitagawa, H. Fujita, N. Miyanaga, K. Nagai, T. Norimatsu, T. Sato, Y. Sentoku, K. Shigemori, A. Sunahara, T. Shozaki, M. tanpo, S. Tohyama, T. Yabuuchi, J. Sheng, T. Yamanaka, P. A. Norreys, R. Evanse, M. Zepf, K. Krushelnic, A. Dangor, R. Stephens, S. Hatchett, M. Tabak, and R. Turner, *Phys. Plasmas* **10**, 1925 (2003).
- [7] S. V. Bulanov, F. Pegoraro, and A. S. Sakharov, *Phys. Fluids B* **4**, 2499 (1992).
- [8] L. I. Rudakov and J. D. Huba, *Phys. Rev. Lett.* **89**, 095002 (2002).
- [9] K. Avinash, S. V. Bulanov, T. Esirkepov, P. Kaw, F. Pegoraro, P. V. Sasorov, and A. Sen, *Phys. Plasmas* **5**, 2849 (1998).
- [10] N. Attico, F. Califano, and F. Pegoraro, *Phys. Plasmas* **7**, 2381 (2000).
- [11] N. Attico, F. Califano, and F. Pegoraro, *Phys. Plasmas* **9**, 458 (2002).
- [12] F. Califano, N. Attico, F. Pegoraro, G. Bertin, and S. V. Bulanov, *Phys. Rev. Lett.* **86**, 5293 (2001).
- [13] J. C. Dorelli and J. Birn, *Phys. Plasmas* **8**, 4010 (2001).
- [14] L. Chacon, A. N. Simakov, and A. Zocco, *Phys. Rev. Lett.* **99**, 235001 (2007).
- [15] D. Biskamp, E. Schwarz, and J. F. Drake, *Phys. Plasmas* **4**, 1002 (1997).
- [16] M. A. Shay, J. F. Drake, R. E. Denton, and D. Biskamp, *Journal of Geophysical Research* **103**, 9165 (1998).
- [17] J. F. Drake, M. Swisdak, C. Cattell, M. A. Shay, B. N. Rogers, and A. Zeiler, *Science* **299**, 873 (2003).

Bibliography

- [18] B. N. Rogers, J. F. Drake, and M. A. Shay, *Geophysical Research Letters* **27**, 3157 (2000).
- [19] R. Horiuchi and T. Sato, *Phys. Plasmas* **1**, 3587 (1994).
- [20] M. Swisdak, J. F. Drake, M. A. Shay, and J. G. McIlhargey, *Journal of Geophysical Research* **110**, A05210 (2005).
- [21] A. Fruchtman, A. A. Ivanov, and A. S. Kingsep, *Phys. of Plasmas* **5**, 1133 (1998).
- [22] R. Shpitalnik, A. Weingarten, K. Gomberoff, Ya. Krasik, and Y. Maron, *Phys. Plasmas* **5**, 792 (1998).
- [23] M. Sarfaty, R. Shpitalnik, R. Arad, A. Weingarten, Ya. E. Krasik, A. Fruchtman, and Y. Maron, *Phys. Plasmas* **2**, 2583 (1995).
- [24] A. Teste and G. K. Perks, *Phys. Rev. Lett.* **102**, 075003 (2009).
- [25] N. Jain and A. S. Sharma, *Phys. Plasmas* **16**, 050704 (2009).
- [26] J. P. Freidberg, *Ideal Magnetohydrodynamics* (Plenum Press, New York, 1987).
- [27] D. Biskamp, *Magnetic Reconnection in Plasmas* (Cambridge University Press, Cambridge, UK, 2000).
- [28] E. Priest, *Solar Magnetohydrodynamics* (D. Reidel, Dordrecht, Holland, 1987).
- [29] A. S. Kingsep, K. V. Chukbar and V. V. Yankov, in *Reviews of Plasma Physics* (Consultants Bureau, New York, 1990), Vol. 16 and references therein.
- [30] A. V. Gordeev, A. S. Kingsep, and L. I. Rudakov, *Phys. Rep.* **243**, 215 (1994).

Bibliography

- [31] A. Das and P. H. Diamond, *Phys. Plasmas* **7**, 170 (2000).
- [32] F. Califano, R. Prandi, F. Pegoraro, and S. V. Bulanov, *Phys. Plasmas* **6**, 2332 (1999).
- [33] S. V. Basova, S. A. Varentsova, A. V. Gordeev, A. V. Gulin, and V. Yu. Shuvaev, *Sov. J. Plasma Phys.* **17**, 362 (1991).
- [34] A. Das and P. Kaw, *Phys. Plasmas* **8**, 4518 (2001).
- [35] V. S. Lukin, *Phys. Plasmas*, **16**, 122105 (2009).
- [36] H. Lamb, *Hydrodynamics* (Dover Publication, Inc, , New York, 1945).
- [37] S. Chandrasekhar, *Hydrodynamic and Hydromagnetic Stability* (Dover Publications, Inc., New York, 1981).
- [38] P. G. Drazin and W. H. Reid, *Hydrodynamic Stability* (Cambridge University Press, Cambridge, London, 1982).
- [39] A. K. Sen, *Phys. Fluids* **6**, 1154 (1963); A, K. Sen, *Phys. Fluids* **7**, 1293 (1964).
- [40] R. A. Gerwin, *Reviews of Modern Physics* **40**, 652 (1968).
- [41] A. Miura and P. L. Pritchett, *J. Geophys. Res.* **87**, 7431-7444 (1982), doi:10.1029/JA087iA09p07431.
- [42] A. Miura, *J. Geophys. Res.* **89**, 801 (1984); A. Miura, *J. Geophys. Res.* **92**, 3195 (1987).
- [43] J. F. Drake, R. G. Kleva, and M. E. Mandt, *Phys. Rev. Lett.* **73**, 1251 (1994); D. Biskamp, E. Schwarz, and J. F. Drake, *Phys. Rev. Lett.* **76**, 1264 (1996).

Bibliography

- [44] J. F. Drake, D. Biskamp, and A. Zeiler, *Geophysical Research Letters* **24**, 2921 (1997).
- [45] N. Jain, A. Das, P. Kaw, and S. Sengupta, *Phys. Plasmas* **10**, 29 (2003).
- [46] N. Jain, A. Das and P. Kaw, *Phys. Plasmas* **11**, 4390 (2004).
- [47] N. Jain, A. Das, P. Kaw, and S. Sengupta, *Phys. Letts. A* **363**, 125 (2007);
N. Jain, A. Das, S. Sengupta, and P. Kaw *Phys. Plasmas* **19**, 092305 (2012).
- [48] Neeraj Jain (2006), *Study of Electron Magnetohydrodynamic (EMHD) Phenomena in Plasmas*: PhD Thesis, Institute for Plasma Research, Bhat, Gandhinagar - 382428, India
- [49] S. I. Vainshtein, S. M. Chitre, and A. V. Olinto, *Phys. Rev. E* **61**, 4422 (2000).
- [50] M. Rheinhardt and U. Geppert, *Phys. Rev. Lett.* **88**, 101103 (2002).
- [51] M. B. Isichenko, and A. N. Marnachev, *Sov. Phys. JETP* **66**, 702 (1987).
- [52] S. V. Bulanov, M. Lontano, T. Zh. Esirkepov, F. Pegoraro, and A. M. Pukhov, *Phys. Rev. Lett.* **76**, 3562 (1996); S. V. Bulanov, T. Zh. Esirkepov, M. Lontano, and F. Pegoraro, *Plasma Phys. Rep.* **23**, 660 (1997).
- [53] S. Sundar and A. Das, *Phys. Plasmas* **17**, 042106 (2010).
- [54] S. K. Yadav and Amita Das, *Phys. Plasmas* **17**, 052306 (2010).
- [55] A. Das, *Plasma Phys. Control. Fusion* **41**, A531 (1999).
- [56] S. Dastgeer (2000), *Coherent, Nonlinear and Turbulence Phenomena in Electron Magnetohydrodynamics Systems*: PhD Thesis, Institute for Plasma Research, Bhat, Gandhinagar - 382428, India

Bibliography

- [57] J. P. McFadden, C. W. Carlson, R. E. Ergun, C. C. Chaston, F. S. Mozer, M. Temerin, D. M. Klumpar, E. G. Shelley, W. K. Peterson, E. Moebius, L. Kistler, R. Elphic, R. Strangeway, C. Cattell, and R. Pfaff, *Geophys. Res. Lett.* **25**, 2045 (1998); G. Parks, L. J. Chen, M. Fillingim, M. McCarthy, *Space Sci. Rev.* **95**, 237 (2001).
- [58] R. A. Treumann and T. Terasawa, *Space Sci. Rev.* **99**, 135 (2001).
- [59] J. Arons, in *General Relativistic Polar Particle Acceleration and Pulsar Death* (Universal Academy Press, Tokyo, 1998), p. 339.
- [60] R. L. Stenzel, J. M. Urrutia, and K. D. Strohmaier, *Phys. Rev. Lett.* **99**, 265005 (2007); R. L. Stenzel, J. M. Urrutia and K. D. Strohmaier, *Phys. Rev. Lett.* **101**, 135002 (2008).
- [61] G. Ravi, S. K. Mattoo, L. M. Awasthi, and V. P. Anitha, *Phys. Plasmas* **10**, 2194 (2003).
- [62] R. S. B. Ong and N. Roderick, *Planet. Space Sci.* **20**, 1 (1972).
- [63] A. Miura, *Geophys. Res. Lett.* **17**, 749 (1990).
- [64] A. Malagoli, G. Bodo, and R. Rosner, *ApJ* **456**, 708 (1996).
- [65] A. Frank, T. W. Jones, D. Ryu, and J. B. Gaalaas, *ApJ* **460**, 777 (1996).
- [66] T. W. Jones, J. B. Gaalaas, D. Ryu, and A. Frank, *ApJ* **482**, 230-244 (1997).
- [67] Jones, T. W., Joseph B. Gaalaas, Dongsu Ryu, and Adam Frank. "*The Role of Weak Magnetic Fields in Kelvin-Helmholtz Unstable Boundary Layers*". In *Computational Astrophysics; 12th Kingston Meeting on Theoretical Astrophysics* **123**, 146 (1997).

Bibliography

- [68] R. Keppens, G. Toth, R. H. Westermann, and J. P. Goedbloed, *J. Plasma Phys.* **61**, 1-19 (1999).
- [69] N. O. Weiss, *Proc. Royal Soc. London A* **293**, 310 (1966).
- [70] J. V. Shebalin, W. H. Matthaeus, and D. Montgomery. *J. Plasma Phys.* **29**, 525 (1983).
- [71] S. Oughton, W. H. Matthaeus, and S. Ghosh, *Phys. Plasmas* **5**, 4235 (1998).
- [72] S. Dastgeer, A. Das, P. Kaw, and P. H. Diamond, *Phys. Plasmas* **7**, 571 (2000);
S. Dastgeer, A. Das, and P. Kaw, *Phys. Plasmas* **7**, 1366 (2000).
- [73] C. S. Ng, A. Bhattacharjee, K. Germaschewski, and S. Galtier, *Phys. Plasmas* **10**, 1954 (2003).
- [74] J. P . Boris and D. L. Book, *Methods Compt. Phys.* **16**, 76 (1976).
- [75] J. P . Boris and D. L. Book, *Journal of Computational Physics* **11**, 38 (1973).
- [76] S. K. Yadav, A. Das and P. Kaw, *Phys. Plasmas* **15**, 062308 (2008).
- [77] S. K. Yadav, A. Das, P. Kaw and S. Sengupta, *Phys. Plasmas* **16**, 040701 (2009).
- [78] A. S. Sandhu, A. K. Dharmadhikari, P. P . Rajeev, G. R. Kumar, S. Sengupta, A. Das, and P. K. Kaw, *Phys. Rev. Lett.* **89**, 225002 (2002).
- [79] A. Das, N. Jain, P. Kaw and S. Sengupta, *Nucl. Fusion* **44**, 98 (2004).
- [80] G. Gaur, S. Sundar, S. K. Yadav, A. Das, P. Kaw, and S. Sharma, *Phys. Plasmas* **16**, 072310 (2009).

Bibliography

- [81] D. Sarto, F. Califano, and F. Pegoraro, Phys. Rev. Lett. **91**, 235001 (2003);
D. Sarto, F. Califano, and F. Pegoraro, Phys. Plasmas **12**, 012317 (2005).
- [82] Sharad K. Yadav (2011), *Electron Magnetohydrodynamic (EMHD) Studies on Electron Transport in An Inhomogeneous Plasma Medium*: PhD Thesis, Institute for Plasma Research, Bhat, Gandhinagar - 382428, India